ABSTRACT

CHOI, WONCHANG. Flexural Behavior of Prestressed Girder with High Strength Concrete. (Under the direction of Dr. Sami Rizkalla)

The advantages of using high strength concrete (HSC) have led to an increase in the typical span and a reduction of the weight of prestressed girders used for bridges. However, growing demands to utilize HSC require a reassessment of current provisions of the design codes. The objective of one of the research projects, recently initiated and sponsored by the National Cooperative Highway Research Program (NCHRP), NCHRP Project 12-64, conducted at North Carolina State University is to extend the use of the current AASHTO LRFD design specifications to include compressive strength up to 18,000 psi (124 MPa) for reinforced and prestressed concrete members in flexure and compression. This thesis deals with one part of this project. Nine full-size AASHTO girders are examined to investigate the behavior of using different concrete compressive strength and subjected to the flexural loadings. The experimental program includes three different configurations of prestressed girders with and without a deck slab to investigate the behavior for the following cases: 1) the compression zone consists of normal strength concrete (NSC) only; 2) the compression zone consists of HSC only; and 3) the compression zone consists of a combination of two different strengths of concrete. An analytical model is developed to determine the ultimate flexural resistance for prestressed girders with and without normal compressive strength concrete. The research also includes investigation of the transfer length and the prestress losses of HSC prestressed girders. Based on materials testing and extensive data collected from the literature, a new equation is proposed to calculate the elastic modulus for normal and high strength concrete.

FLEXURAL BEHAVIOR OF PRESTRESSED GIRDER WITH HIGH STRENGTH CONCRETE

By
Wonchang Choi

A dissertation submitted to the Graduate Faculty of
North Carolina State University
in partial fulfillment of the
requirement for the degree of
Doctor of Philosophy

Civil Engineering

Raleigh, North Carolina

2006

Approved by:

Dr. Sami Rizkalla	Dr. Paul Zia
Chair of Advisory Committee	Advisory Committee
Civil Engineering	Civil Engineering
Dr. Amir Mirmiran	Dr. Kara Peters
Advisory Committee	Advisory Committee
Civil Engineering	Mechanical Engineering

BIOGRAPHY

Wonchang Choi obtained a Bachelor's Degree in Chemistry from Kyung Hee University, and a second Bachelor's Degree in Civil Engineering from Hongik University, Seoul Korea. He continued his studies in structures and completed research with the use fiber reinforced polymer girder for compression members, completing his Master's Degree in 2002.
In 2003, he relocated to Raleigh, North Carolina State University under the supervision of Dr. Sami Rizkalla to pursue his Doctor of Philosophy.

ACKNOWLEGEMENTS

It would have been impossible to complete this dissertation without the intellectual, emotional and financial support and friendship of my advisor, my colleague and my family.

It is with sincere gratitude that I thank my advisor, Dr. Sami Rizkalla, for his continuous supervision and mentoring. I would also like to thank Dr. Paul Zia for providing valuable insight. It is truly an honor to work with such an outstanding man who is willing to share his wealth of knowledge and his extensive personal experience. Thanks are extended to Dr. Amir Mirmiran for providing an opportunity to join this research program.

The technical assistance provided by the staff of the Constructed Facilities Laboratory (Bill Dunleavy, Jerry Atkinson, and Amy Yonai) are greatly appreciated. Thanks are extended to all of my fellow graduate students at the Constructed Facilities Laboratory for their help and friendship. Special thanks are extended to Mina Dawood, as my officemate who was a tremendous help to encourage me.

And lastly, I sincerely thank my parent and my lovely wife. I couldn't imagine standing here without their unconditional love and support.

I know that this thesis is not the conclusion, but rather the starting point.

TABLE OF CONTENTS

LIST OF FIGURES ..... **v**

LIST OF TABLES ..... **vii**

1 INTRODUCTION **1**

1.1 GENERAL 1
1.2 OBJECTIVES 2
1.3 SCOPE 3

2 LITERATURE REVIEW **6**

2.1 INTRODUCTION 6
2.2 MATERIAL PROPERTIES 8
2.3 STRESS BLOCK PARAMETERS 12
2.4 PRESTRESS LOSSES 14
2.5 FLEXURAL BEHAVIOR OF GIRDERS WITH HIGH STRENGTH CONCRETE 16

3 EXPERIMENTAL PROGRAM **18**

3.1 INTRODUCTION 18
3.2 DESIGN OF THE TEST SPECIMENS 18
3.3 FABRICATION OF TEST SPECIMENS 22
3.4 INSTRUMENTATION 29
3.5 MATERIAL PROPERTIES 35
3.6 FLEXURAL TEST DETAILS 45

4 RESULTS AND DISCUSSION **54**

4.1 INTRODUCTION 54
4.2 MATERIAL PROPERTIES STUDY 55
4.3 PRESTRESS LOSSES 65
4.4 TRANSFER LENGTH 72
4.5 CAMBER 74
4.6 FLEXURAL RESPONSE 75

5 ANALYTICAL MODEL **100**

5.1 INTRODUCTION 100
5.2 CODE PROVISONS 101
5.3 SECTION ANALYSIS 120

6 SUMMARY AND CONCLUSIONS **135**

6.1 SUMMARY 135
6.2 CONCLUSIONS 136
6.3 RECOMMENDATION AND FUTURE WORK 140

LIST OF FIGURES

Figure 3-1 Cross-section showing prestressing strand configurations 21
Figure 3-2 Prestressing bed: a) Elevation schematic view of prestressing bed, b) Strand lay-out, c) Pretensioning 24
Figure 3-3 Sequence of girder fabrication 26
Figure 3-4 Formwork for the 5 ft. and 1 ft. wide deck slabs 28
Figure 3-5 Load cell installation 30
Figure 3-6 Locations of weldable strain gauges 33
Figure 3-7 Installation of weldable strain gauge 34
Figure 3-8 Installation of the strain gauges attached to #3 steel rebar 35
Figure 3-9 Specimen preparation and test set-up for elastic modulus 39
Figure 3-10 Test set-up for elastic modulus and modulus of rupture 40
Figure 3-11 Material property for prestressing strand 44
Figure 3-12 Test set-up schematic 45
Figure 3-13 Typical test set-up for nine AASHTO girder specimens 46
Figure 3-14 Location of LMTs to measure deflections 49
Figure 3-15 Location of Strain and PI gages for 10PS – 5S, 14PS- 5S and 18PS-5S 50
Figure 3-16 Location of Strain and PI gages for 10PS–1S, 14PS-1S and 18PS-1S 51
Figure 3-17 Location of Strain and PI gages for 10PS-N, 14PS–N and 18PS-N 53

Figure 4-1 Comparison of the elastic modulus between test results and predicted value 57
Figure 4-2 Comparison between predicted E and measured E with various equations; a) AASHTO LRFD and ACI318; b)ACI363R; c) Cook's; d) Proposed 59
Figure 4-3 Normal distribution for the ratio of predicted to measured elastic modulus 62
Figure 4-4 Modulus of rupture versus compressive strength 64
Figure 4-5 Load-deflection behavior for 10, 14, 18PS-5S 76
Figure 4-6 Strain envelopes for 18PS-5S 78
Figure 4-7 Moment – N.A. depth location for 10PS – 5S, 14PS – 5S and 18PS – 5S 80
Figure 4-8 Typical failure mode for the AASHTO girder with a 5 ft. wide deck 81
Figure 4-9 Load-deflection behavior for 10PS – 1S, 14PS – 1S and 18PS-1S 84
Figure 4-10 Strain envelopes for 10PS-1S 86
Figure 4-11 Moment – N.A. depth location for 10PS – 1S, 14PS – 1S and 18PS – 1S 88
Figure 4-12 Typical failure modes for the AASHTO girder with a 1 ft. wide deck 90
Figure 4-13 Load-deflection behavior for 10PS - N, 14PS – N and 18PS-N 92
Figure 4-14 Strain envelopes for 18PS-N 94
Figure 4-15 Moment – N.A. depth location for 10PS - N, 14PS – N and 18PS - N 96
Figure 4-16 Typical failure modes for the AASHTO girder without deck 97
Figure 4-17 Ultimate strain at peak load for tested AASHTO girders 99

Figure 5-1 Cracking strength ratio for three different calculations 104
Figure 5-2 Compressive stress distribution (a) cross-section; (b) strain compatibility; (c) meausred strain-stress distribution in compression zone; (d) the equivalent rectangular stress block in compression zone 111

Figure 5-3 Compressive stress distribution (a) cross-section; (b) strain compatibility (c) measured strain-stress distrubution in compression zone, (d) simplified stress distribution (e) the equvalent rectagular stress block 114
Figure 5-4 Compressive stress distribution (a) cross-section; (b) strain compatibility; (c) measured strain-stress distribution in compression zone; (d) the equivalent rectangular stress block 116
Figure 5-5 Failure evaluation for each configuration 118
Figure 5-6 Cross-section and assumed strain profile for 18PS - 5S 121
Figure 5-7 Measured stress-strain behavior of 10PS-5S and a best-fit curve with analytical model 124
Figure 5-8 Definition of the four factors adopted from Collins (1997) 127
Figure 5-9 Analytical modeling of the prestressing strand 127
Figure 5-10 Measured and predicted load deflection responses 130
Figure 5-11 Measured and predicted load deflection responses 131
Figure 5-12 Measured and predicted load deflection responses 132
Figure 5-13 Flexural strength ratio of the measured versus predicted results 134

LIST OF TABLES

Table 3.1 Detailed Design of the Test Specimens 20
Table 3.2 Construction Sequence Summary 23
Table 3.3 Measured Data from Load Cells 31
Table 3.4 Order of Prestressing Strands and Elongation 32
Table 3.5 Detailed Mix Design for Girder Specimens 36
Table 3.6 Concrete Properties for Girder Specimens 37
Table 3.7 Concrete Mix Design for Deck Slab 38
Table 3.8 Concrete Properties for Cast-in-place Deck 38
Table 3.9 Test Results for Material Properties 42
Table 3.10 Compressive Strength Test for Deck Concrete 42
Table 3.11 Material Property for Each AASHTO Girder Specimen 43

Table 4.1 Range of the Collected Data 58
Table 4.2 Results of Statistical Analysis 61
Table 4.3 Elastic Shortening at Transfer 68
Table 4.4 Creep and Shrinkage Prediction Relationships by AASHTO LRFD 70
Table 4.5 Test Results for Prestressed Losses at Test Day 71
Table 4.6 Summary of End Slippage and Transfer Length 73
Table 4.7 Summary of Camber Results 74
Table 4.8 Observed Test Results for 10PS–5S, 14PS–5S and 18PS-5S 76
Table 4.9 Observed Test Results for 10PS-1S, 14PS–1S and 18PS-1S 84
Table 4.10 Observed Test Results for 10PS-N, 14PS–N and 18PS-N 93

Table 5.1 Comparison between Observed and Computed Cracking Strength 103
Table 5.2 Calculation Method for the Flexural Strength 106
Table 5.3 Comparison of Design Calculation 110
Table 5.4 Design Calculations for Composite AASHTO Girders 112
Table 5.5 Design Calculation for Composite AASHTO Girders 115
Table 5.6 Design Calculation for AASHTO Girders without a Deck 117
Table 5.7 Failure Evaluation for All Specimens 119
Table 5.8 Concrete Material Model for the Specimens 125

1 INTRODUCTION

1.1 GENERAL

1.1.1 High Performance versus High Strength Concrete

The performance of concrete has been improved through the use of chemical and mineral admixtures such as fly ash, slag, silica fume, and high-range water reducing agents. These admixtures have the potential to influence particular properties of concrete and, as such, influence the compressive strength, control of hardening rate, workability, and durability of the concrete. Thus, more rigid criteria are needed to define the performance of concrete.

Zia (1991), in a study undertaken through the Strategic Highway Research Program (SHRP), defines high performance concrete (HPC) by using three requirements: a maximum water-cementitious ratio less than 0.35; a minimum durability factor of 80 percent, and a minimum compressive strength. Russell (1999) states that HPC in the ACI definition is that "concrete meeting special combinations of performance and uniformity requirements that cannot always be achieved routinely using conventional constituents and normal mixing, placing, and curing practices." Neville (4th Edition) specifies that HPC includes two major properties, high compressive strength and low permeability.

The term, *high performance concrete*, may be a more comprehensive expression than *high strength concrete*. However, this project focuses on the behavior of high compressive strength. Therefore, instead of *high performance concrete*, the term, *high strength concrete* (HSC), is used in this study.

1.1.2 High Strength Concrete

Research by Carasquillo et al. (1981) on HSC highlighted the uncertainty and potential inaccuracy of using current code provisions that have been developed for normal concrete strength. Accordingly, several studies have been conducted to gain a better understanding of HSC flexural members including prestressed concrete girders. However, the definition and boundaries of HSC contain too many ambiguities to specify stringent conditions. Therefore, many specifications mainly specify the compressive strength for HSC. According to the ACI 363R *State-of the Art Report on High Strength Concrete* (1992), the definition of HSC is based on the compressive strength of 6,000 psi (41 MPa) or greater at the age of 28-day. However, one must note that the definition of HSC has changed over the years and will no doubt continue to change.

1.2 OBJECTIVES

The main objective of this research is to evaluate the behavior of prestressed concrete girder with high strength concrete with and without a cast-in-place normal strength deck slab. The specific objective can be summarized as follows:

1. Due to the lack of complete knowledge of the material properties of HSC, the prediction of the material properties using current design specifications may be inaccurate in determining the behavior and the strength. This may include unreliable predictions of the cracking strength and ultimate flexural strength. This introduced the

needs for reassessment of the material properties of HSC using more accurate test results.

2. This research program proposes to validate the analytical models typically used to determine the flexural response of prestressed HSC AASHTO type girders with and without a cast-in-place normal strength deck. The intent of the tests is to validate the use of stress block parameters in calculating the flexural resistance of flanged sections with HSC. This experiment also investigates the effect of the presence of normal strength deck in composite action with HSC girders.

3. Evaluate the applicability of the current code equations to predict the prestress losses in HSC girders, including recently proposed equations by Tadors (2003), based on the measured prestress losses of prestressed concrete girders.

4. Provide recommendations for the design of prestressed concrete girders with HSC.

1.3 SCOPE

To study the behavior and prestress loss of prestressed high strength concrete girder, a total of nine AASHTO type II girders were tested with and without normal strength concrete deck slab.

All girders were simply supported with 40 ft. long. The nine AASHTO Type II girders were fabricated and tested up to failure under static loading conditions using four-point loading.

Three girders were cast without a concrete deck. Therefore, the entire section consists of HSC only. The rest of the girders were cast with a concrete deck. The concrete decks were cast at the Constructed Facilities Laboratory (CFL) at North Carolina State University, Raleigh, NC after the girders were fabricated. The design concrete strengths for the nine girders ranged from 10,000 psi (69 MPa) to 18,000 psi (124 MPa). The concrete strength of the cast-in-place deck was in the range of 4,000 psi (28 MPa).

The flexural response of the prestressed girders was investigated in a three-phase experimental research program. In the first phase, three HSC AASHTO with three different target strength and a cast-in-place NSC deck were fabricated. This allowed the compression zone will be located within the NSC deck slab. In the second phase, included three prestressed girders with HSC and the narrow width cast-in-place NSC deck. Therefore, the compression zone consists of HSC and NSC. In the third phase, three prestressed girder with HSC without deck slab was subjected to flexure to study the behavior when the entire compression zone consisted of HSC only.

The nine girders were extensively instrumented to measure the different limit states including cracking and deflections at various loading stages, as well as prestress losses measurements.

The research includes modeling of the behavior of the prestressed girders based on strain compatibility and equilibrium approach. The measured values were also compared to the predictions according to code equations. Based on the findings, design model is proposed for the prediction of the ultimate moment resistance of HSC prestressed girders.

Chapter 2 of this thesis presents a relevant literature review of the flexural behavior of prestressed AASHTO girders with HSC. The literature review includes material properties, stress block parameters, prestress losses, and the flexural behavior of HSC girders.

Chapter 3 of this thesis describes in details the experimental program, including design considerations, fabrication procedures of the prestressed AASHTO girders, instrumentation, the flexural test setup, and separate test results for each phase.

Chapter 4 summarizes the test results and discussion the material properties, transfer length, prestress losses and flexural response of the tested girders under static loading conditions.

Chapter 5 presents the analytical model for the flexural behavior of the prestressed concrete girders using HSC. A comparison of the measured and computed values is discussed.

The summary and conclusion of the research program are presented in Chapter 6.

2 LITERATURE REVIEW

2.1 INTRODUCTION

High strength concrete has been used and studied as a workable construction material for several decades. In the United States, HSC was applied to major prestressed girders in 1949. Walnut Lane Bridge in Philadelphia was the first bridge reported to use HSC in its design and construction (Russell, 1997). This bridge was constructed with a 160 ft. center main span with two 74 ft. side spans. The required strength of 5,400 psi (37 MPa) was obtained in 14 to 17 days. Zollman (1951) reported that the compressive strength at 28 days was usually high about 6,500 psi (45 MPa). ACI 363R-97 notes that concrete with a compressive strength of 5,000 psi (34 MPa) was considered to be HSC in the 1950s. However, at about that same time, the introduction of prestress design methods would have been considered to be more remarkable than the use of HSC. The development of high-range water reducing admixtures in the 1960s and further improvements of material technology increased the possibilities for HSC production in the construction industry.

From the late 1970s, the major research into the application of prestressed bridge girders using HSC was conducted at Cornell University, the Louisiana Transportation Research Center, the University of Texas at Austin, North Carolina State University, the Portland Cement Association and Construction Technology Laboratory, the Minnesota Department of Transportation and others. In general, this research focused on three subjects: the development of concrete mix designs to produce HSC using regional materials; the assessment of equations used to predict the material properties of HSC; and the application of prestressed girders with HSC, including cost effectiveness.

Additional research (Law and Rasoulian, 1980; Cook, 1989; Adelamn and Cousins, 1990) shows that concrete compressive strength in excess of 10,000 psi (69 MPa) using regional materials can be produced by the construction industry. In addition to mix design development, an increase in concrete design compressive strength, from 6,000 psi (41 MPa) to 10,000 psi (69 MPa), results in an average 10 percent increase in span capability for prestressed girders used in routine bridge design (Adelamn and Cousins, 1990). For this type of bridge construction, it has been shown that an increase in concrete strength and stiffness can also result in increased cost effectiveness.

Concrete with a compressive strength of 10,000 psi (69 MPa) can now be routinely produced commercially. Based on HSC's advantages, the application of prestressed girders with HSC has increased in the United States. Moreover, the need for a reassessment of current design code has broadened.

This section provides a description of selected test results and the design parameters for predicting the flexural behavior of prestressed girders with HSC. Topics in this section include: 1) material properties, 2) stress block parameters, 3) prestress losses and 4) the flexural behavior of girders with HSC.

2.2 MATERIAL PROPERTIES

The material properties of HSC constitute the essential factors in the design and analysis of longer bridge spans due to the increasing use of HSC in such bridge design. A more accurate prediction methodology for the material properties of HSC is required to determine prestress losses, deflection and camber, etc. Many researchers have proposed methods for the prediction of material properties for HSC. This section addresses the major findings related to the material properties for HSC.

2.2.1 Pauw (1960)

The ACI Committee 318 Building Code (ACI 318-77) has accepted the findings of Pauw (1960) for the elastic modulus. Pauw utilized other researchers' test results for the modulus of elasticity and derived the empirical equation for normal-weight concrete by using the least squares method based on a function of the unit weight and compressive strength of concrete. The proposed empirical modulus of elasticity, E_c, equation shows good agreement for the normal-weight concrete. These equations are recommended in the current ACI 318 Building Code and in the AASHTO LRFD specifications. They are given as:

$E_c = 33 \cdot w^{1.5} \cdot \left(f_c'\right)^{0.5}$ (psi) and **Equation 2-1**

$E_c = 0.043 \cdot w^{1.5} \cdot \left(f_c'\right)^{0.5}$ (MPa) , **Equation 2-2**

where

w_c = dry unit weight of concrete at time of test;

f_c' = compressive strength of concrete.

2.2.2 Carasquillo et al. (1981)

Research into HSC was conducted at Cornell University by Carasquillo et al. (1981). The ACI Committee 363's *State-of-the-Art Report of High-Strength Concrete* (ACI 363R-84 1984) accepted the findings of their research as well as their proposed equations for the elastic modulus and the modulus of rupture for HSC. The Carasquillo team investigated the compressive concrete strength range from about 3,000 to 11,000 psi (21 to 76 MPa). Carasquillo et al. suggested that the ACI 318-77 equations, based on the proposal of Pauw (1960), overestimate the modulus of elasticity for HSC ranging from 6,000 psi (41 MPa) or more because the stiffness of the concrete is due to a combination of mortar and aggregate strength. The Carasquillo study also discusses the effects of coarse aggregate type and proportions on the modulus of rupture and the modulus of elasticity. However, no consideration was given to the effects of the use of different aggregates on the modulus. Regarding the Poisson's ratio of concrete, Carasquillo et al. state that the value of Poisson's ratio of concrete is close to 0.2 regardless of the compressive strength or the age of the test. Currently, ACI 363R-97 relates these properties to the specified compressive strength ranging from 3,000 psi (21 MPa) to 12,000 psi (83 MPa) and still accepts the Carasquillo research results. The equations are given below for the elastic modulus, E_c and modulus of rupture, f_r are;

$$E_c = \left[40{,}000 \cdot \left(f_c'\right)^{0.5} + 10^6\right] \cdot \left(w_c/145\right)^{1.5} \text{ (psi),} \qquad \textbf{Equation 2-3}$$

$$E_c = \left[3{,}320 \cdot \left(f_c'\right)^{0.5} + 6900\right] \cdot \left(w_c/2320\right)^{1.5} \text{ (Mpa),} \qquad \textbf{Equation 2-4}$$

$$f_r = 11.7\sqrt{f_c'} \text{ (psi) and} \qquad \textbf{Equation 2-5}$$

$f_r = 0.94\sqrt{f_c'}$ (Mpa) **Equation 2-6**

2.2.3 Ahmad and Shah (1985)

Empirical equations for the material properties of HSC were derived from experimental data from other researchers. The research of Ahmad and Shah is limited to compressive concrete strength up to 12,000 psi (84 MPa). Ahmad and Shah found that the difference in the characteristics of the stress-strain curve between NSC and HSC is significant. They also stated that the modulus of rupture of HSC in ACI318-83 is very conservative, while the modulus of elasticity in ACI318-83 computes 20 percent higher values. Ahmad and Shah suggested new equations for the modulus of rupture and the modulus of elasticity of HSC. The equations are given below as reference.

$E_c = w_c^{2.5} \cdot (f_c')^{0.325}$ (psi) , **Equation 2-7**

$E_c = 3.385 \cdot 10^{-5} \cdot w_c^{2.5} \cdot (f_c')^{0.325}$ (MPa), **Equation 2-8**

$f_r = 2(f_c')^{2/3}$ (psi) and **Equation 2-9**

$f_r = 0.38(f_c')^{2/3}$ (MPa). **Equation 2-10**

2.2.4 Zia et al. (1993)

The Strategic Highway Research Program on mechanical behavior of high performance concrete was conducted by Zia et al. at North Carolina State University. The concrete specimens referred to as Very High Strength show 28-day compressive strengths ranging

from 8,080 to 13,420 psi (55.7 to 92.5 MPa). Based on Zia et al.'s research findings, the test results correlate well with the ACI 318 equation for the elastic modulus, which is similar to the AASHTO LRFD. Zia et al. (1993) found that the equation in ACI 363R, developed by Carasquillo et al. (1981), underestimates the measured elastic modulus. For the modulus of rupture, they found that at the design age, the ratio of the observed value to the value predicted by ACI 318 is 1.06 for concrete made with fly ash and 1.15 for concrete made with silica fume. In a comparison of the modulus rupture between the measured values and those predicted by ACI 363R, the ratio is as low as 0.68.

2.2.5 Mokhtarzadeh and French (2000)

More recent research has been conducted by Mokhtarzadeh and French (2000). Their research included extensive test results and predictions regarding the material properties for HSC. They conducted tests using 98 mixtures with compressive strengths ranging from 6,000 to 19,500 psi (41.4 to 135 MPa) for the modulus of elasticity and 280 modulus rupture beams made from 90 HSC mixtures with compressive strengths ranging from 7,500 to 14,630 psi (51.7 to 101 MPa), including heat-cured and moist-cured conditions. Their data showed that the ACI 318-99 equation overestimates the elastic modulus of HSC, while the ACI 363R-92 equation provides a more reasonable prediction of the elastic modulus for moist-cured specimens and slightly overestimates heat-cured test results. For the modulus of rupture, Mokhtarzadeh and French found that values measured for the moist-cured specimens are adequately predicted by the ACI 363R-92 equation. Values from the heat-cured specimens fall in between the values predicted by the ACI 363R-92 and ACI 318-99 equations. The authors proposed a new relationship for the modulus of rupture that uses a coefficient of 9.3 in lieu of the 7.5 in the ACI 318 equation.

2.3 STRESS BLOCK PARAMETERS

The equivalent rectangular stress block has been widely used to determine the ultimate flexural strength of reinforced and prestressed beams and columns. Through the application of ultimate strength design theory, stress block parameters have been developed to make equivalent rectangular stress blocks that can simplify the actual stress distribution. The proposed stress block by many researches are given in Appendix A. This section presents major findings in the use of stress block parameters for predicting the ultimate flexural strength.

2.3.1 Mattock et al. (1961)

The ACI 318 and AASHTO LRFD specifications regarding the use of stress block parameters to compute flexural strength were originally developed by Mattock et al. (1961). The Mattock research used studies previously conducted by Whiney (1937) and Hognestad et al. (1995) as reference. Mattock et al. suggested the use of stress block parameters, α_1 and β_1, to determine ultimate strength and α_1 is taken as 0.85 of the cylinder strength; β_1 is taken as 0.85 for concrete cylinder strength up to 4,000 psi (28 MPa); and thereafter is reduced by 0.05 for each 1,000 psi of strength in excess of 4,000 psi. Based on design examples for bending and compression, they concluded that the proposed stress block parameters allow sufficient accuracy of the prediction of ultimate strength in bending and compression.

2.3.2 Nedderman (1973)

In Nedderman's research (1973), plain concrete columns with compressive strengths up to 14,000 (98 MPa) were tested under eccentric loading conditions. Nedderman suggests that the depth of the stress block, β_1 in ACI318 (ACI 318, 1971), becomes an unrealistic value at a compressive concrete strength of 21,000 psi (147 MPa). This research also proposes the lower limits of β_1 to be 0.7 with a compressive concrete strength higher than 7,000 psi (49 MPa).

2.3.3 Ibrahim et al. (1996, 1997)

In the Ibrahim research, 20 HSC columns up to 14,500 psi (100 MPa) and UHSC with the compressive concrete strength over 14,500 psi were tested that incorporates concrete strength, confinement steel, and the shape of the compression zone. The test specimens consisted of fourteen C-shaped sections with a rectangular cross-section and six C-shaped sections with a triangular section. A better understanding of the flexural behavior of HSC and UHSC sections without confinement or with less confinement than required in seismic regions was also sought in this test. The Ibrahim study concluded that the ACI stress block parameters (ACI 318, 1989) overestimate the moment capacity of HSC and UHSC columns in compression. The researchers proposed new stress block parameters, as follows:

$$a_1 = 0.85 - \frac{f_c'}{800} \geq 0.725 \qquad f_c' \text{ (MPa) and} \qquad \textbf{Equation 2-11}$$

$$b_1 = 0.95 - \frac{f_c'}{400} \geq 0.70 \qquad f_c' \text{ (MPa).} \qquad \textbf{Equation 2-12}$$

2.4 PRESTRESS LOSSES

Concrete is a time-dependent material. In particular, concrete experiences creep under a sustained load and experiences shrinkage due to changes in moisture content. These physical changes increase over time. The prestress losses due to concrete creep and shrinkage result in the loss of compressive force onto the concrete. Ngab et al. (1981) measured less creep and slightly more shrinkage of HSC in comparison to NSC. The creep coefficient for HSC was 50 to 70 percent that of NSC. In a similar study, Nilson (1985) found that the ultimate creep coefficient for HSC is much less than that of NSC. This section describes findings regarding the prestress losses of full-size prestressed girders with HSC.

2.4.1 Roller et al. (1995)

A project undertaken in Louisiana investigated prestress losses in HSC girders. Two bulb-tee sections, 70 ft. (21.3 m) long and 54 in. (1372 mm) deep and designed according to AASHTO standard specifications (AASHTO 1992), were tested for long-term study. The design compressive strength at 28 days for the girders' concrete and releasing strength was 10,000 psi (69MPa) and 6000 psi (41 MPa), respectively. The concrete strain due to prestress losses of the girders was measured using internal Carlson strain meters under the full design dead load for 18 months. Roller et al. concluded that concrete strains measured at 28 days indicate that prestress losses are significantly less that the losses calculated using the provisions found in the AASHTO standard specifications.

2.4.2 Tadros (2003)

A more recent published study, National Cooperative Highway Research Program (NCHRP) Report 496 by Tadros (2003), developed design guidelines for estimating prestress losses in

pretensioned HSC. Tadros' research included a review of the extensive relevant literature to determine the applicable range of concrete strengths for the AASHTO (2003) provisions for estimating prestress losses in pretensioned concrete bridge girders. Based on this information, Tadros investigated the affecting factors, such as material properties, curing, exposure, and loading conditions. He concluded that the AASHTO LRFD (2003) refined method overestimates creep because it ignores the reduction in the creep coefficient associated with the increase in concrete strength. Tadros proposed new equations for each parameter to calculate the creep coefficient and shrinkage of HSC. His research results are included in the current AASHTO LRFD specifications (2004).

2.4.3 Waldron (2004)

Comprehensive research for prestress losses of HSC was conducted by Waldron (2004). Comparisons between measured and calculated prestress losses were made using AASHTO LRFD (1998) refined and lump sum methods, the AASHTO standard specifications, PCI-1975, PCI BDM, and NCHRP Report 469. This research draws some conclusions for estimating prestress losses. The methods for estimating prestress losses presented in the AASHTO Standard Specification (AASHTO 1996) and LRFD Specification (AASHTO 1998) overestimate the measured total losses for each set of girders by 18 percent (5 ksi) to 98 percent (27 ksi). The NCHRP Report 496 refined and approximate methods for estimating prestress losses predict within ±18 percent for the normal-weight HPC and over-predict the measured total losses of the light-weight HPC by less than 22 percent (8 ksi). Consequently, the NCHRP Report 496 refined the methods for estimating prestress losses. They recommended for estimating the prestress losses at the end of the service life for girders with normal-weight HPC.

2.5 FLEXURAL BEHAVIOR OF GIRDERS WITH HIGH STRENGTH CONCRETE

The principle for determining flexural response has been well established by using equilibrium of force and strain compatibility conditions. As described in the literature, due to the different material characteristics of HSC, as compared to conventional strength concrete, the flexural behavior, including prestress losses, transfer length, load-deflection relationship, camber, ultimate flexural strength, and cracking load may be affected. This section describes major findings regarding the flexural response for full-size prestressed girders with HSC.

2.5.1 Shin et al. (1990)

Shin, Kamara and Ghosh (1990) tested three sets of 12 specimens with compressive strengths of 4, 12, and 15 ksi (27.6, 82.7 and 103.4 MPa). Although the specimens were clearly reinforced as columns, they were cast horizontally and cured under field conditions. The specimens were tested in flexure under two-point loading conditions. This research concluded that the equivalent rectangular stress block parameters addressed in ACI318-83 are appropriate for determining the flexural strength of HSC beams to 15 ksi (103.4MPa). Shin et al. also confirmed that there is no need for change in the ACI procedure for computing flexural strength. However, the ultimate strain of HSC is recommended to be 0.0025 as a lower bound instead of 0.003.

2.5.2 Bruce and Martin (1994)

Bruce and Martin (1994) investigated the behavior of prestressed concrete girders with HSC under sponsorship of the Louisiana Transportation Research Center. This research focused on the flexure and shear behaviors of composite girders under static and fatigue loading conditions. Four full-size prestress bulb-tee girders, 70 ft (21.3 m) long and 54 in. (1372 mm)

deep and designed according to AASHTO standard specifications (AASHTO 1992), were fabricated. Three of them had a 9 ½ in. (240 mm) thick and 10 ft. (3.05 m) wide deck. Each girder specimen had a 28-day compressive concrete strength of 10,000 psi (69 MPa). Bruce and Martin concluded that the AASHTO standard specification (AASHTO 1992) is conservatively applicable for members with concrete compressive strengths up to 10,000 psi (69 MPa). Based on the findings of this research, HSC has potential benefits for highway bridge structures, including wider girder spacing and lower prestress losses. Bruce and Martin recommended the use of HSC for highway bridge structures.

2.5.3 Ahlborn, French, and Shield (2000)

Ahlborn et al. (2000) investigated the long-term and flexural behavior of HSC prestressed bridge girders under the sponsorship of the Minnesota Department of Transportation. This study began with an extensive parametric study to better understand the limitations of using HSC in prestressed bridge girder sections in Minnesota. Two long-span, high-strength, composite, prestressed bridge girders (MNDOT 45M) were fabricated. Test specimens had a 28-day concrete compressive strength that exceeded 11,100 psi (77Mpa) for girders and 4,500 psi (31 MPa) for a composite deck. This research focused on the structural behavior and the adequacy of AASHTO standard provisions (AASHTO 1993), including prestress losses, transfer length, cyclic load response and ultimate flexural strength. Ahlborn et al. suggest that the prediction of prestress losses using the AASHTO provisions ignores the concrete stress prior to release as well as overestimates the elastic modulus of HSC and creep and shrinkage. Their research indicates that the prediction of the ultimate flexural strength using AASHTO standard specifications is conservative.

3 EXPERIMENTAL PROGRAM

3.1 INTRODUCTION

This experimental research program was conducted to evaluate the flexural behavior of prestressed composite girders with high strength concrete (HSC). A total of nine prestressed AASHTO girders were fabricated and tested under static loading conditions to determine the different limit states behavior including ultimate and mode of failure of HSC girders. Each of the AASHTO girders was instrumented with internal strain gauges to measure prestress loss. Concrete cylinders for each of the AASHTO girders were also cast to determine material properties. This section will provide details related to design considerations, fabrication procedure, test set-up, loading scheme, instrumentation, and test descriptions.

3.2 DESIGN OF THE TEST SPECIMENS

A total of nine AASHTO girders with HSC were designed and tested to evaluate their flexural response. All specimens for this research program were designed in accordance with two specific design considerations.

The first design consideration is the concrete strength because the application of current code provisions limits the use of HSC over 10,000 psi. Therefore, three different nominal design concrete strengths, 10,000, 14,000, and 18,000 psi, were considered so that the current LRFD provisions can be extended up to 18,000 psi compressive strength for reinforced and prestressed concrete.

The second design consideration is the location of the compression zone of the specimens in the flexure. Design of the girders allows three configurations of the compressive zone. The first configuration of the compressive zone is located within the top flange of the girder without the deck slab. Therefore, the strength of the concrete of the compressive zone is controlled by the HSC. The second configuration allows the neutral axis to be located within the top flange of the girder with the deck slab cast with NSC; therefore, the strength within the compressive zone is controlled by the HSC used in the girder and the normal strength concrete of the deck slab. The third type of configuration allows the neutral axis to be located within the cast-in-place deck; therefore, the flexural strength is controlled entirely by the NSC.

Depending on the strength of the concrete and the location of the compression zone, the required number of prestressing strands were 16, 18 and 20 strands for the nominal design compressive strength concrete of 10,000, 14,000, and 18,000 psi (69 to 124 MPa), respectively. All strands were straight. The design of the nine AASHTO Type II prestressed concrete girders were finalized using three design concrete strengths. Table 3.1 presents a summary and identification of each girder specimen. Typical AASHTO Type II girder sections, each shown with the order and location of strands, are given in Figure 3-1.

All girders are designed to avoid premature failure due to shear and bond slippage before flexural failure. A preliminary design of this reinforcement is based on the AASHTO LRFD specifications. Each girder employed No. 4 stirrups at a spacing of 3 in. near the end blocks and every 6 in. along the entire length of the girder. More information about the reinforcements of the test specimens are presented in Appendix B.

Table 3.1 Detailed Design of the Test Specimens

Girder				
Design Strength		10 ksi (69 Mpa)	14 ksi (97 Mpa)	18 ksi (124 Mpa)
Section		AASHTO Type II	AASHTO Type II	AASHTO Type II
Total Length		41 ft. (12.5 m)	41 ft. (12.5 m)	41 ft. (12.5 m)
Clear Span Length		40 ft. (12.2 m)	40 ft. (12.2 m)	40 ft. (12.2 m)
Strand (1/2" f 270 k Low Relaxation)				
Required Number		16	18	20
Pattern		Straight	Straight	Straight
Deck Slab				
Design Strength		4 ksi (28 Mpa)	4 ksi (28 Mpa)	4 ksi (28 Mpa)
Thickness		8 in.	8 in.	8 in.
Identification				
Width of the deck slab	None	10 PS - N	14 PS - N	18 PS - N
	1 ft.	10 PS - 1 S	14 PS - 1 S	18 PS - 1 S
	5 ft.	10 PS - 5 S	14 PS - 5 S	18 PS - 5 S

*1 ft. = 30.48cm; 1 ksi = 6.9 Mpa

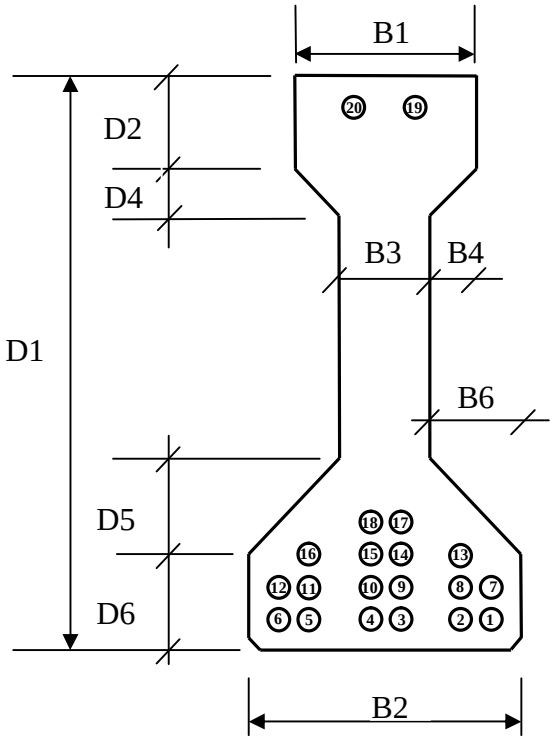

Dimensions

Type	AASHTO TYPE II
D1	36.0 (in.)
D2	6.0
D4	3.0
D5	6.0
D6	6.0
B1	12.0
B2	18.0
B3	6.0
B4	3.0
B6	6.0

Properties

Area	369 $in.^2$
y_{bottom}	15.83 in.
Inertia	50,980 $in.^4$
Weight	0.384 kip/ft.

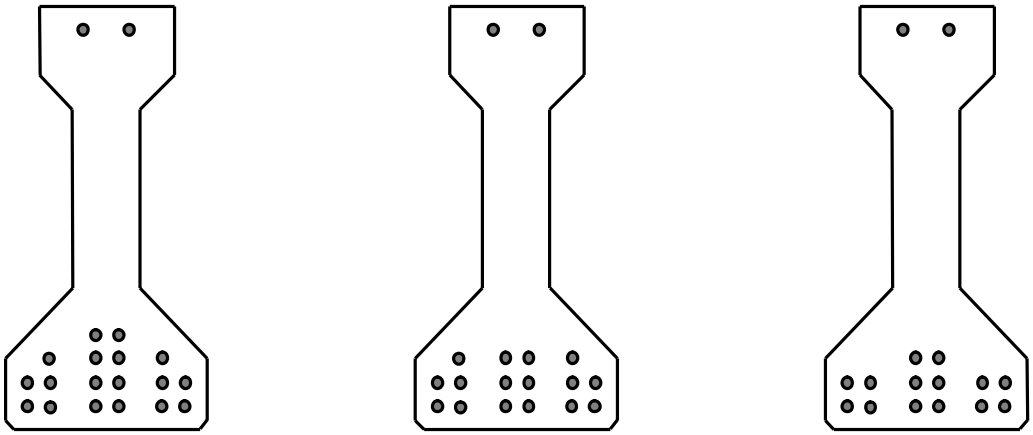

For 18 PS-5 S, 1 S, and N For 14 PS-5 S, 1 S, and N For 10 PS-5 S, 1 S, and N

Figure 3-1 Cross-section showing prestressing strand configurations

3.3 FABRICATION OF TEST SPECIMENS

Fabrication of the composite girder specimens with variable deck widths consists of two steps. First, the AASHTO girders were fabricated at a pre-cast, prestress plant. Second, the cast-in-place decks were cast on the AASHTO girders at the CFL. This section presents a description of the fabrication of the test specimens.

3.3.1 AASHTO Girder Specimens

A total of nine prestressed concrete girders were fabricated by the Standard Concrete Products prestressing plant in Savannah, GA. Construction of the prestressed girders can be summarized in the following event, as presented in Table 3.2. All load cells and strain gauges were attached before tensioning of the prestressing strands. A total of 20 strands were placed on the prestressing bed simultaneously. The strands for the nine girder specimens were tensioned individually, as shown in Figure 3-2 (b). Each prestressing strand was tensioned to 75 percent of its ultimate strength for a total load of 31 kips. Then, reinforcement and formwork were positioned. The casting and curing of the girders were completed following the typical procedure used by Standard Concrete Products. Figure 3-2 (a) and (c) show elevation views of the prestressing bed for the nine girders and the prestressing procedure, respectively.

Table 3.2 Construction Sequence Summary

Date	Time	Event
July 15 -17, 2005	7:00 am - 5:00 pm	Load cell and strain gauge installation
July 18, 2005	Morning	Tensioning 20 strands
	Afternoon (4:00 - 6:00 pm)	Casting 18 ksi design strength
July 19, 2005	Morning	Releasing 2 strands
	Afternoon (4:00 - 6:00 pm)	Casting 14 ksi design strength
July 20, 2005	Morning	Releasing 2 strands
	Afternoon	None
July 21, 2005	Morning (9:00 - 11:00 am)	Casting 10 ksi design strength
July 22, 2005	Morning (10:00 am - 1:00 pm)	De-molding and releasing remaining strands

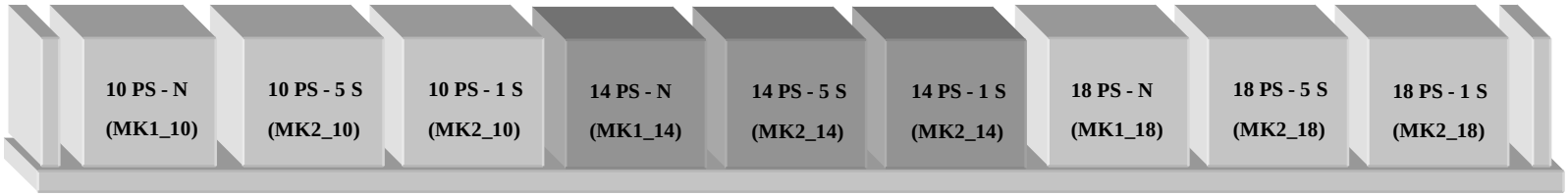

Dead End (Anchored End)
(WEST)

Live End (Jacking End)
(EAST)

(a)



(b)



(c)

Figure 3-2 Prestressing bed: a) Elevation schematic view of prestressing bed, b) Strand lay-out, c) Pretensioning

After applying prestressing force to the strands and installing the instrumentations, steel reinforcements were placed and the formwork was positioned. The three girders for each design concrete strength were cast using four batches of the same concrete mix. In order to determine the material property of each AASHTO girder, 15 concrete cylinders, 4 x 8 in. for the modulus of elasticity and compressive strength and nine 6 x 6 x 20 in. beams for the modulus of rupture, were made from each of the first three batches of concrete and cured next to the girders prior to shipping to the CFL, then air-cured in the laboratory. Additionally, the concrete supplier cast ten 4 x 8 in. concrete cylinders from each batch of mix for determining compressive concrete strength. The supplier provided the results of the compressive concrete strength at 1, 7, 14, 28, and 56 days.

The girders were vibrated using a internal vibrator while the concrete was placed. The top surface of the girders was intentionally roughened. After the girders for each design concrete strength were cast, they were then covered with burlap and plastic, and a water hose was placed on top of the girders for curing. Pictures of this procedure are provided in Figure 3-3.

As seen in Table 3.2, there are three casting schedules for each design concrete strength. After casting for the 18,000 psi (124 MPa) design compressive strength, two strands, the 18th and 17th (see Figure 3-1), were released and removed. After casting for the 14,000 psi (97 MPa) design compressive strength, two more strands, the 13th and 16th (see Figure 3-1), were also released and removed. Finally, 16 strands remained in the prestressing bed. Before their release, the required compressive strength was tested and provided by the concrete supplier. Most of the girders reached the required release strength after 1 day. All strands were flame cut at both ends of the AASHTO girder. Strain data, obtained from installed weldable strain

gauges on the selected strands, were recorded before and after release, and the end slippage was measured at specified points, as will be described in later sections.



(a) Reinforcing



(b) Casting concrete



(c) Covering with burlap



(d) Curing

Figure 3-3 Sequence of girder fabrication

After the nine AASHTO Type II girders were fabricated, they were stored in the plants. Approximately 56 days after fabrication, on September 19, 2005, three girders for the 10,000 psi design strength concrete were shipped from the plant to the CFL for testing. The others also were shipped to the CFL within 3 months after fabrication. They were stored inside the laboratory.

3.3.2 Cast-in-place Deck

Approximately three months after girder fabrication, deck slabs (three 1 ft. wide and three 5ft. wide) were cast on six AASHTO girders at the CFL. The width of the deck slab was determined based on the design consideration. The 28-day nominal design compressive strength of the cast-in-place deck was specified as 4,000 psi (28 MPa). Other details, including the deck slab dimensions and reinforcement specifications for the 5 ft. and 1 ft. wide deck slabs, are presented in Appendix C.

A single 5 ft. wide cast-in-place deck was cast each week for three consecutive weeks, and three 1 ft. wide cast-in-place decks were cast at the same time during the following week. Concrete was provided by Thomas Concrete of Raleigh, NC. The measured concrete slump was 3 to 4 in. at the time of casting. The concrete deck slabs were covered with plastic for 1 day, after which the forms were removed and the beams were air cured. The completed formwork for 1 ft. and 5 ft. wide slabs is shown in Figure 3-4. Figure 3-4 (a) shows two AASHTO girders that were used temporarily to support the deck concrete.

Internal strain gauges were embedded into the deck slabs during the fabrication process. Detailed information about internal gauges can be found in the Section 3.4.



a) 5 ft. wide deck slab



b) 1ft. wide deck slab

Figure 3-4 Formwork for the 5 ft. and 1 ft. wide deck slabs

3.4 INSTRUMENTATION

3.4.1 AASHTO Girder Specimens

Applied prestressing force, strain, elongation, and end slippage, were measured during the fabrication process. Specifically, load cells were used to verify the applied load on the strands at the dead end of the prestressing bed. The locations of the load cells corresponds to the strands are shown in Figure 3-5 (a). Four load cells were installed on the bottom-most strands. A portable indicator, shown in Figure 3-5 (b), was used to measure the load indicated by the load cells. The bearing plate was used only for the two outside strands due to the limited space available, as shown in Figure 3-5 (c).

After the installation of the load cells, the strands were lightly tensioned to a load of 4 kips and then fully tensioned up to 31 kips. The load cells measured the applied force after jacking, during casting, curing, and at the release of the strands. Data obtained from the load cells are given in Table 3.3.

In addition to the use of load cells, the applied prestressing force was verified by measuring the elongation of the prestressing strands. After the strands were fully tensioned up to a specified prestressing force, the elongation of each prestressing strand was measured. For a comparison between applied force and computed force, 0.153 $in.^2$ for the area of the prestressing strand, 29,000 ksi for the modulus, and 5061 in. for the prestressing bed length were used to calculate the prestressing force. Detailed results for elongation are given in Table 3.4.

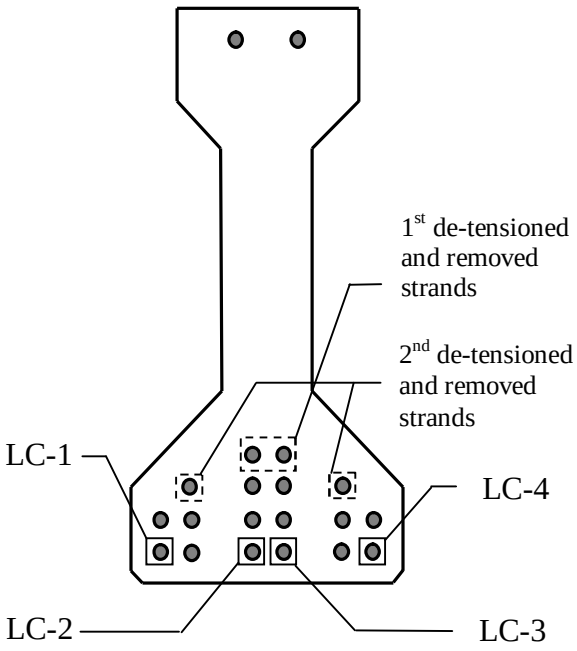

a) Location of load cells (LC) and of de-tensioned strands

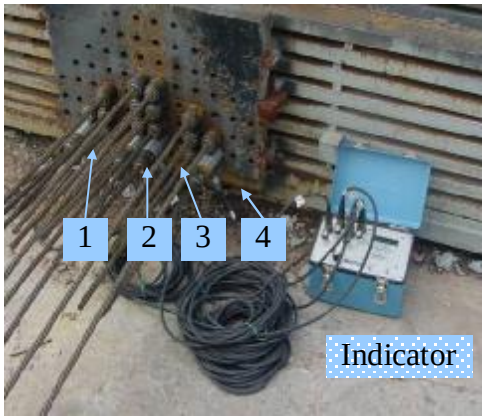

b) Installed load cell and indicator

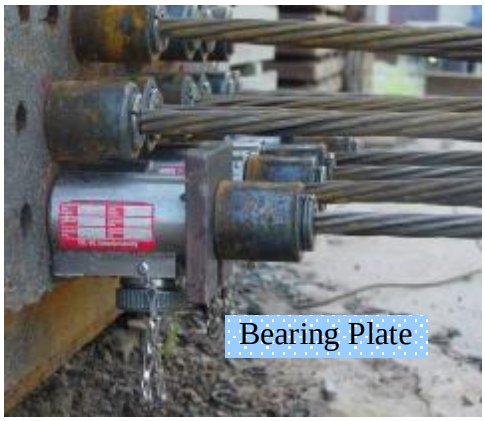

c) Bearing plate

Figure 3-5 Load cell installation

Table 3.3 Measured Data from Load Cells

Date (2005)	Time		Load Cell 1	2	3	4	Etc.
July 18	Jacking	1st reading (P.G. = 4 kips)	3.5	3.5	3.7	3.4	
		2nd reading (P.G. = 10 kips)	-	-	-	10.4	
		3rd reading (P.G. = 20 kips)	-	-	-	19.8	
		4th reading (P.G. = 30 kips)	30.5	30.9	29.5	30.8	
	After 18 ksi casting		30.7	30.8	29.7	30.8	
July 19	Morning		30.8	31.0	29.8	31.1	1st de-tensioned, removed strands
	After 14 ksi casting		30.8	30.9	29.6	30.9	
July 20	Morning		31.1	31.3	29.9	31.3	2nd de-tensioned, removed strands
	Afternoon		31.3	31.4	30	31.3	
July 21	Morning		32.0	32.3	30.9	31.3	
	After 10 ksi casting		30.4	30.6	29.3	30.5	
July 22	Morning		33.0	33.1	31.8	33.3	
	Afternoon		32.8	33.0	31.6	33.1	
	At release		-0.1	-0.1	-0.2	0	Releasing

Table 3.4 Order of Prestressing Strands and Elongation

Strand #	Applied force (lb.)	Measured Elongation (in.)	Computed force (lb.)	Applied/Com.
1	31600	30 5/8	26849	1.18
2	31600	31 1/2	27616	1.14
3	31600	30 3/8	26630	1.19
4	31600	30 1/8	26411	1.20
5	31600	31	27178	1.16
6	31600	31	27178	1.16
7	31600	30 7/8	27068	1.17
8	31600	31 3/8	27507	1.15
9	31600	31 7/8	27945	1.13
10	31600	31 1/4	27397	1.15
11	31600	31	27178	1.16
12	31600	31 1/4	27397	1.15
13	31600	31	27178	1.16
14	31600	30 1/4	26520	1.19
15	31600	31 7/8	27945	1.13
16	31600	31	27178	1.16
17	31600	31 3/4	27835	1.14
18	31600	31 7/8	27945	1.13
19	31600	30 3/4	26959	1.17
20	31600	30 3/8	26630	1.19

During the construction of the girder specimens, as indicated in Table 3.2, two internal weldable strain gauges for each girder were attached to the selected bottom-most strands of each girder near the mid-span prior to pretensioning the strands. These gauges were used to indicate the strain of the embedded strands during the entire testing process. Welded strain gauges provide prestress losses and the strain of the strand during flexural testing. The weldable gauges were located in accordance with three phases. These locations, as shown in Figure 3-6, were duplicated for each girder according to each girder's design strength of concrete. These gauges were located approximately at the middle of the span.

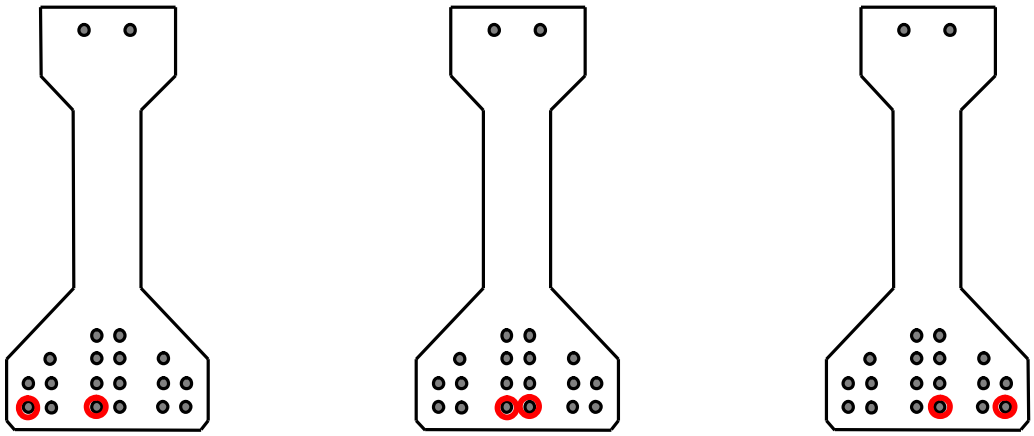

For 18 PS - 1 S For 18 PS - 5 S For 18 PS - N

Figure 3-6 Locations of weldable strain gauges

To install the weldable strain gauges, several steps were taken, as given in Figure 3-7. First, the surfaces of the strands were polished with 180 grit sand paper and cleaned with acetone. Second, the strain gauges were welded with a 10-12 watt-second spot welder with a 0.8 mm diameter probe. Finally, the welded gauges were covered with friction tape for protection against damage during the casting process.



a) Welder



b) Weldable strain gauge

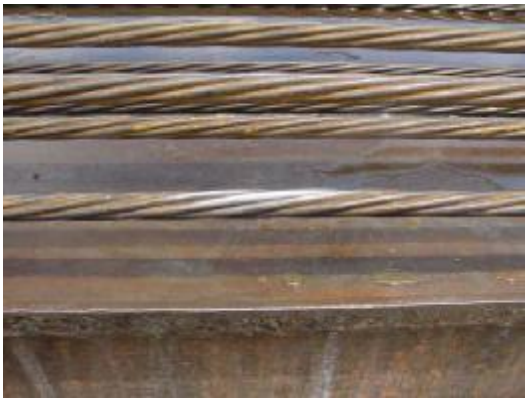

c) Surface preparation



d) After installation

Figure 3-7 Installation of weldable strain gauge

3.4.2 Cast-in-place Deck

The deck slab was instrumented by strain gauges attached to #3 reinforcing bars located near the mid-span of the girder, parallel to the top layer of the longitudinal reinforcement. These gauges were used to measure the strain at the level of the top steel reinforcement and, consequently, the concrete at the same level of the deck slab. Typical locations of the instrumented individual bars for each specimen with various deck widths are shown in Figure 3-8.

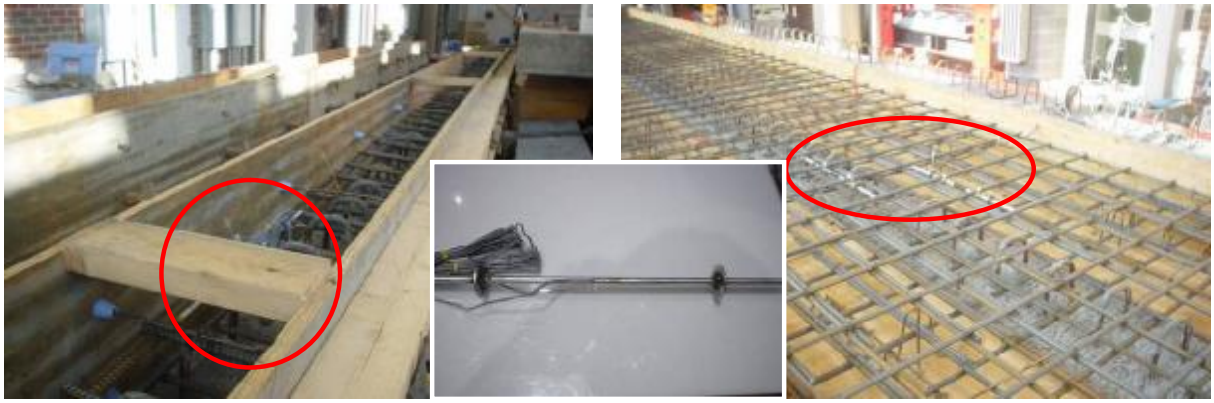

Figure 3-8 Installation of the strain gauges attached to #3 steel rebar

3.5 MATERIAL PROPERTIES

3.5.1 Concrete Properties

All concrete mix designs were developed by the Standard Concrete Products prestressing plant using several lab batches to achieve the specified design compressive concrete strength. Representative concrete mix designs for each of the three target strengths are given in Table 3.5. As described in the section on fabrication of the girders, three concrete batches were used for three girders. The concrete mix design for each batch is given in Appendix D.

Table 3.5 Detailed Mix Design for Girder Specimens

NCHRP12-64 HSC Mix			
Design compressive strength (psi)	10,000	14,000	18,000
Cement (lbs.)	670	703	890
Fly ash (lbs.)	150	192	180
Microsilica (lbs.)	50	75	75
#67 Granite (lbs.)	1727	1700	1700
Concrete sand (river) (lbs.)	1100	1098	917
Water (lbs.)	280	250	265
Recover (hydration stabilizer) (oz.)	26	50	50
ADVA 170 (water reducer) (oz.)	98	125	135
W/cementitious material	0.32	0.26	0.23

As described earlier, one batch of concrete was insufficient for a single girder. Therefore, 15 4 x 8 in. concrete cylinders for measuring the modulus of elasticity and compressive strength, and nine 6 x 6 x 20 in. beams for measuring the modulus of rupture were made from each of the first three batches of concrete and cured next to the girder. Additionally, the concrete supplier made ten 4 x 8 in. concrete cylinders for each batch mix for measuring compressive strength. Table 3.6 shows the concrete properties for the first three batches for each design mix. The unit weight for the concrete used in the girders indicates that the concrete is normal-weight.

Table 3.6 Concrete Properties for Girder Specimens

Design Strength	Mix Design	Batch	Con. Temp. (^oF)	% Air	Slump (in.)	Unit Weight (pcf)
10 ksi	MIX 1 P	1	91	3	8 1/2"	144.6
		3	82	3.5	8 3/4"	145.5
14 ksi	MIX 2 P	1	98	3.2	6 3/4"	148.5
		2	100	2.9	8.75"	-
		3	97	2.6	10"	148.9
18 ksi	MIX 3 P	1	100	2.98	7 1/2"	-
		2	98	1.48	10 1/2"	-
		3	100	2.78	6 1/4"	-

The decks for the three AASHTO girders with the 1 ft. wide deck slab and the 5 ft. wide deck slab were cast at the CFL. The width of the deck slab was determined based on the design consideration. The 28-day nominal design compressive strength of the deck concrete was specified as 4,000 psi (28 MPa). The detailed mix design for the deck concrete is given in Table 3.7. Concrete properties for the deck are given in Table 3.8.

Table 3.7 Concrete Mix Design for Deck Slab

	5 ft. wide deck slab	1 ft. wide deck slab
Deck cast date	10-20-2005	11-10-2005
Amount ($yd.^3$)	5.5	3.5
#67 Stone (lb.)	4978	6335
River Sand (lb.)	3742	4740
Cement (lb.)	1628	2072
Recycle water (gal.)	106	45
200 N (oz.)	47	60

Table 3.8 Concrete Properties for Cast-in-place Deck

Identification	Air Content (%)	Slump (in.)	Unit Weight (pcf)
10 PS – 5 S	2.4	3.5	149.87
14 PS – 5 S	1.7	3	149.36
18 PS – 5 S	2	4 3/4	154.63
10, 14, and 18 PS – 1 S	1.3	4 1/2	149.84

3.5.2 Compressive Strength, Elastic Modulus, and Modulus of Rupture

Three concrete cylinders for compressive strength and elastic modulus were tested according to ASTM C39-03 specifications. A review of the studies related to end treatments shows that

grinding the cylinders provides the highest strength and the lowest coefficient of variation Zia et al. (1987). Therefore, all of the cylinders were first prepared by grinding both end surfaces to remove irregularities in the surfaces and to ensure that the ends were perpendicular to the sides of the cylinders, as shown in Figure 3-9 (a). As mentioned earlier, the girder producers also provided cylinders for measuring the compressive strength of the concrete in each girder at 1, 7, 14, 28, 56 days. Test cylinders were grinded on the both end surfaces using a hand grinder, as shown in Figure 3-9 (b). Test results for the compressive strength are given in Appendix E.



a) Grinder b) Hand grinder

Figure 3-9 Specimen preparation and test set-up for elastic modulus

The concrete material property tests, that is, the elastic modulus and modulus of rupture tests, were conducted at the concrete age of 28 and 56 days in the CFL. Tested cylinders were placed in air-cured conditions at the CFL. Therefore, the compressive strength is slightly different between the data provided by the concrete supplier and the data obtained from the CFL. All of the tests for the determination of material properties were conducted in accordance with ASTM designations. Each value represents the average of two cylinders

from one batch of one design strength. The test set-up for the elastic modulus and modulus of rupture is shown in Figure 3-10 (a) and (b), respectively.



a) Cylinder test set-up

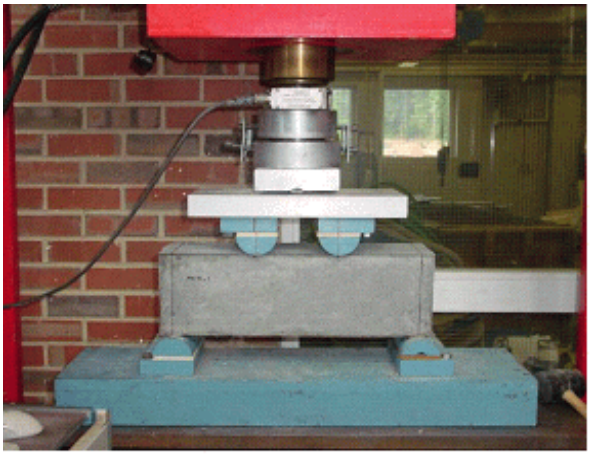

b) Beam test set-up

Figure 3-10 Test set-up for elastic modulus and modulus of rupture

The elastic modulus from the 4 x 8 in. concrete cylinders was determined in accordance with ASTM C496. Firstly, one of the three cylinders was tested solely to determine the compressive strength. Subsequently, the remaining two cylinders from each specified day were used to determine the elastic modulus and then tested to failure to determine the compressive strength. Strains were determined using four linear motion transducers (LMTs) attached to two fixed rings. The LMTs were used to measure the axial deformation. The collected data were used to calculate the elastic modulus. The apparatus consists of two aluminum rings with set screws that attach to the cylinder. The rings were initially joined by three aluminum bars to maintain the specified gauge length used to determine the axial strains from the recorded deformation. The elastic modulus test consisted of three loading cycles. The first loading cycle, which was only intended to seat the gauges and the specimen,

began at zero applied load and unloaded at 40 percent of the expected capacity of the specimen. The second and third loading cycles were applied up to 40 percent of the expected capacity of the specimen. Finally, the specimen was loaded to failure to obtain the compressive strength. From the measured average strain under twice loading phase, the elastic modulus was determined.

The modulus of rupture tests were carried out using the 6 x 6 x 20 in. beam specimens. The specimens were tested under four-point loading in accordance with AASHTO T 97. A 90-kip hydraulic jack mounted inside a structural steel test frame was used to apply the load. A load cell was used to measure the applied load. A spherical head and a plate/roller assembly were located beneath the load cell to distribute the load evenly on the two loading points at the top surface of the specimen. The span length of the specimen was 18 in., and the spacing between supports and the nearest loading point as well as the space between the two loading points was 6 inches. The load was applied such that the stress at the extreme bottom surface of the specimen increased at an approximate rate of 150 psi/sec.

As indicated in Table 3.9, the average 28- and 56-day compressive concrete strength of each representative design mix reached the design strength except Mix 3P, which called for 18,000 psi (124 MPa) design compressive strength. However, a study of concrete shows that fly ash redistributes the pore size in the concrete. Capillary pores are better able to retain water, which can then be available for long-term hydration (Neville, 4th Edition). For this possibility of long-term hydration, the development of the compressive strength for each specimen at each test day could be expected.

As indicated in Table 3.10, the average 28-day compressive strength for the deck concrete reached the design strength ranging from 3450 to 5560 psi. The deck concrete is considered normal-strength concrete.

Table 3.9 Test Results for Material Properties

Mix Design	Concrete Age	f_c (psi)	E (ksi)	f_r (psi)
Mix 1P (10 ksi)	28 days	11430	5450	828
	56 days	11880	5750	n/a
Mix 2P (14 ksi)	28 days	12960	5430	813
	56 days	14020	5500	n/a
Mix 3P (18 ksi)	28 days	15870	6100	853
	56 days	16810	5590	n/a

( ) is the design concrete strength

Table 3.10 Compressive Strength Test for Deck Concrete

Specimen Identifications	f_c (psi) at 28 days	Average f_c (psi)
10 PS – 5 S	3880 3770 3680	3780
14 PS – 5 S	5150* 4900* 4910*	4990
18 PS – 5 S	3390 3500	3450
10, 14, and 18 PS-1 S	5570 5350 5760	5560

* Concrete cylinders were tested at 31 days.

As indicated, using fly ash in concrete mix results in the development of compressive concrete strength over longer time. Test results, as given in Table 3.11 for compressive strength, elastic modulus, and modulus of rupture, indicate that the compressive cylinder strengths of each AASHTO girder reached the design compressive strengths of 10,000, 14,000, and 18,000 psi, with the exception of girder 18 PS–1 S. These test results for compressive strength were expected due to the test results provided by the concrete supplier, as given in Appendix E.

Table 3.11 Material Property for Each AASHTO Girder Specimen

Specimens	Age (days)		f_c (psi)	E (ksi)	f_r (psi)
10 PS – 5 S	Girder	120	11490	5360	768
	Deck	29	3780	2690	-
14 PS – 5 S	Girder	143	16160	5560	711
	Deck	43	5340	3300	-
18 PS – 5 S	Girder	175	18060	5970	872
	Deck	67	3990	2660	-
10 PS – 1S	Girder	189	13190	5630	820
	Deck	77	5040	2770	-
14 PS- 1 S	Girder	184	15530	5440	751
	Deck	70	5040	2770	-
18 PS – 1S	Girder	199	14490	5150	680
	Deck	84	5040	2770	-
10 PS - N	Girder	222	11810	5540	820
14 PS - N	Girder	228	15660	5330	717
18 PS - N	Girder	232	18110	6020	706

3.5.3 Prestressing Strands

Prestressing strands typically used in the girder specimens were ½ in. in diameter, 7-wire, Grade 270, low relaxation strands. The material properties of the prestressing strands were provided by the supplier. The strength-strain relationship is given in Figure 3-11.

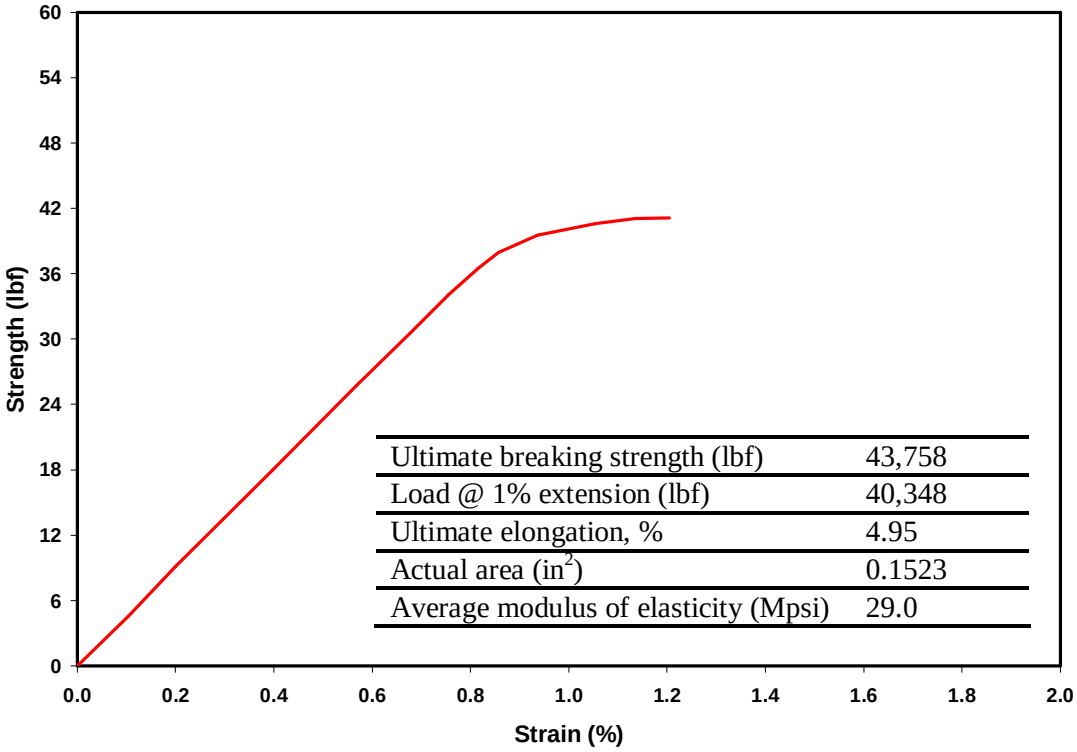

Figure 3-11 Material property for prestressing strand

3.6 FLEXURAL TEST DETAILS

3.6.1 Test Set-up and-Procedure

The test setup used for the flexural tests is schematically shown in Figure 3-12. Girders were simply supported with a steel plate above a neoprene pad. The load was commonly applied for all of the girders at two locations spaced 6 ft. at mid-span. Load was applied to the girders using a 440 kip MTS closed-loop actuator. The AASHTO girder specimens were loaded and unloaded using a stroke control at a rate of 0.1in./min. prior to the cracking of the girders and reloaded using a stroke control rate of 0.1in./min. up to the yielding of the prestressing strands and a stroke control rate of 0.25 in./min. after the prestressing strands yielded. Then, the specimens were loaded up to failure.

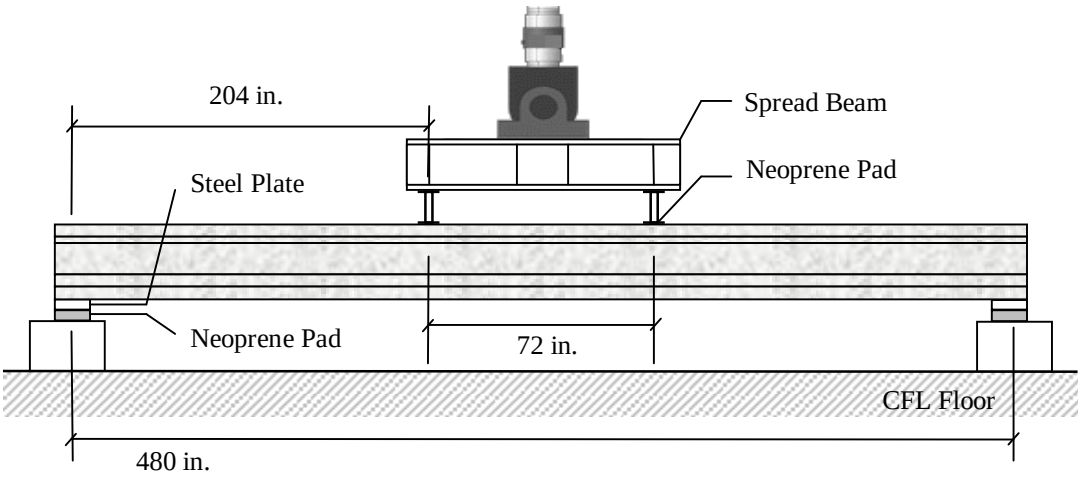

Figure 3-12 Test set-up schematic

The first test specimen, 10 PS–5 S, which is the 10 ksi girder with a 5 ft. wide slab, indicated the possibility of rotation of the specimens at failure due to local crushing of the concrete as

shown in Figure 3-13 (a). To prevent any instability in the test set-up, a frame was installed diagonally near the loading location. Figure 3-13 (b) indicates the supporting conditions with a 1 in. steel place above a 2 in. neoprene pad, respectively. Figure 3-13 (c) and (d) show the test set-up for the AASHTO girder specimens with 5 ft wide decks installed with and without the lateral frame, respectively. Additionally, Figure 3-13 (e) and (f) show the test set-up for AASHTO girder specimens with a 1ft wide deck and without a deck.



a) Local crushing at failure



b) Support conditions



c) Test set-up for girder with 5 ft. without lateral frame

Figure 3-13 Typical test set-up for nine AASHTO girder specimens



d) Test set-up for girder with 5 ft. with lateral frame



e) Test set-up for girder with 1 ft. deck with lateral frame

Figure 3-13 (continued) typical test set-up for nine AASHTO girder specimens



f) Test set-up for girder without deck with lateral frame

Figure 3-13 (continued) typical test set-up for nine AASHTO girder specimens

3.6.2 External Instrumentation

After placement on the supporting block, the girder specimens with the 1 ft. and 5 ft. wide deck slab and without the deck slab, were instrumented for measurement of displacements and strains at several locations along the beam.

3.6.2.1 Deflection Measurement Device

As shown in Figure 3-14, both string transducers and linear motion transducers (LMTs) were used to measure girder deflections at both ends, at the quarter-span location, at the loading

points, and at the mid-span of the girders. Two conventional linear transducers at the ends were used to measure the relative deflection between the concrete girder and the neoprene pad.

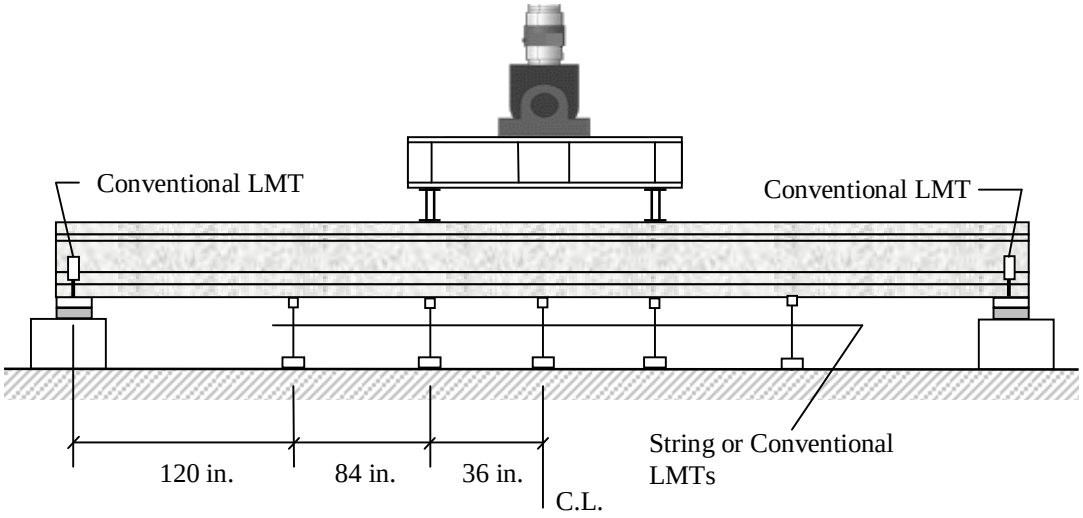

Figure 3-14 Location of LMTs to measure deflections

3.6.2.2 Strain Measurement Device

Strain measurement devices were placed on the top, bottom, and side surface of concrete girder to measure the strains at the various loading stage. Both electrical resistance strain gages and PI gages were installed on extreme top surface of concrete, and within constant moment zone. Additionally, PI gages were attached to the bottom and side surface of girders to obtain the strain profile at the given section. In particular, top surface instrumentations were used to determine the ultimate strain of HSC girder. For the composite AASHTO girder with a 5ft wide deck, Figure 3-15 shows the locations of both electric strain gages and PI gages. In the case of AASHTO girder with a 1ft wide deck and without deck, the width of deck is same with the flange width of AASHTO girder. The locations as shown in Figure

3-16 and Figure 3-17 for both electric strain gages and PI gages represents AASHTO girders with 1ft wide deck and without deck respectively. The locations for top and bottom surface for AASHTO girder without deck are duplicated as same as Figure 3-16 (a) and (b).

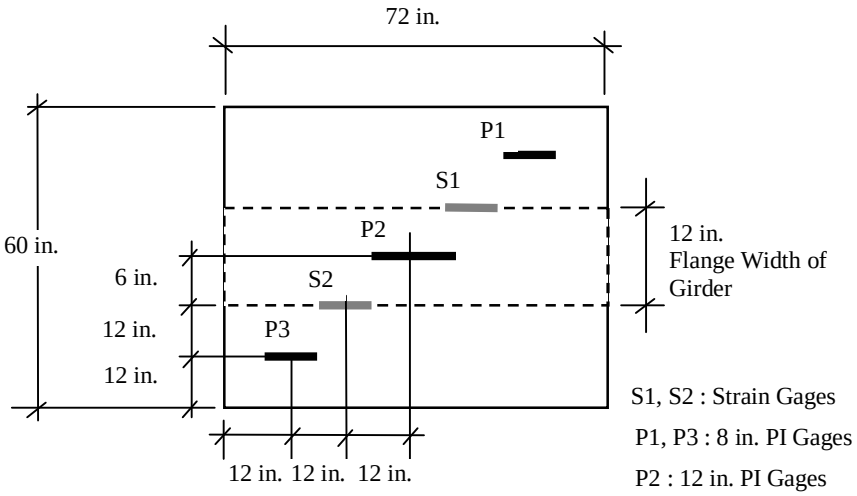

a) Top surface

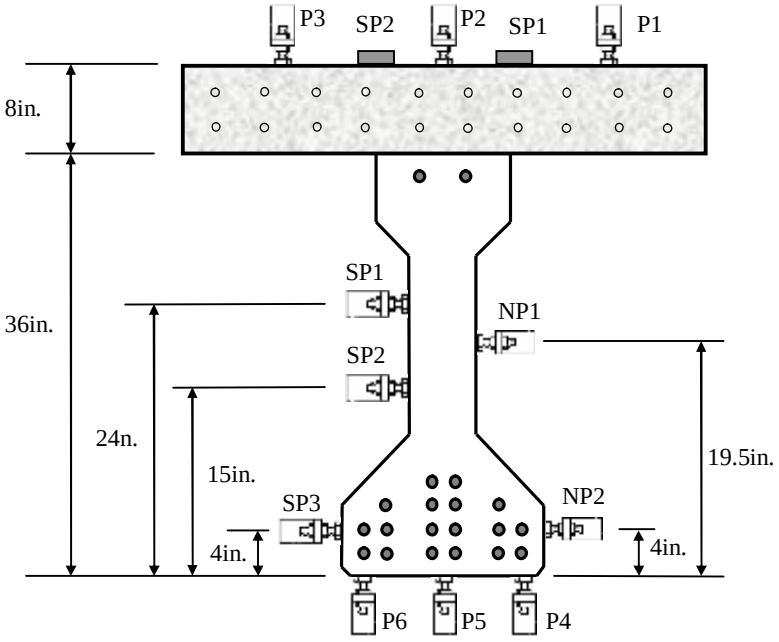

b) Cross section

Figure 3-15 Location of Strain and PI gages for 10PS – 5S, 14PS- 5S and 18PS-5S

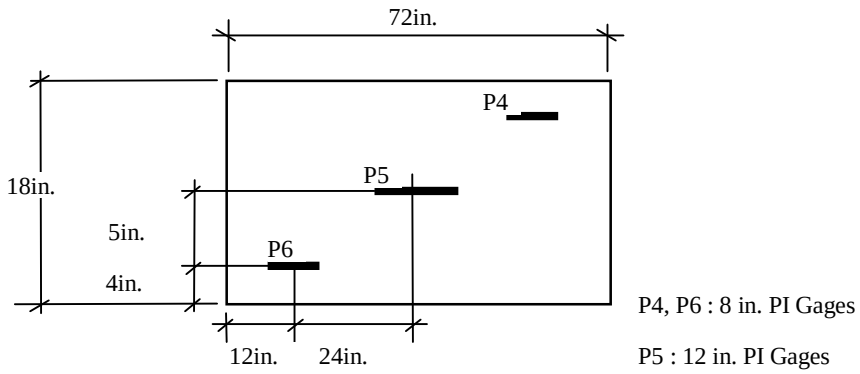

c) Bottom surface

Figure 3-15 (continued) Location of Strain and PI gages for 10PS-5S, 14PS–5S and 18PS-5S

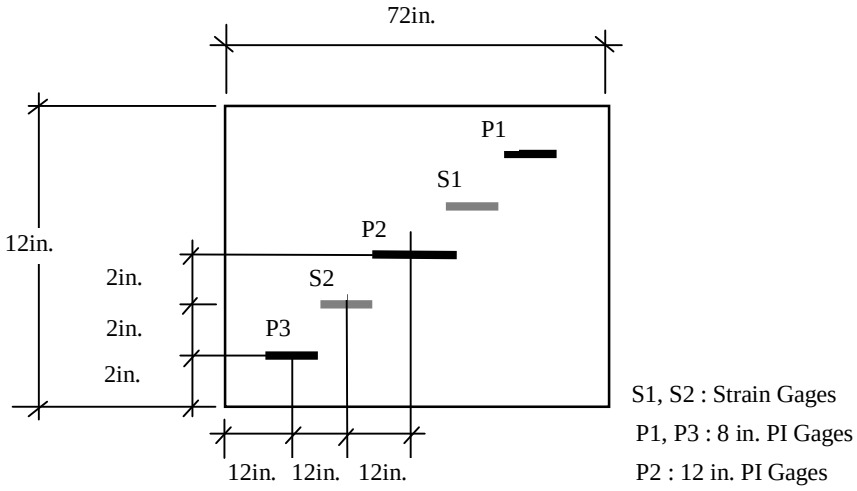

a) Top surface

Figure 3-16 Location of Strain and PI gages for 10PS–1S, 14PS-1S and 18PS-1S

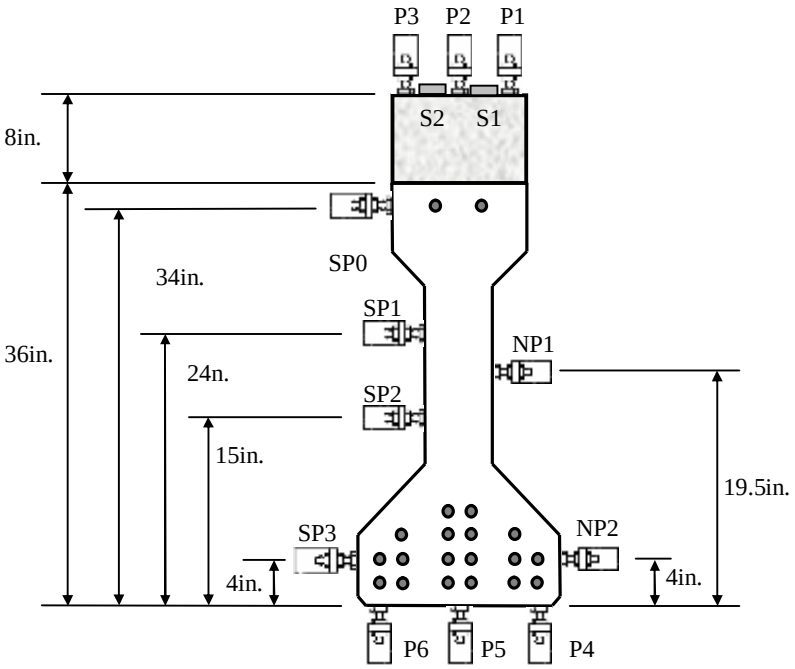

b) Cross section

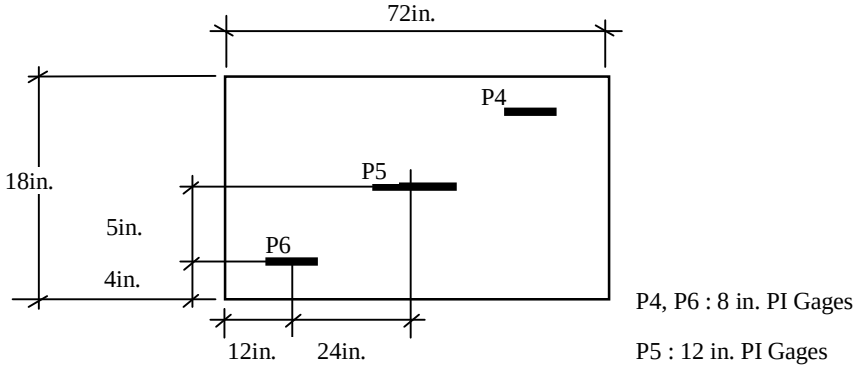

c) Bottom surface

Figure 3-16 (continued) Location of Strain and PI gages for 10PS–1S, 14PS–1S and 18PS-1S

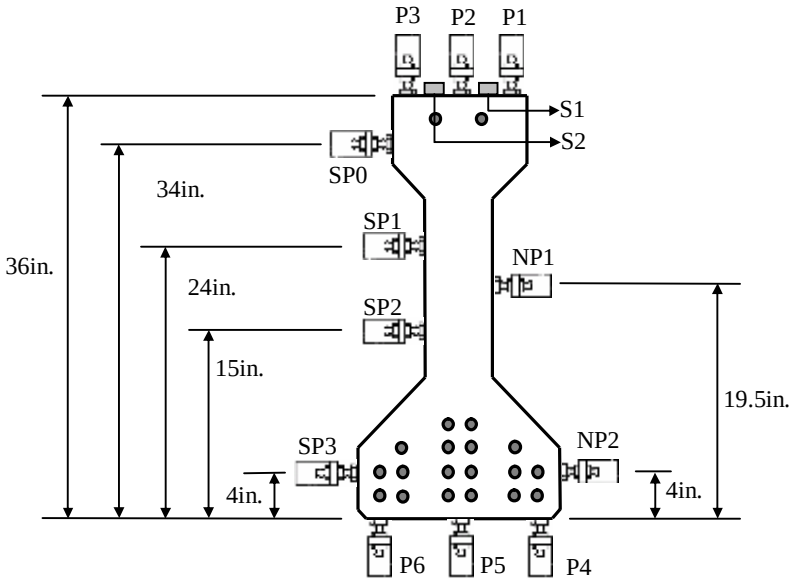

Figure 3-17 Location of Strain and PI gages for 10PS-N, 14PS–N and 18PS-N

3.6.3 Data Acquisition System

An OPTIM MEGADAC data acquisition system, controlled by the TCS (Test Control Software) program, was used to record data, including load, stroke, strain, and deflection for each test. Using this system, the results were graphically monitored using Microsoft Excel during the data acquisition process.

4 RESULTS AND DISCUSSION

4.1 INTRODUCTION

This chapter provides test results and the discussion regarding the flexural response of prestressed AASHTO girders with HSC.

Section 4.2 summarizes the material properties of the specimens and proposes a recommended equation for a prediction of the elastic modulus based on statistical analysis. In addition, the test results are evaluated based on a comparison of the proposed equation and previous research and current specifications.

Section 4.3 provides the measured prestress losses by the use of internal weldable strain gauges. The test results are compared with the current AASHTO LRFD specifications (2004) which contain the most recent research results for HSC, as obtained from tests conducted by Tadros (2003).

Section 4.4 discusses the measured end slippage that are used to investigate transfer length. These results are evaluated against the references, as found in AASHTO LRFD specification (2004) and Oh and kim (2000).

Section 4.5 describes the flexural test results, including ultimate flexural strength and cracking strength for each of the nine AASHTO girders with HSC tested under static loading conditions. The measured load-deflection relationships and failure modes are also provided in this section.

4.2 MATERIAL PROPERTIES STUDY

4.2.1 Elastic Modulus

The measured material properties for this study were provided in Section 3.5.2. In addition to the test results for material properties, the proposed equations for elastic modulus by the statistical analysis were briefly discussed in Section 2.2.

As published in both AASHTO LRFD (2004), which is similar to the ACI318 (2005), and ACI363R (1992), the predictive equation for elastic modulus is expressed in terms of the compressive strength and the dry unit weight of concrete. More specifically, these code provisions use the relationship of the root of the compressive strength of concrete, as seen in the Chapter 2.

However, Cook (2005) has developed a predictive equation for the elastic modulus with the following relationship:

$$E_c = w_c^{2.6738} \cdot (f_c')^{0.2453}, \qquad \textbf{Equation 4-1}$$

where

w_c = dry unit weight of concrete (pcf) and

f'_c = specified strength of concrete (psi).

However, in practical application, Cook's equation may be difficult to apply in design. Therefore, that equation was modified using the experimental results obtained from this

study and analytical results discussed in the following section. It is proposed that the equation for the modulus of elasticity, E_c, be revised as follows:

$$E_c = w_c^{2.5} \cdot (f_c')^{0.33} \quad \textbf{Equation 4-2}$$

The measured elastic modulus results obtained from each specimen in this study and other researchers collected from test results by Andrew (2005) are shown in Figure 4-1 along with the current code equations, Cook's equation and the above proposed equation for the elastic modulus. The predictive equations were generated using a unit weight of 149 pcf as an average of the measured value. It indicates clearly that the AASHTO LRFD (2004) equation overestimates the measured results in the high strength concrete. On the other hand, the elastic modulus in the ACI363R (1992) equation shows a better agreement with measured test results. In the case of the Cook and the above proposed equations, they were within the predictions by the LRFD equation and ACI363R equation. However, the Cook's equation seems to overestimate the elastic modulus under 10,000 psi concrete compressive strength and yields relatively high value beyond 10,000 psi concrete.

The research on material properties of HSC performed by Andrew (2005) at North Carolina State University indicates that the measured values are generally in good agreement with the ACI 363R-92 equation, regardless of the curing method or compressive strength. The test results also support the findings of ACI 363R-92 that the AASHTO-LRFD (ACI318-05) equation consistently overestimates the elastic modulus for HSC.

However, it is difficult to judge which one provides more appropriate prediction due to the limited number of test results and collected data from other researcher. Therefore, more comprehensive comparison is required to evaluate the predictive equation for the elastic modulus over the full range of the concrete compressive strength up to 18,000 psi or more.

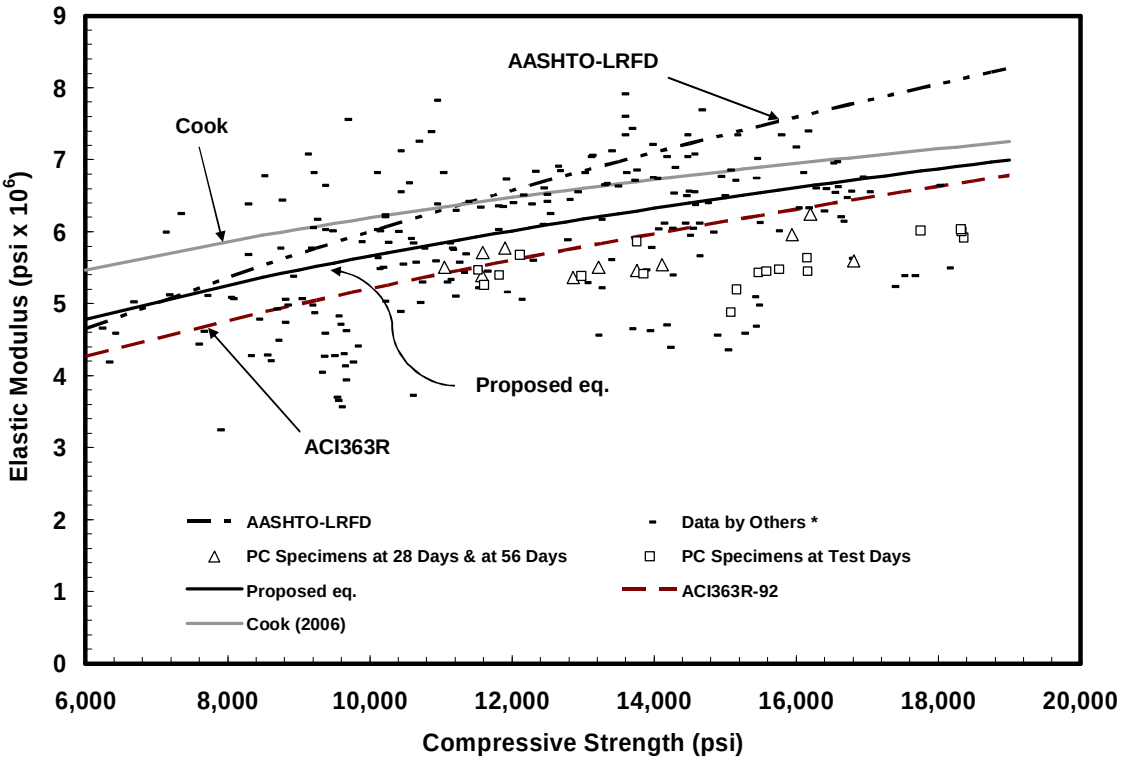

Figure 4-1 Comparison of the elastic modulus between test results and predicted value

To provide a more comprehensive comparison, the 4388 test data entries were collected from J. Cook (2005), the Noguchi Lab in Japan, M. Tadros (2003), and NCHRP12-64 (2006). The ranges of parameters in the collected data, including the compressive strength, unit weight, and measured elastic modulus, are shown in Table 4.1. Detailed information, including the distribution of the compressive concrete strength and the unit weight, is given in Appendix F.

Table 4.1 Range of the Collected Data

Test Data Entries	Compressive Strength (psi)	Unit Weight (lbf)	Elastic Modulus (x106 psi)
4388	370 to 24000	90 to 175.95	0.71 to 10.78

Figure 4-2 (a), (b), (c) and (d) compare the measured elastic modulus data to the following equations: AASHTO LRFD (2004), ACI 363R-92, Cook's (2006) and the proposed, respectively. The figures indicate that the collected data are widely scattered in terms of unit weight. Based on a comparison of the predicted and measured elastic modulus, Cook's equation seems to have a better correlation with the highest R squared values. However, the majority of the data beyond the elastic modulus value of 4×10^6 psi is overestimated. This comparison confirms the trend in the Figure 4-1. Similarly, the AASHTO LRFD equation overestimates the majority of the data beyond the elastic modulus value of 4×10^6 psi. On the other hands, the ACI363-92 and the author's proposed equation provide a slightly better correlation with a higher R^2 value.

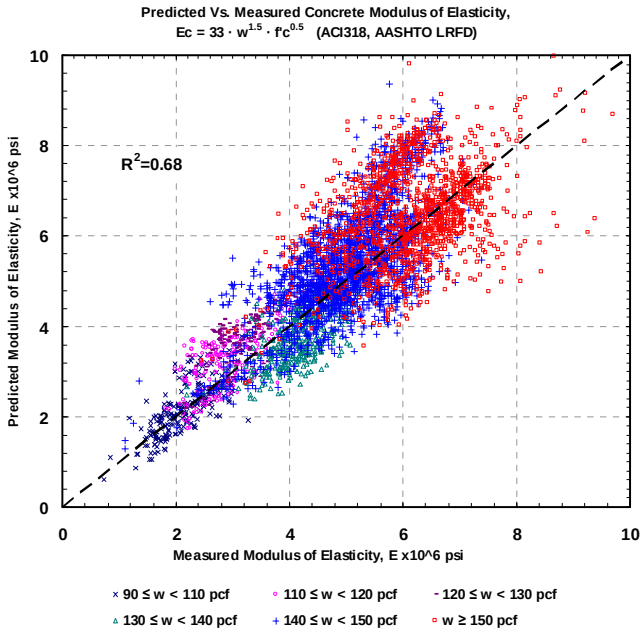

a) AASHTO LRFD and ACI318

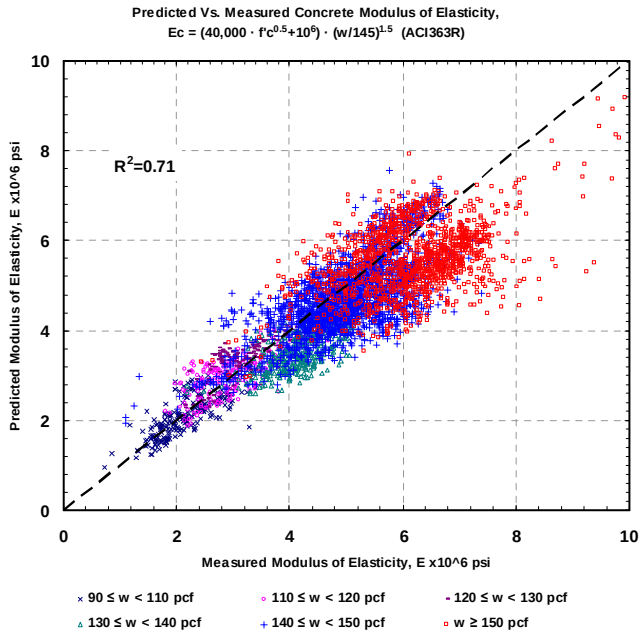

b) ACI363R

Figure 4-2 Comparison between predicted E and measured E with various equations; a) AASHTO LRFD and ACI318; b)ACI363R; c) Cook's; d) Proposed

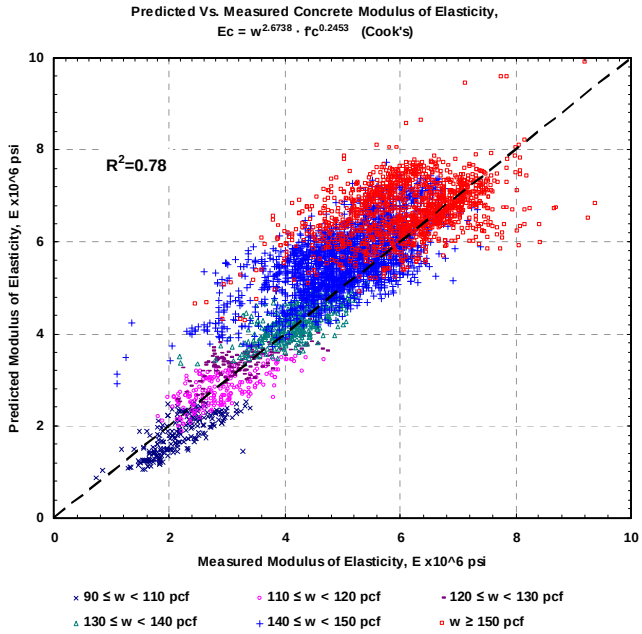

c) Cook's equation

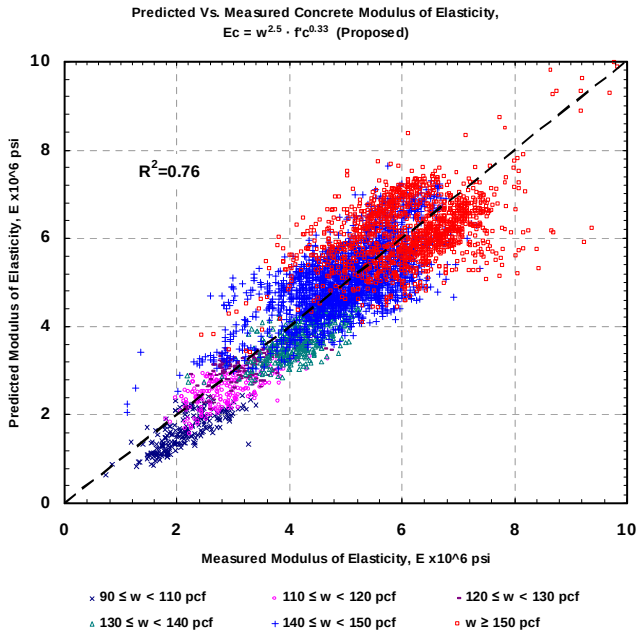

d) Proposed equation

Figure 4-2 (continued) Comparison between predicted E and measured E with various equations; a) AASHTO LRFD and ACI318; b)ACI363R; c) Cook's; d) Proposed

To evaluate the accuracy of the current equations and the proposed equation, a statistical analysis was conducted using the following normal distribution formula. The normal distributions of the collected data with respect to the current AASHTO LRFD (2004), ACI 363R-92, Cook's (2005) and the proposed equation are shown in Figure 4-3 in which P(x) is the probability function, defined as follows:

$$P(x) = \frac{1}{s\sqrt{2p}} \exp\left(-\frac{(x-m)^2}{2s^2} \right), \qquad \textbf{Equation 4-3}$$

where

σ = the standard deviation,

exp = the exponential function,

μ = the mean and

x = the variable.

Results of the statistical analysis for the ratio of the predicted to the measured elastic modulus with respect to the various predictive equations are shown in Table 4.2.

Table 4.2 Results of Statistical Analysis

Equation	Mean (m)	Standard Deviation (σ)	$1/\left(s\sqrt{2p}\right)$
AASHTO LRFD	1.06	0.18	2.18
ACI363R	0.95	0.15	2.72
Cook's	1.09	0.18	2.22
Proposed	0.99	0.16	2.48

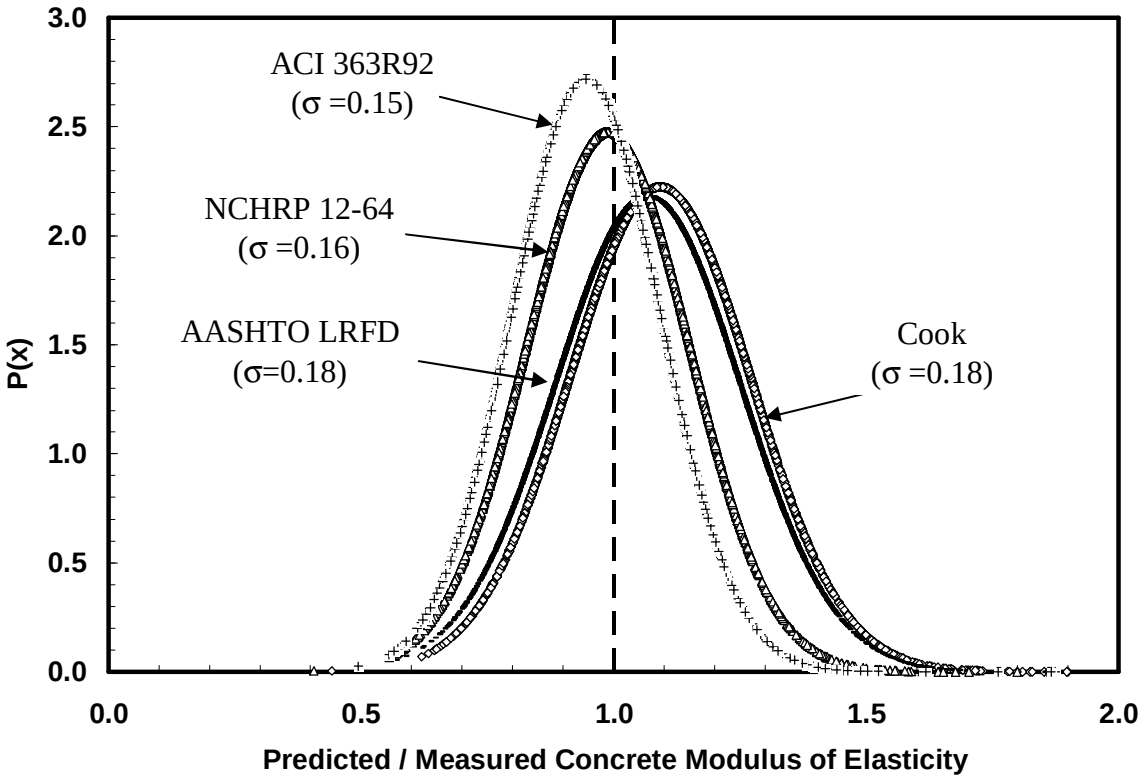

Figure 4-3 Normal distribution for the ratio of predicted to measured elastic modulus

As described previously, both AASHTO LRFD and Cook's prediction result in overestimation of the elastic modulus with higher standard deviation. It seems difficult to cover all of the compressive strength up to 18,000 psi. The ratio of the predicted elastic modulus using the ACI 363R equation to the measured elastic modulus shows a lower standard deviation than the other predictions. As mentioned previously, the equation presented in ACI 363R-92 provides a good estimation of the elastic modulus for this research program. However, the mean in the ratio of the predicted to the measured elastic modulus shows that the prediction using the ACI 363R equation is more conservative than the proposed equation. On the other hand, the proposed equation from this study, which is a

modified Cook's equation, shows that the mean of the ratio of the predicted to the measured elastic modulus is closest to 1, even though the standard deviation is slightly higher than that of the ACI 363R-92 equation. On the basis of these findings, the proposed equation for the elastic modulus is believed to be more appropriate for the compressive concrete strength up to 18,000 psi.

4.2.2 Modulus of Rupture

The modulus of rupture provides an indirect measurement of tensile strength of concrete. Typically, most design codes include an equation for the modulus of rupture of concrete as it relates to the compressive strength. LRFD Specification gives two the modulus rupture value, one is for calculating deflection and the other is used to determine the minimum reinforcement ratio. The smaller value of the two, equation for calculating the deflection and camber is presented as follows:

$$f_r = 7.5\sqrt{f_c'} \text{ (psi)}, \qquad \textbf{Equation 4-4}$$

where

f_r = the modulus of rupture and

f'_c = the specified compressive strength.

On the other hand, the equation for determining minimum reinforcement in the LRFD specification as well as the presented equation in ACI 363R-92 (1981) discussed in Section 2.2.2 is given as follows:

$f_r = 11.7\sqrt{f_c'}$ (psi). **Equation 4-5**

The measured modulus of rupture for the nine girders given in Section 3.5.2, as well as the data collected from Légeron and Paultre (2000), Paultre and Mitchell (2003), the Noguchi Laboratory, and NCHRP 12-64 (2006) are graphically shown in Figure 4-4. This figure obviously shows that the ACI 363R is in a good agreement with the measured test results obtained from other researches, whereas, the smaller value in the LRFD specification shows a better agreement with the test results conducted in this study. Andrew, (2006) and Mokhtarzadeh, (1996) showed that the modulus of rupture was mainly affected by the moisture condition and curing condition.

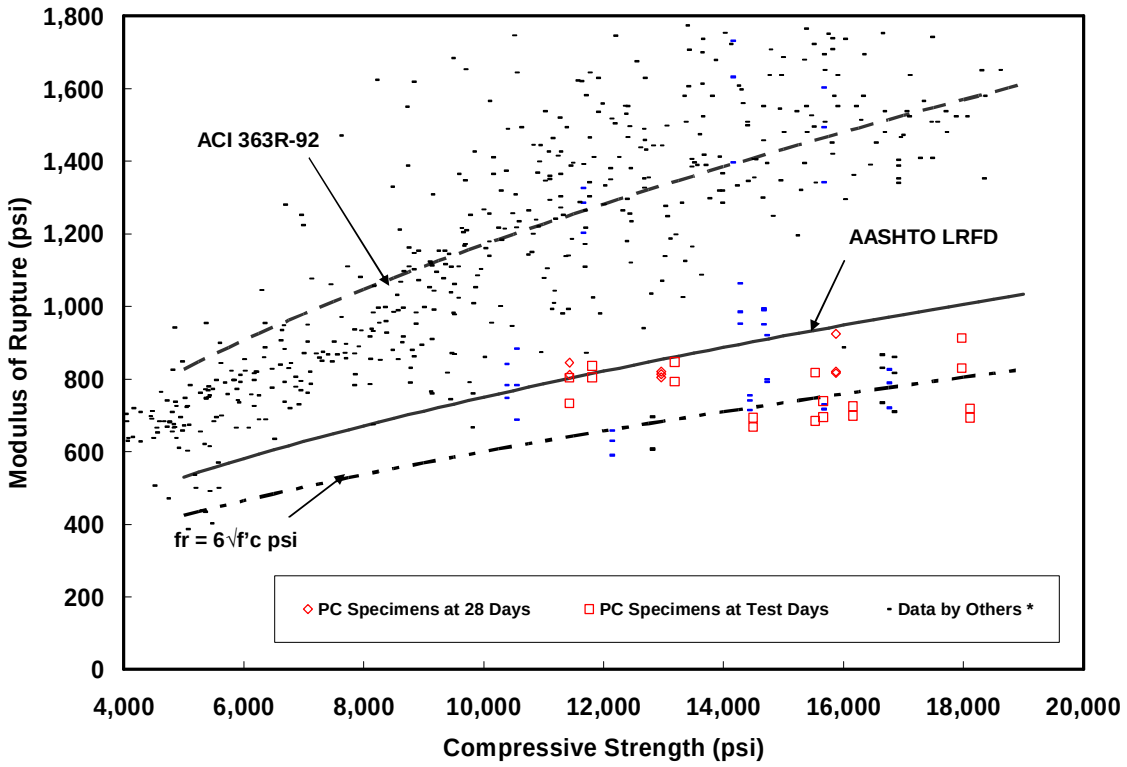

Figure 4-4 Modulus of rupture versus compressive strength

The results from NCHRP 12-64 (2006) suggest that the equation published in ACI 363R-92 correlates well with the measured values obtained from specimens that are moist-cured continuously up to the time of testing. However, in most practical applications, the curing period of concrete is shorter than that study would suggest. Therefore, the case of the prestressed concrete girders may be more similar to the specimens that had been air cured after moist curing or heat curing for several days. The fabricated girder specimens for this study were air cured the initial moist curing for one or two days.

The test results from this study provide good examples for practical applications. The smaller value in the AASHTO LRFD specification (2004) appears to be more suitable for estimating the modulus of rupture for those girder specimens. These test results are in good agreement with the test results conducted by Andrew (2005). Andrew states that, "The equation published in ACI 363R-92 overestimates the modulus of rupture for the ASTM curing methods. The smaller value in the LRFD specification suggested applicable prediction of modulus of rupture for these two different curing conditions which are moisture and heat curing." On the basis of these findings, the current AASHTO LRFD (2004) equation for the modulus of rupture seems more appropriate for HSC. However, in this research, the lower bound equation for modulus of rupture, which is $6\sqrt{f'_c}$ was used for the following study.

4.3 PRESTRESS LOSSES

As described in the instrumentation Section 3.4.1 previously, internal weldable strain gauges were installed on the bottom strand of each girder specimen and monitored regularly in order

to monitor the prestress force in the strands. The measured strains from the internal strain gauges were then used to determine the elastic shortening at transfer and the long-term effects.

In prestressed concrete girders, the primary instant loss of prestress at transfer is due to the elastic shortening of the concrete member. In addition to elastic shortening, the long-term effects consist of concrete shrinkage, creep, and relaxation of the prestressing strand.

The AASHTO-LRFD Refined Method (2004), developed by Tadros (2003), is used in this study to evaluate and compute the prestress losses in members that are constructed and prestressed in a single stage. The equation is composed of the sum of individual loss components, as follows:

$$\Delta f_{pT} = \Delta f_{pES} + \Delta f_{pLT}, \qquad \textbf{Equation 4-6}$$

where

Δf_{pT} = total loss (ksi),

Δf_{pES} = sum of all losses or gains due to elastic shortening or extension at the time of application of prestress and/or external loads (ksi),

Δf_{pLT} = losses due to long-term shrinkage and creep of concrete, and relaxation of the steel (ksi).

After applying prestress force onto the girders, stress reduction occurs in the structure due to elastic shortening, creep, shrinkage, and relaxation. These reductions, or prestress losses, interact with each other. When the prestress force is transferred to the girder concrete through

the contraction of the strands, the adjacent concrete immediately shortens. This shortening of the concrete called elastic shortening results in the loss of part of the prestress force. The computed elastic shortening can be determined by using the AASHTO LRFD equation, as follows:

$$\Delta f_{pES} = \frac{E_p}{E_{ci}} f_{cp}, \qquad \textbf{Equation 4-7}$$

where

f_{cp} = concrete stress at the level of most bottom strands due to the prestress force at transfer and the self-weight of the member at the section of maximum moment;

E_p = modulus of elasticity of prestressing steel; and

E_{ci} = modulus of elasticity of concrete at transfer.

The primary parameters used to determine elastic shortening are the elastic modulus of concrete at transfer and the concrete stress at the level of the most bottom prestressing tendons. Specifically, the two equations – the code equation and the proposed equation by author to predict the elastic modulus of concrete – are considered in this study. Table 4.3 shows the comparison between the measured elastic shortening and the prediction.

Table 4.3 Elastic Shortening at Transfer

Identification	Gauge Number	Measured Strain (με)	Loss %	Measured Average Losses	Computed Elastic Shortening with	
					Code E	Proposed E
18PS-1S	1_4	465	7%	9.5%	7.9%	7.9%
	1_6	761	12%			
18PS-5S	2_3	261	4%	5.0%	7.8%	7.9%
	2_4	396	6%			
18PS-N	3_1	403	7%	7.0%	7.6%	7.7%
	3_3	398	7%			
14PS-1S	4_4	487	8%	8.0%	7.7%	7.5%
	4_6	502	8%			
14PS-5S	5_3	431	7%	7.0%	8.2%	7.9%
	5_4	464	7%			
14PS-N	6_1	477	8%	8.5%	8.2%	7.9%
	6_3	486	9%			
10PS-1S	7_4	498	8%	8.5%	6.8%	6.6%
	7_6	545	9%			
10PS-5S	8_3	532	8%	8.0%	6.8%	6.6%
10PS-N	9_1	472	7%	7.0%	6.7%	6.6%
Average				7.6%	7.5%	7.4%

Based on the measured strain at the most bottom strands, the losses due to elastic shortening are averages 7.6 percent of the initial prestressing stress. These results are slightly higher

than the LRFD equation with using the elastic modulus in the code equation and in the proposed equation. However, from the practical point of view, the measured results provide a reasonable agreement with the LRFD equation.

After instantaneous prestress loss, concrete structures under a sustained load experience creep and shrinkage at the same time. Test results measured by internal strain gauges were compared to the current creep and shrinkage predictions specified by AASHTO LRFD Bridge Design Specifications (2004), developed by Tadros (2003). The major equations to calculate creep and shrinkage of concrete are given in Table 4.4. In the table:

ε_{sh} = the predicted shrinkage strain;

Ψ = the predicted creep coefficient;

t = he age of the concrete after loading, in days;

t_i = the age of the concrete when the load is initially applied for accelerated curing or the age minus 6 days for moist-curing, in days;

f'_{ci} = the specified compressive strength in ksi at transfer for prestressed members or 80 percent of the strength at service for non-prestressed members;

V/S = the volume-to-surface ratio, in inches; and

H = the relative humidity of the ambient air.

Several steps are required to determine the prestress losses based on the AASHTO LRFD equation. For example, a detailed calculation procedure adopted from Tadros (2003) to determine prestress losses for 10PS-5S is given in Appendix H.

Table 4.4 Creep and Shrinkage Prediction Relationships by AASHTO LRFD

	Shrinkage	Creep
Equation	$e_{sh} = 480\times10^{-6} k_{td} k_s k_{hs} k_f$	$\Psi(t,t_i) = 1.90 k_{td} k_{la} k_s k_{hc} k_f$
k_{td} **(time development factor)**	$k_{td} = \frac{t}{61 - 4f'_{ci} + t}$	
$k_{hs,hc}$ **(humidity factor)**	$k_{hs} = 2.00 - 0.0143H$	$k_{hc} = 1.56 - 0.008H$
k_s **(size factor)**	$k_s = \frac{1064 - 94V/S}{735}$	
k_f **(concrete strength factor)**	$k_f = \frac{5}{1 + f'_{ci}}$	
k_{la} **(loading age factor)**	-	$k_{la} = t_i^{-0.118}$

Table 4.5 shows the comparison between the measured prestress loss at test day and the predicted value from the AASHTO LRFD (2004) using the two different equations of the elastic modulus, i.e., code and proposed by author. As can be seen in the Table 4.5, the measured prestress losses at the level of the most bottom strands result are not consistent. However, it appears that roughly 11.4 percent of the losses stem from the initial prestressing force. On the other hand, the predicted results in the LRFD specification with two types of elastic modulus are approximately 15 percent of the initial prestressing force.

Additionally, the effective prestressing force can be evaluated with the cracking strength and the measured modulus of rupture. Related study about the cracking strength will be discussed in the following Section 5.2.1. Herein, the calculated prestress losses with the measured values are also given in the same table. On the basis of the calculated prestressed losses with

the measured cracking strength and modulus rupture, the prestress losses are approximately 11 percent of the initial prestressing force. These results show that the predicted prestress losses using the LRFD specification are quite conservative.

Additionally, the long term prestress losses due to creep, shrinkage and relaxation of prestressing strands are only a small portion of the total losses at the test day.

Table 4.5 Test Results for Prestress Losses at Test Day

Identification	Measured Average Losses	AASHTO LRFD		Calculated (with M_{cr} and f_r)
		Code E	Proposed E	
10PS-5S	7.8%	13.9%	13.7%	12.9%
14PS-5S	16.7%	15.3%	15.0%	11.2%
18PS-5S	7.9%	14.2%	14.2%	12.9%
10PS-1S	11.3%	15.1%	14.8%	13.9%
14PS-1S	8.0%	15.8%	15.6%	10.8%
18PS-1S	13.0%	15.0%	15.1%	11.3%
10PS-N	8.1%	14.9%	14.7%	8.3%
14PS-N	8.5%	17.6%	17.2%	7.3%
18PS-N	21.7%	14.1%	14.3%	10.1%
Average	11.4%	15.1%	14.9%	11.0%
Standard Dev.	0.053	0.01	0.01	0.022

4.4 TRANSFER LENGTH

In this study, the transfer length was not measured directly. However, the transfer length can be evaluated for each of the AASHTO girders by measuring the end slippage of the prestressing strand at transfer. End slippage was measured using tape measurement readings taken before and after release at specified locations. The required transfer length for a prestressing strand provided in the AASHTO LRFD specifications is:

$$l_t = 60 d_b, \qquad \textbf{Equation 4-8}$$

where l_t is the transfer length and d_b is the nominal diameter of the prestressing strand.

On the other hands, the predicted equation for transfer in ACI318 specifications is 50 d_b. These required transfer length in the LRFD and ACI 318 for ½ in. diameter strand is 30 in. and 25 in., respectively.

In addition to these code values, Oh et al. (2000) proposed an equation as a function of end slippage to predict the transfer length. The equation for the transfer length is as follows:

$$l_t = \frac{2E_p d}{f_{pi}}, \qquad \textbf{Equation 4-9}$$

where l_t is the transfer length, E_p is the modulus of elasticity of the strand, d is the strand end slippage, and f_{pi} is the initial prestress of the strand just before detensioning.

Using the above equations to compute the transfer length, the computed transfer lengths for each girder specimen are listed in Table 4.6.

Table 4.6 Summary of End Slippage and Transfer Length

Specimen	d* (in)	Oh and Kim (2000) (in.)
18PS-1S	2/16	29
18PS-5S	1/16	23
18PS-N	1/16	23
Average	1/16	25
14PS-1S	1/16	12
14PS-5S	2/16	35
14PS-N	2/16	29
Average	2/16	25.3
10PS-1S	2/16	29
10PS-5S	3/16	55
10PS-N	1/16	15
Average	2/16	33

* indicates a round up value

The average computed transfer length using end slippage as shown in Table 4-6 are in the range from 25 to 33 in. These estimated transfer lengths within the requirement of these two provisions are in reasonable agreement. Consequently, the equation in the LRFD specification seems to predict the transfer length reasonably well.

4.5 CAMBER

The measured cambers for each girder specimen were compared in the Table 4.7. To calculate camber with different elastic modulus of concrete, the average initial prestressing force by the load cells for each target strength girder, and assuming 10 percent prestress losses were used. The elastic modulus was predicted with unit weight of concrete for 149 pcf.

As can be seen in Table 4.7, the calculated camber by the proposed elastic modulus provided less value than that by the elastic modulus in the LRFD specification.

Table 4.7 Summary of Camber Results

Specimen	Measured Camber (in)	Calculated Camber (in.) using		
		Code E	Proposed E	Measured E
18PS-1S	5/8	0.51	0.51	0.49
18PS-5S	1/2	0.50	0.51	0.47
18PS-N	1/2	0.49	0.50	0.44
14PS-1S	5/8	0.50	0.49	0.42
14PS-5S	5/8	0.53	0.51	0.44
14PS-N	1/2	0.53	0.51	0.46
10PS-1S	1/2	0.44	0.43	0.38
10PS-5S	1/2	0.44	0.43	0.39
10PS-N	5/8	0.44	0.43	0.35

4.6 FLEXURAL RESPONSE

This section presents the flexural test results of nine AASHTO girders under static loading conditions. The ultimate flexural resistance, cracking resistance, load-deflection relationship and failure mode for all the girder specimens are summarized in this section. Based on the test results, the major findings in this study are discussed.

4.6.1 AASHTO Girders with a 5 ft. Wide Deck

Three composite AASHTO girders, each with a 5 ft. wide deck, and identified as 10PS-5S, 14-PS-5S and 18PS-5S, were tested under static loading conditions. As mentioned in the design consideration, three girders were designed to be subjected to the compressive force controlled by the deck concrete with NSC. The load-deflection relationships for the composite girders with a 5 ft. deck slab are presented in Figure 4-5. The figure shows the net deflection at mid span, after accounting for the deflections measured at both supports.

As described previously in the loading procedure, load was applied twice before failure of the girders. Once the initial cracking of the concrete girder was observed, the girders was unloaded and reloaded up to failure. The initial flexural stiffness of the three composite girders was linearly elastic up to the yielding of the prestressing strands and the cracking of the concrete girders. Moreover, the initial flexural stiffness of the composite girders prior to initial cracking is not significantly different with respect to the strength of the girder, that is, whether it is 10,000, 14,000 or 18,000 psi. Figure 4-5 indicates that the flexural stiffness of the girders is not proportional to the compressive strength of the girder concrete. In the figure, it is clear that the load-deflection behavior becomes nonlinear after the section was cracked.

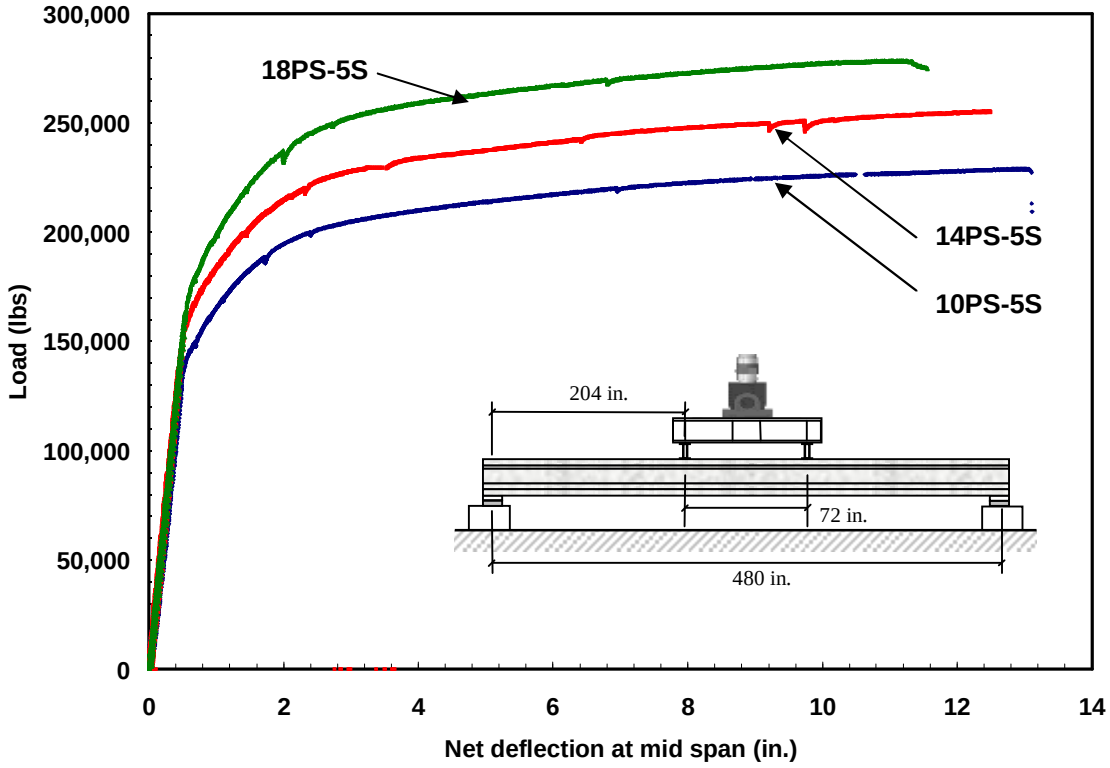

Figure 4-5 Load-deflection behavior for 10, 14, 18PS-5S

As can be seen in the above figure, the net deflection at mid span was relatively large at the failure. The observed initial cracking load and ultimate load at failure for each specimen are given in Table 4.8.

Table 4.8 Observed Test Results for 10PS – 5S, 14PS – 5S and 18PS-5S

Identification	Cracking Load (kips)	Ultimate Load (kips)
10PS-5S	129	229.0
14PS-5S	149	255.5
18PS-5S	162	278.4

As discussed in section 3.4, during the static loading phase, the strain envelopes for each specimen were measured at top surface of the deck concrete, at bottom surface and side surface of the girder. For 18PS-5S, the measured strain envelopes at three locations were given in the Figure 4-6. Locations of the strain gauge are given in Figure 4-6 (a). Figure 4-6 (b) indicates a typical strain envelope by the PI gauges and the concrete strain gauges at the top surface of the deck. Figure 4-6 (c) provides the strain profile at the bottom surface. Figure 4-6 (d) presents the strain at the bottom surface of the girder. All strain envelope clearly show that the strain became a nonlinear response after the girder was cracked. Detailed strain envelopes for the rest of two specimens are given in Appendix G. In all cases of the three composite AASHTO girders with a 5 ft. wide deck, the measured strain at the top surface of the deck concrete at failure was higher than the ultimate strain of the concrete, that is, 0.003, as specified in AASHTO LRFD (2004).

Using the strain envelope at a specific location, the average strains at the top surface and bottom surface under a given loading stage were used to determine the neutral axis location by the plane section assumption. The applied moment at the mid span in Figure 4-7 was determined from the measured load, but the dead load moment was not included in the calculation.

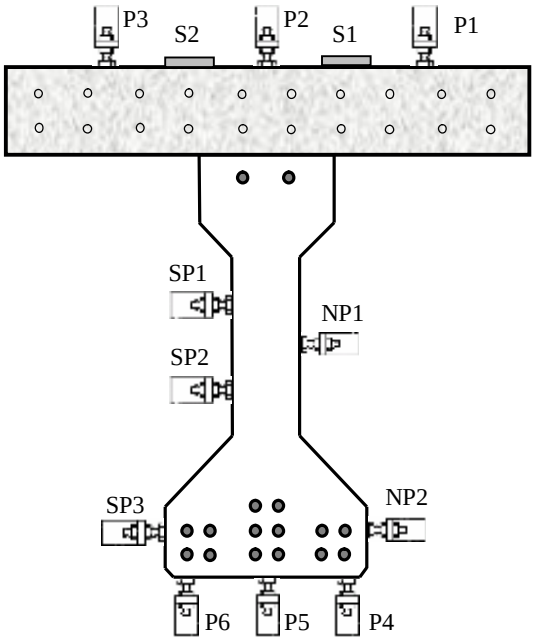

a) Location of the strain gauges

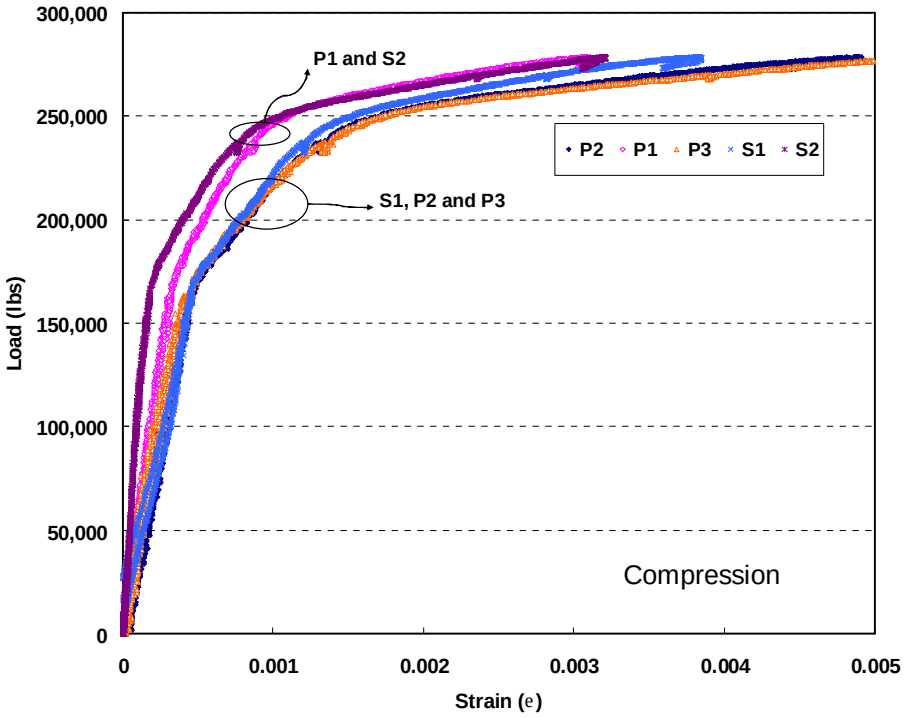

b) Strain at the top surface

Figure 4-6 Strain envelopes for 18PS-5S

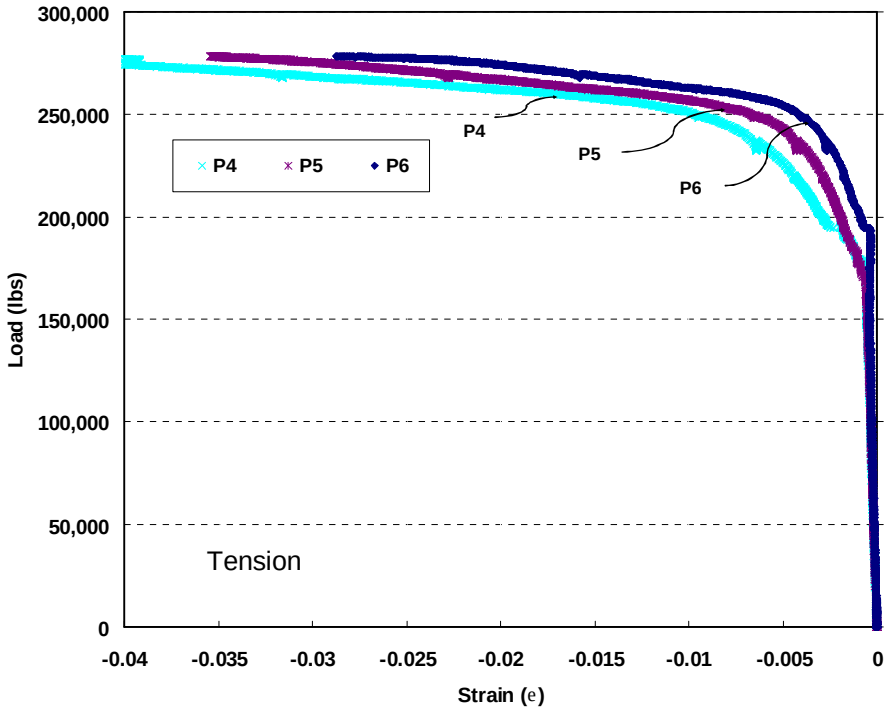

c) Strain at the bottom surface

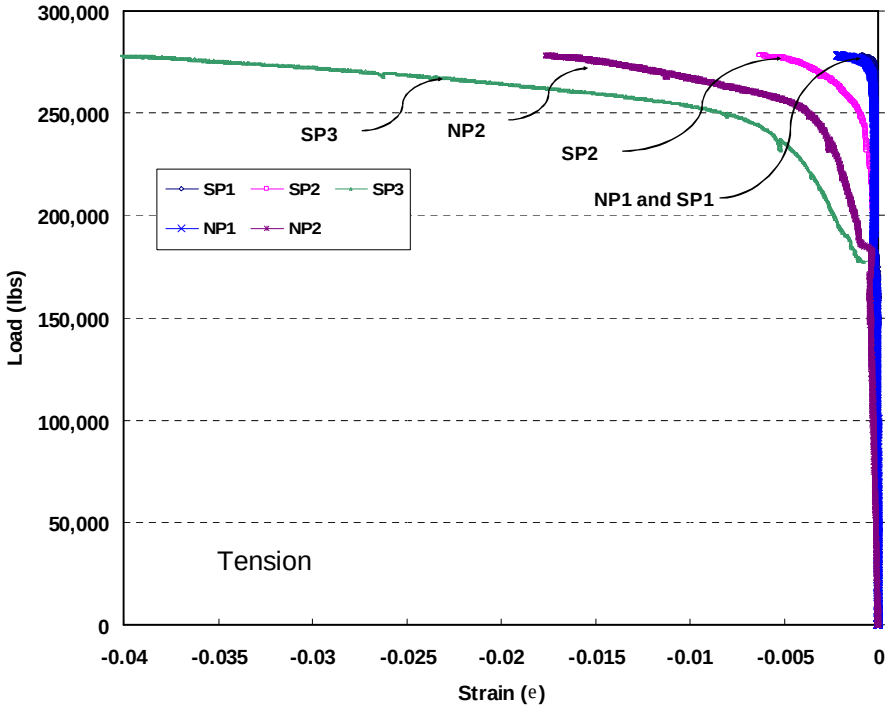

d) Strain at the side surface

Figure 4-6 (continued) Strain envelopes for 18PS-5S

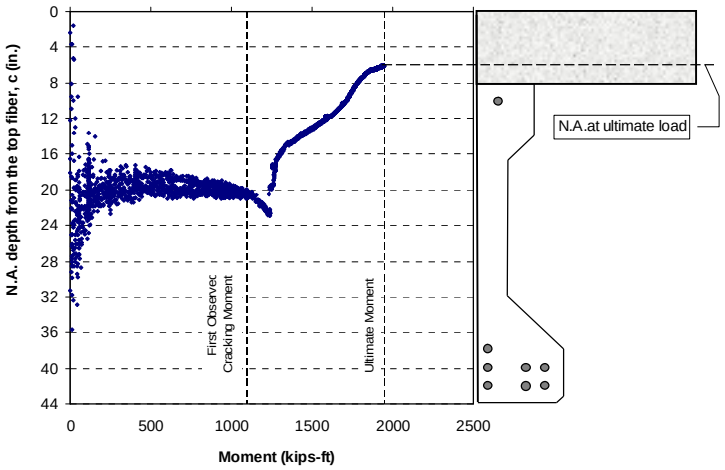

a) Moment-N.A. depth relationship for 10PS-5S

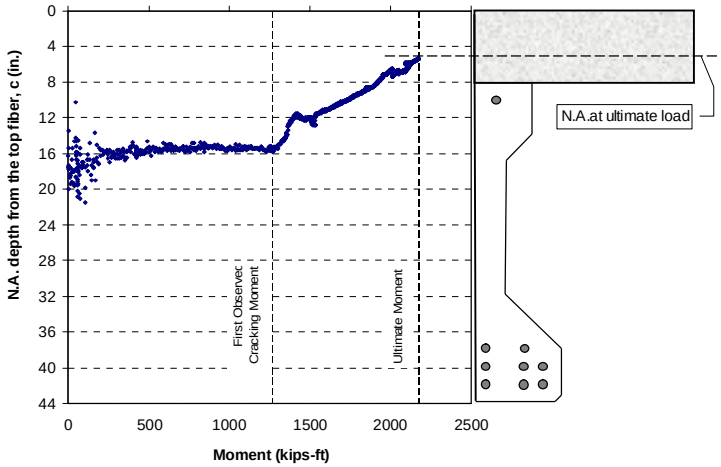

b) Moment-N.A. depth relationship for 14PS-5S

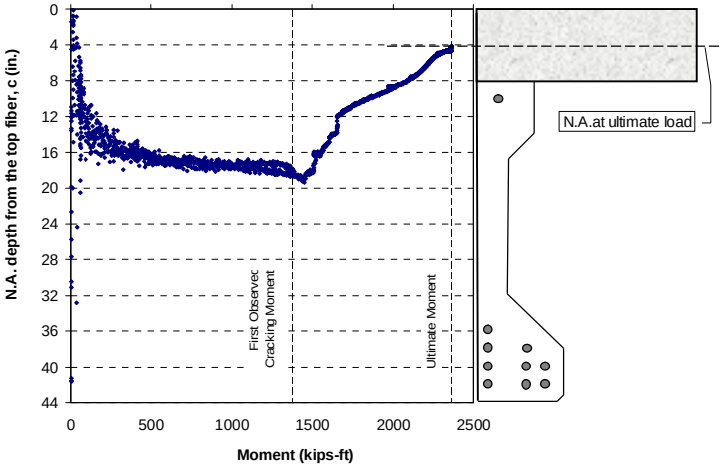

c) Moment-N.A. depth relationship for 18PS-5S

Figure 4-7 Moment – N.A. depth location for 10PS – 5S, 14PS – 5S and 18PS – 5S

It is clear that the neutral axis at the failure was located in the deck concrete as shown in Figure 4.7.

Figure 4-8 indicates a typical failure mode for AASHTO girders with a 5 ft. wide deck. At the first loading phase, once the initial crack was observed, the load was recorded and unloaded as shown in Figure 4-8 (a). At the second loading phase, after the prestressing strands were ruptured, failure of the specimens occurred due to the crushing of the deck concrete near one of the load locations as shown in Figure 4-8 (b). Whereas, Figure 4-8 (c) shows the typical deformed shape of the girders immediately after the deck concrete is crushed. Deflection at failure of the composite girders was quite large (see Figure 5-4). All three of the specimens failed due to the compressive force controlled by the NSC, and the crack was propagated to the deck concrete as expected in the design. The flexural cracks developed along the girder length. They seemed to match with the location of the stirrup with every 6 in. along with the girder.



a) The initial observed crack b) Crushing of deck concrete at failure

Figure 4-8 Typical failure mode for the AASHTO girder with a 5 ft. wide deck



c) Deformed shape after failure

Figure 4-8 (continued) Typical failure mode for the AASHTO girder with a 5 ft. wide deck

4.6.2 AASHTO Girders with a 1 ft. Wide Deck

Three composite AASHTO girders, each with a 1 ft. wide deck and identified as 10PS-1S, 14-PS-1S and 18PS-1S, were tested under static loading conditions. As mentioned in the design consideration, these girders were designed to have the compressive force controlled by the combination of two types of concrete strength, that is, the NSC for the cast-in-place deck and the HSC for the girder.

The load-deflection curves for the three composite girders with a 1 ft. deck slab are presented in Figure 4-9. The figures show the net mid-span deflection after the deflections measured at the support were accounted for.

In the same manner as the girders with the 5 ft. wide deck, the load was applied twice before failure of the girders. Once the initial cracking of the concrete girder was observed, the girders were unloaded and reloaded up to failure. The initial flexural stiffness of the three composite girders was linearly elastic up to yielding of the prestressing strands and cracking of the concrete girders. Moreover, the initial flexural stiffness of the composite girder prior to the initial cracking was not proportional to the strength of girder, that is, whether it is 10,000, 14,000 or 18,000 psi. Figure 4-9 indicates that the flexural stiffness of girder 18PS-1S is lower than that of 14PS-1S. This result is in good agreement with the test results of the material properties of girder concrete. A small drop in load level was observed due to the shifting of the internal compressive force to the HSC flange of the girder near the point of failure. Deflection at failure of the composite girders was relatively small in compression with that of the composite girder with 5 ft. wide deck slab.

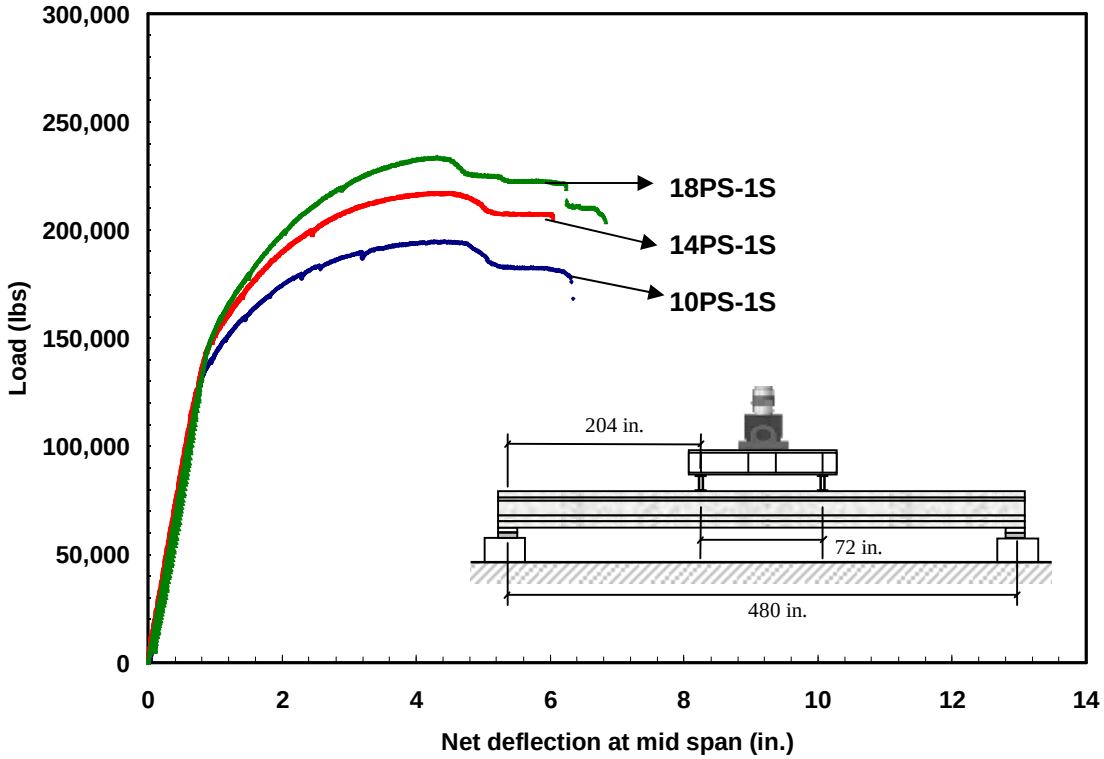

Figure 4-9 Load-deflection behavior for 10PS – 1S, 14PS – 1S and 18PS-1S

The observed initial cracking load and ultimate load at failure for each specimen are given in Table 4.9.

Table 4.9 Observed Test Results for 10PS - 1S, 14PS – 1S and 18PS-1S

Identification	Cracking Load (kips)	Ultimate Load (kips)
10PS-1S	110	194.7
14PS-1S	124	217.0
18PS-1S	133	233.7

Figure 4-10 (a), (b), (c) and (d) indicate the strain gauge locations, a typical strain envelope by the PI gauges and the concrete strain gauges at the extreme top surface, at the bottom surface and at the side surface of the specimen, respectively in 10PS-1S. The strain envelope for specimens: 14PS-1S and 18PS-1S are given in Appendix G. In all three cases, the measured strain at the top surface of the deck concrete where the concrete was crushed is higher than the ultimate strain of the concrete, 0.003, as specified in AASHTO LRFD (2004). The discrepancy in the strain envelope for each gauge on the top surface of the deck concrete most likely resulted from the shrinkage cracks on the surface of the deck concrete. As the composite girder with a 5ft wide deck, the moment versus neutral axis location from top fiber is shown in Figure 4-11.

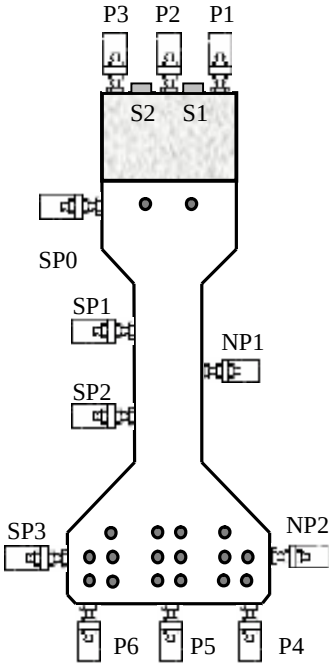

a) Strain gauge location for 10PS-1S

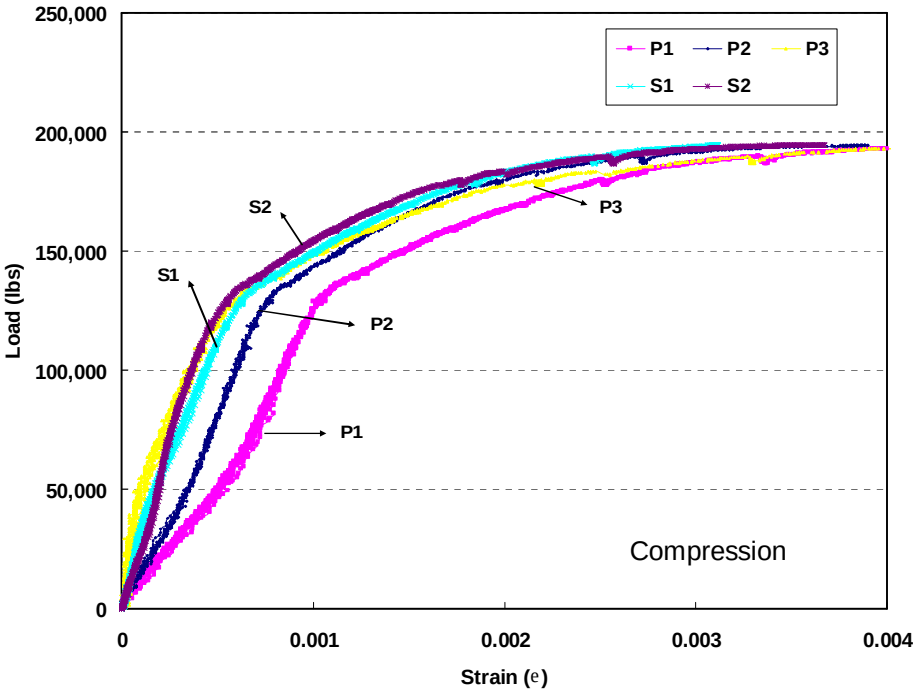

b) Strain at the top surface

Figure 4-10 Strain envelopes for 10PS-1S

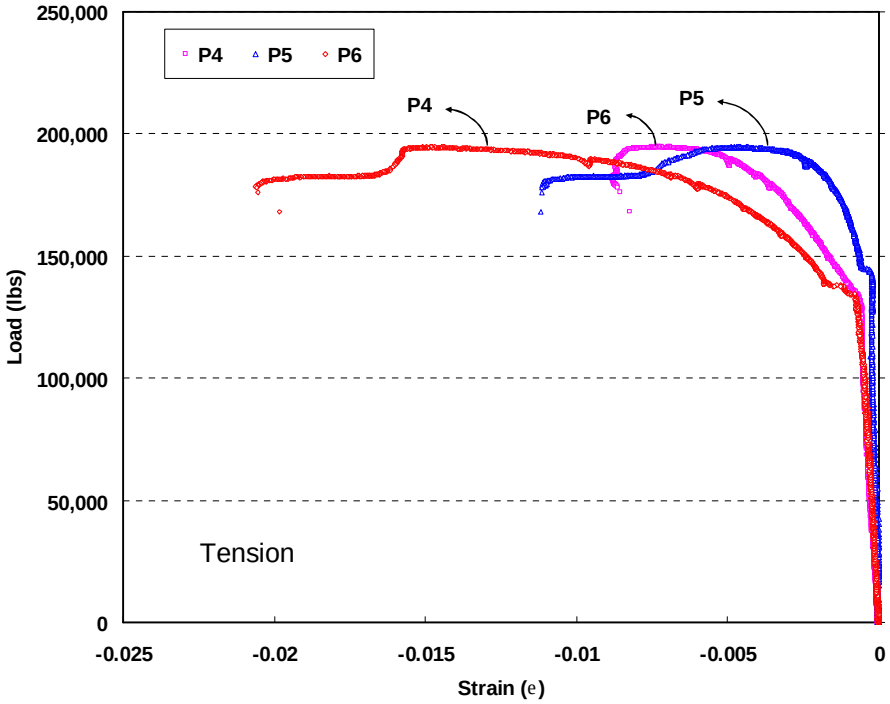

c) Strain at the bottom surface

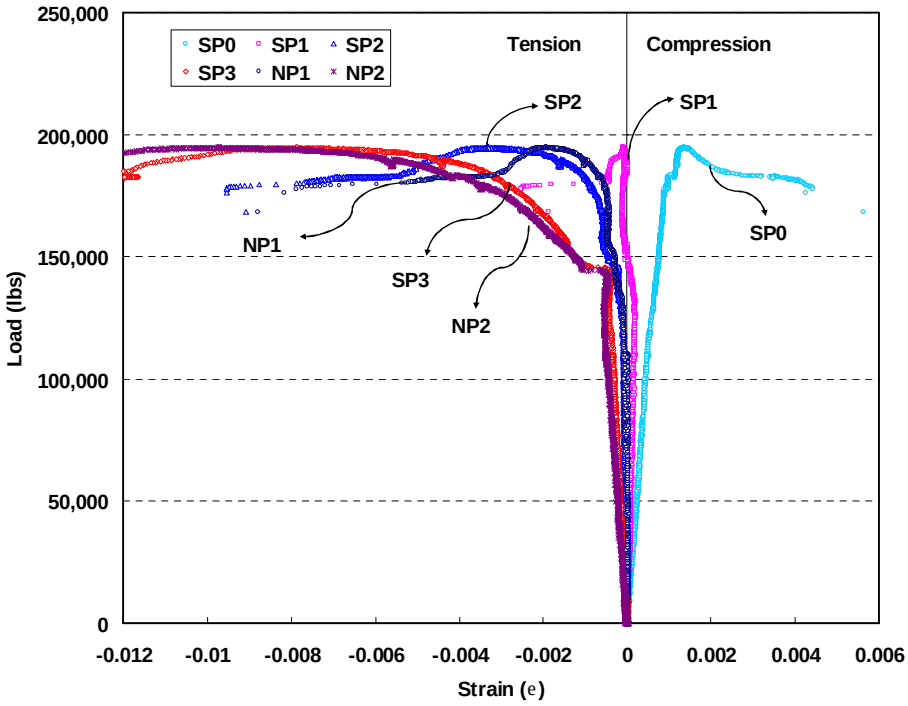

d) Strain at the side surface

Figure 4-10 (continued) Strain envelopes for 10PS-1S

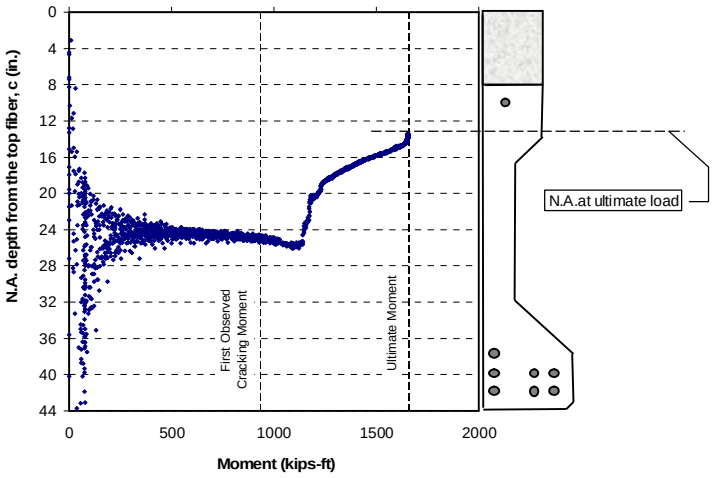

a) Moment-N.A. depth relationship for 10PS-1S

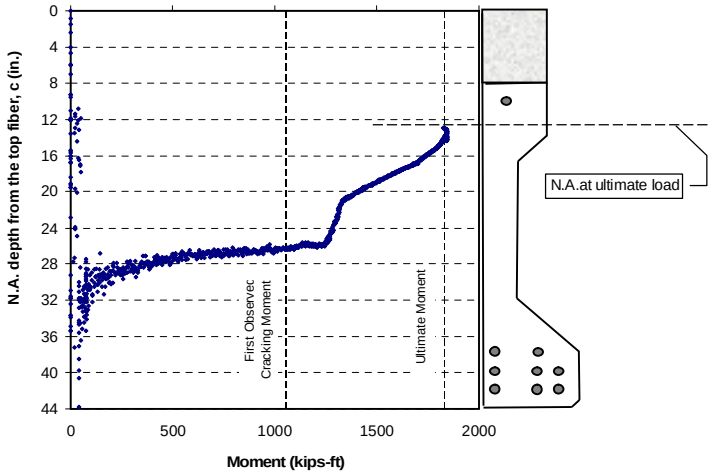

b) Moment-N.A. depth relationship for 14PS-1S

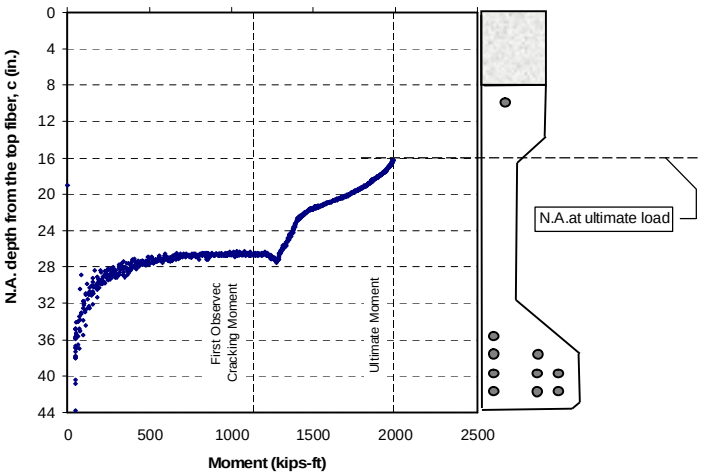

c) Moment-N.A. depth relationship for 18PS-1S

Figure 4-11 Moment – N.A. depth location for 10PS – 1S, 14PS – 1S and 18PS – 1S

As can be seen in Figure 4-11, the neutral axis depth is located in the flange of the girder as called for by the design.

For this case, the internal compressive force was resisted by two types of concrete with different compressive strength. Figure 4-12 shows the typical failure mode of the composite girder with a 1ft wide deck. Failure of the AASHTO girder with a 1 ft. wide deck was preceded by the crushing of the deck concrete and the crushing of the girder concrete. In the first loading phase, once the initial crack was observed, the load was recorded and unloaded as shown in Figure 4-12 (a). As described in the load-deflection relation for the composite girder with a 1ft deck, the internal compressive force shifted downward onto the girder with high strength concrete as can be seen in Figure 4-12 (b). Consequently, the equilibrium force was slightly reduced after the peak load. For a while, the girder concrete resisted against the compression force. Afterward, the sudden failure was observed at the constant moment region as shown in Figure 4-12 (c). The strain envelope, SP0 in the Figure 4-10 (c) confirms this phenomenon.

Additionally, the reinforcement on the deck and the strands on the girder were buckled at failure as shown in Figure 4-12 (d).

Figure 4-12 (e) shows the typical deformed shape of the girders immediately after the girder concrete was crushed. All three specimens failed due to the compressive force controlled by the combination of the NSC for the deck and the HSC for the girder that was expected in the design consideration.



a) The initial observed crack

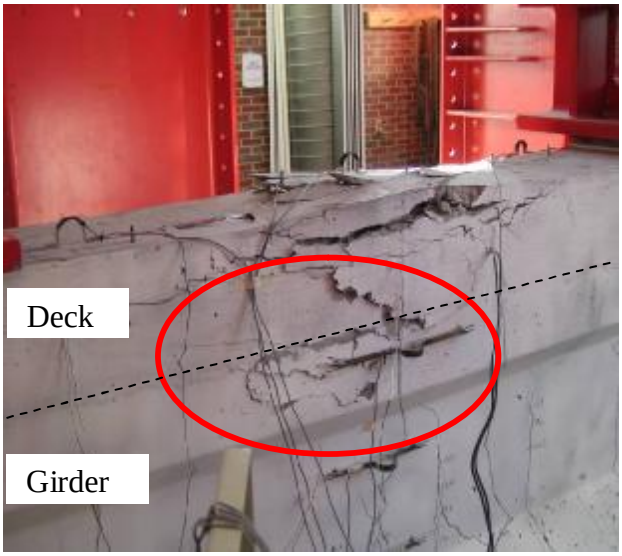

b) Transfer of compression force

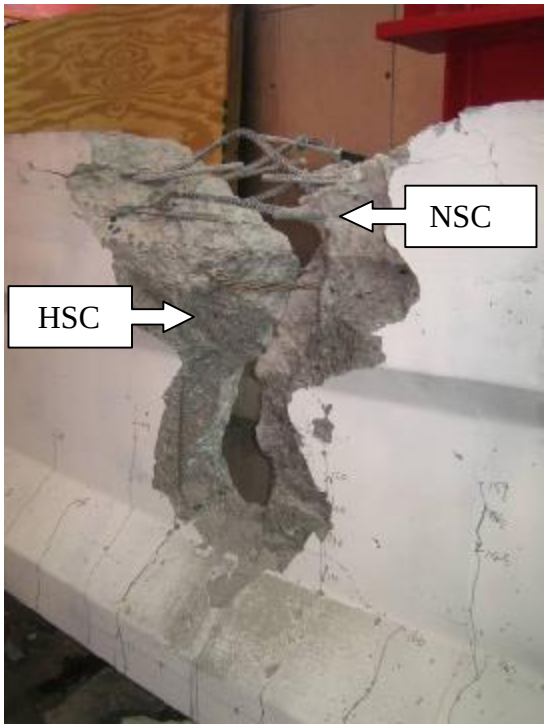

c) At failure



d) Bucking of the reinforcement and strand

Figure 4-12 Typical failure modes for the AASHTO girder with a 1 ft. wide deck



e) Deformed shape after failure

Figure 4-12 (continued) Typical failure modes for the AASHTO girder with a 1 ft. wide deck

4.6.3 AASHO Girder without Deck

Three AASHTO girders without a deck, 10PS-N, 14PS-N and 18PS-N, were tested under static loading conditions. As mentioned in the design consideration, these girders were designed to be have the compressive zone of the girder controlled only by HSC. The load-deflection relationships for the three girders are presented in Figure 4-13. The figure shows the net mid-span deflection, after eliminating the effect of the deflections at both supports.

In the same manner as noted for the other girders, the load was applied twice before the failure of the girders. Once the initial cracking of the concrete girder was observed, the girders were unloaded and reloaded up to failure. The initial flexural stiffness of the three composite girders was linearly elastic up to the yielding of the prestressing strands and the cracking of the concrete. Moreover, the initial flexural stiffness of the girder prior to the

initial cracking was not affected by the concrete compressive strength of 10,000, 14,000 or 18,000 psi. Figure 4-13 indicates that the flexural stiffness of the girders is not proportional to the compressive strength of the girder concrete. After the section was cracked, the load-strain behavior becomes nonlinear. Failure was less ductile than what was observed at the failure of the other six girders.

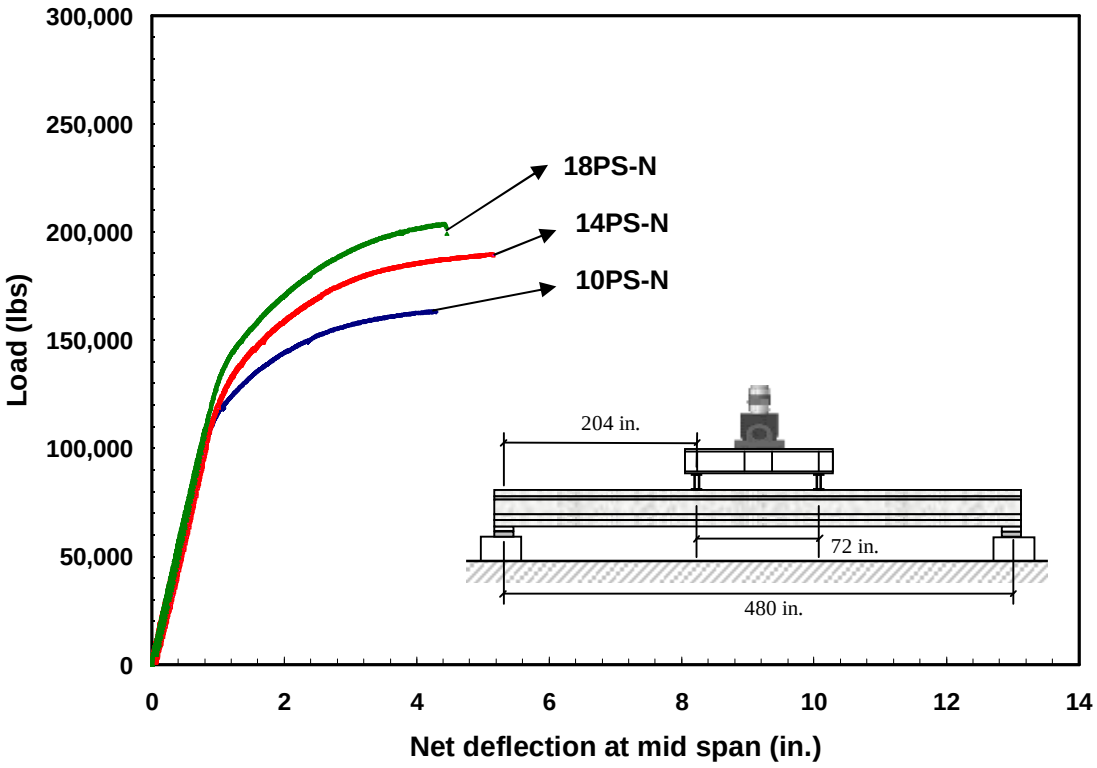

Figure 4-13 Load-deflection behavior for 10PS - N, 14PS – N and 18PS-N

The observed initial cracking load and ultimate load at failure for each specimen are given in Table 4.10.

Table 4.10 Observed Test Results for 10PS - N, 14PS – N and 18PS -N

Identification	Cracking Load (kips)	Ultimate Load (kips)
10PS-N	94	163.3
14PS-N	102	189.5
18PS-N	108	203.7

The strain gauge locations for 18PS-N are given in Figure 4-14 (a). Figure 4-14 (b) indicates a typical strain envelope measured by the PI gauges and concrete strain gauges at the extreme top surface of the flange of specimen. Figure 4-14 (c) provides the strain profile at the bottom surface. Figure 4-14 (d) presents the stain at the side surface of the girder.

Detailed strain envelopes for specimens: 10PS-N and 14PS-N are given in Appendix G. In all three cases of the girders without a deck, the average measured strain at the top surface of the flange of the girder at the location where the concrete was crushed is slightly less than the ultimate strain of the concrete, 0.003, as specified in AASHTO LRFD (2004). More detail discussion for the ultimate strain of the extreme top fiber is given in section 4.5.4.

As before, the average strain from the top surface and bottom surface a specific loading stage was used to determine the neutral axis location by the plane section assumption. The applied moment at the mid span in Figure 4-15 was determined from the measured load, but the dead load moment was not included in this calculation.

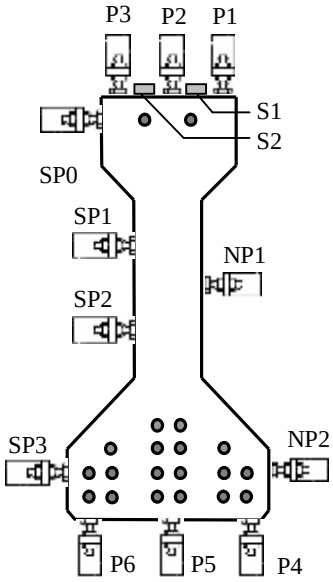

a) Strain gauge locations for 18PS-N

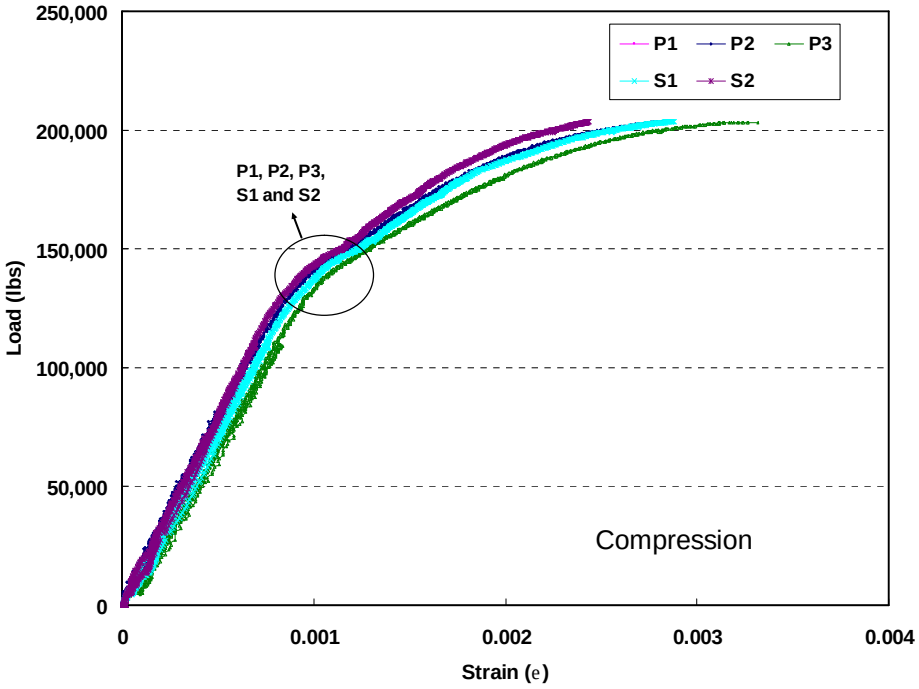

b) Strain at the top surface

Figure 4-14 Strain envelopes for 18PS-N

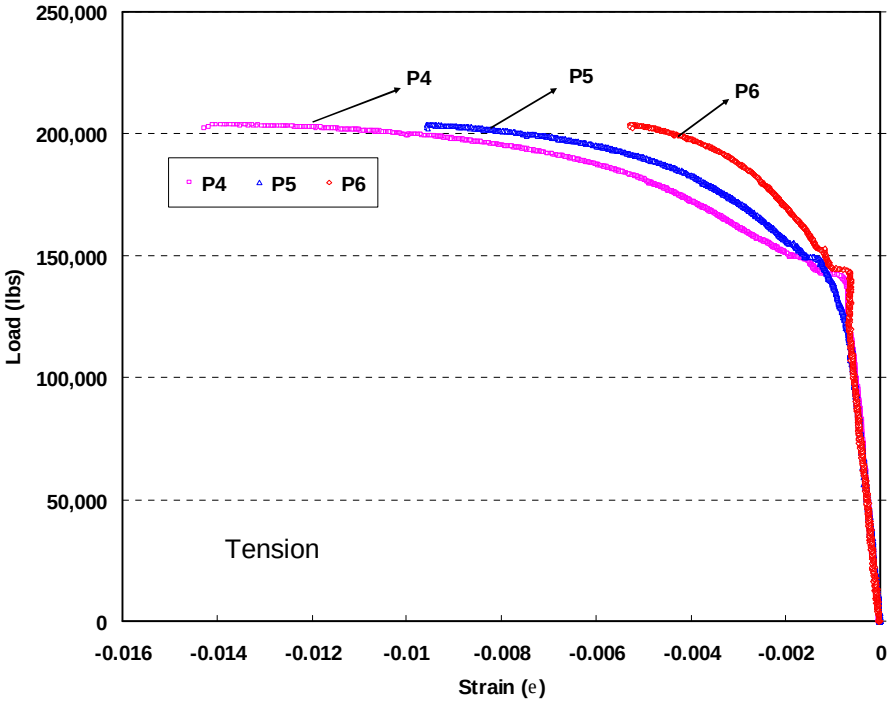

c) Strain at the bottom surface

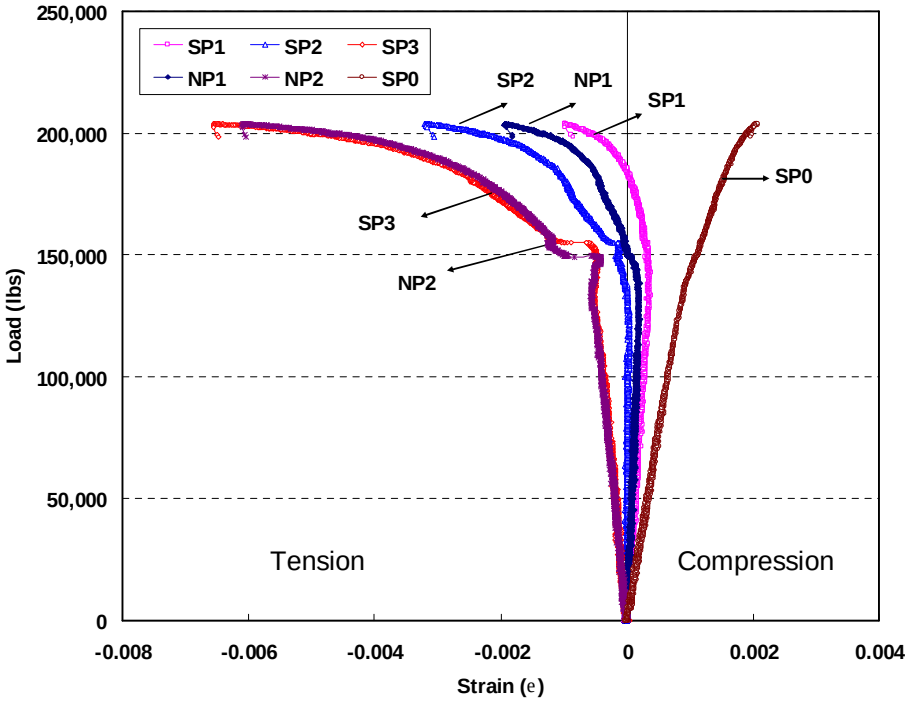

d) Strain at the side surface

Figure 4-14 (continued) Strain envelopes for18PS-N

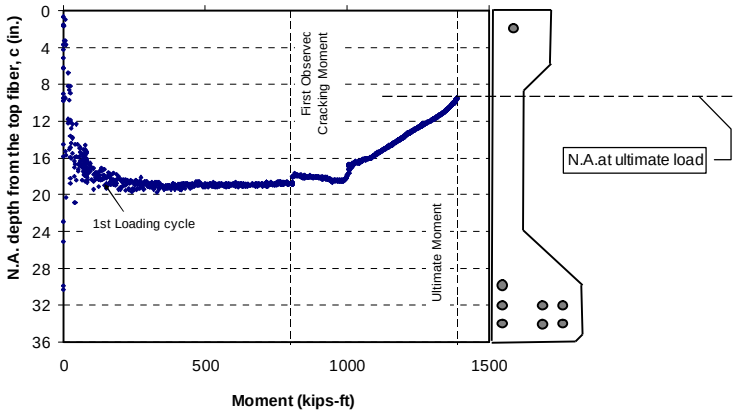

a) Moment-N.A. depth relationship for 10PS-N

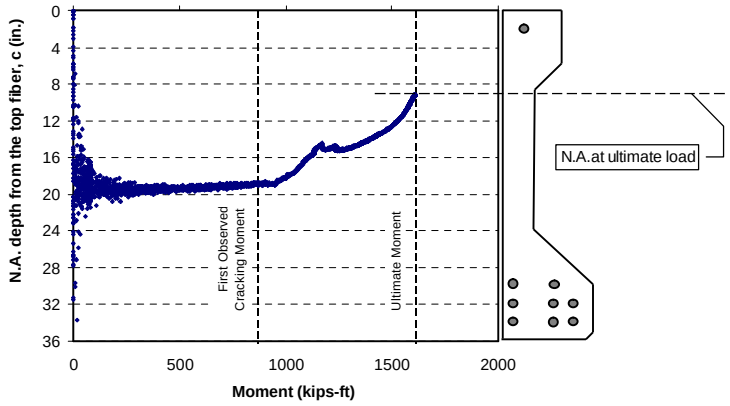

b) Moment-N.A. depth relationship for 14PS-N

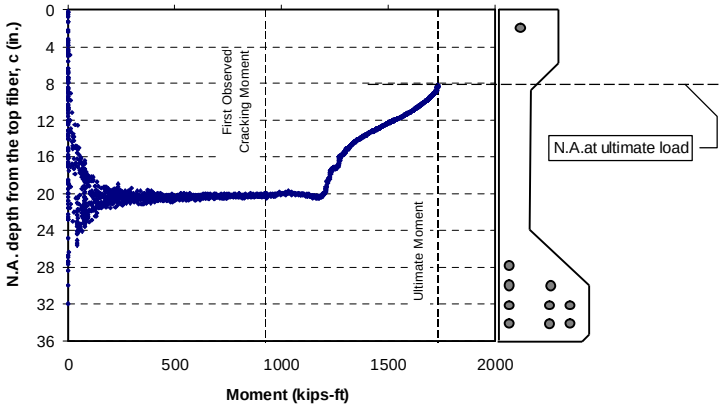

c) Moment-N.A. depth relationship for 18PS-N

Figure 4-15 Moment – N.A. depth location for 10PS - N, 14PS – N and 18PS - N

Figure 4-16 (a) shows a typical crushing failure mode for the AASHTO girder without a deck. Figure 4-16 (b) shows the typical deformed shape of the girders immediately after the girder concrete is crushed. Brittle failure of all three specimens was caused by the internal compressive force controlled by the HSC of the girders, as expected in the design.



a) Crushing of the flange concrete at failure

Figure 4-16 Typical failure modes for the AASHTO girder without deck



b) Deformed shape after failure

Figure 4-16 (continued) Typical failure modes for the AASHTO girder without deck

4.6.4 Ultimate Strain of Concrete

The ultimate strains of the concrete measured prior to failure of a specimen can be by whether the compression force was controlled by the normal strength concrete for a deck or by the high strength concrete for the girder.

The measured maximum strain of concrete at flexural failure is shown in Figure 4-17. These strains were based on reading of 5 strain gauges installed at the extreme top fiber of the concrete in the compressive zone. Results indicate that measured strain for girder with NSC deck slabs exceeds 0.003, as shown in the figure for concrete strength ranging from 4 to 6 ksi. The measured maximum ultimate strain for the girder without deck slabs was in the proximity of 0.003. These results indicate that the limiting strain, 0.003 for concrete in compression is acceptable for HSC up to 18,000 psi.

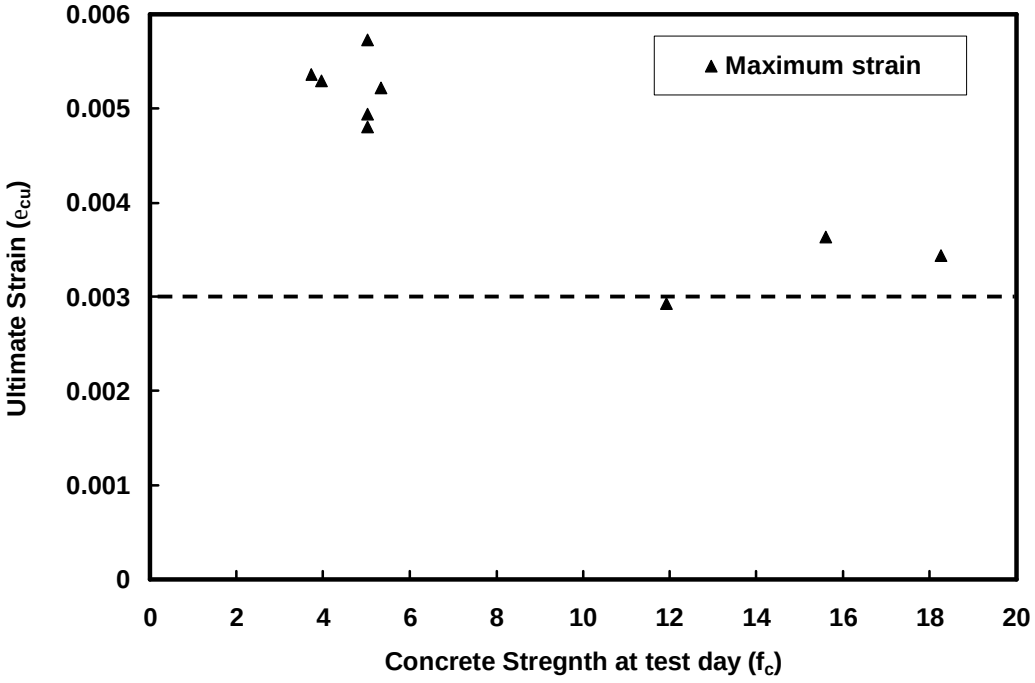

Figure 4-17 Ultimate strain at peak load for tested AASHTO girders

5 ANALYTICAL MODEL

5.1 INTRODUCTION

The major objective of this chapter is to validate the analytical models typically used for the flexural response of prestressed girders with and without concrete decks. Specifically, an analysis of the test results helps to validate the use of stress block parameters of the compressive concrete strength up to 18,000 psi. Moreover, the tests help verify the analytical models typically used for moment curvature and load deflections in prestressed girders subjected to flexure.

The measured flexural resistance and cracking resistance for each girder specimen under static loading conditions are validated by three analytical models, described in this chapter.

1. The ultimate flexural resistance and cracking resistance are determined by the AASHTO LRFD specifications (2004) with the measured concrete strength.

2. The ultimate flexural resistance and cracking resistance are calculated by the AASHTO LRFD specifications (2004) along with the measured concrete strength and the proposed equation for the elastic modulus discussed in Chapter 4.

3. A sectional analysis based on the actual measured material properties and prestress losses is used to predict the moment-curvature and load-deflection behavior of prestressed girders in flexure.

Generally accepted assumptions – i.e., plane sections remaining plane after deformation, force equilibrium and strain compatibility – are recognized in this study.

5.2 CODE PROVISONS

The required values used to determine flexural response, i.e., material properties and prestress losses, are discussed earlier in Section 4.2 and Section 4.3. This section, however, discusses the analytical model used to determine flexural strength and cracking strength based on the code conditions and recommended conditions found in the LRFD specifications.

5.2.1 Analysis of Flexural Cracking Strength

Once the initial load phase is applied, the initially observed cracking load on the specimens is recorded for each specimen. The initially observed cracking strength can be determined using the observed cracking load as follows:

$$M_{cr} = a \cdot (P/2), \qquad \textbf{Equation 5-1}$$

where

M_{cr} = observed cracking strength, ft.-kips;

a = length of shear span, ft.;

P = total applied load coincident with the first flexural crack, kips.

For the evaluation of the observed cracking strength in each specimen, this study considers two calculation methods; based on the design conditions and the recommended conditions. For the design conditions, the material properties for the specimens and prestress losses are determined by the LRFD equation (2004), as discussed in the design calculation shown in Table 5.3. For the recommended conditions, the revised equations for elastic modulus,

modulus of rupture and prestress losses are used. The equations used for computing flexural cracking strength are summarized in detail in Table 5.3.

The computed cracking strength based on the design and recommended equations is obtained using the following equation:

$$M_{cr} = S_{bc}\left(f_r + f_{ce} - f_{d/nc}\right), \qquad \textbf{Equation 5-2}$$

where

S_{bc} = composite section moduli;

f_r = modulus of rupture;

f_{ce} = compressive stress due to effective prestress only at the bottom fibers;

$f_{d/nc}$ = stress due to noncomposite dead loads.

As can be seen in Equation 5-2, the primary factors affecting the computed cracking strength are the modulus of rupture and the effective prestressing stress. Previously, as explained in Chapter 4, these factors of the equation were evaluated by the experimental program in this research.

The observed cracking moment during the first loading phase is used to assess the cracking moment ratio ($M_{measured}/M_{predicted}$) for three different calculations, as shown in Table 5.1. The following comparison shows that the computed results obtained from the AASHTO LRFD specifications, recommendations and measured values for estimating cracking strength provide an appropriate prediction in all cases. In particular, the recommended conditions

from this research provide more conservative results than the current AASHTO LRFD specifications (2004). As can be seen in the prestress losses comparison, the design conditions for prestress losses are slightly different between the LRFD specifications and the recommended conditions due to the use of different elastic modulus of concrete.

Table 5.1 Comparison between Observed and Computed Cracking Strength

I.D.	Experiment	Computed Cracking Strength					
		AASHTO LRFD		Recommendation		with measured value	
	(kips-ft)	(kips-ft)	Exp. /Pre.	(kips-ft)	Exp. /Pre.	(kips-ft)	Exp. /Pre.
10PS-5S	1097	1123	0.98	1061	1.03	1157	0.95
14PS-5S	1267	1314	0.96	1244	1.02	1189	1.07
18PS-5S	1377	1436	0.96	1373	1	1450	0.95
10PS-1S	935	974	0.96	922	1.01	959	0.98
14PS-1S	1054	1084	0.97	1034	1.02	1095	0.96
18PS-1S	1131	1183	0.96	1130	1	1111	1.02
10PS-N	799	751	1.06	708	1.13	800	1
14PS-N	867	843	1.03	796	1.09	879	0.99
18PS-N	918	964	0.95	908	1.01	814	1.13
Average			0.98		1.03		1.01
Standard. Dev.			0.04		0.05		0.06

The cracking moment ratio ($M_{measured}/M_{predicted}$) for the three different calculations is graphically shown in Figure 5-1. This figure clearly shows that the recommended conditions are applicable for the purpose of design, because the lower bound equation for the modulus

of rupture is recommended in this study. Therefore, the lower the modulus of rupture value, the more conservative the prediction.

Additionally, the computed cracking strength using the measured values provides more precise results compared to the other predicted values, except in the case of two specimens, 14PS-5S and 18PS-N. This finding may be due to the measured prestress losses. Recall that the measured prestress losses for 18PS-N are 21.7% of the initial prestressing force. This factor may result in the underestimation of the cracking strength of the specimens: the more the prestress losses, the less cracking strength. In addition, recall that the measured modulus rupture for 14PS-5S is 711 psi, which is the relatively lower modulus rupture result corresponding to the compressive concrete strength. This factor may result in the underestimation of the cracking strength.

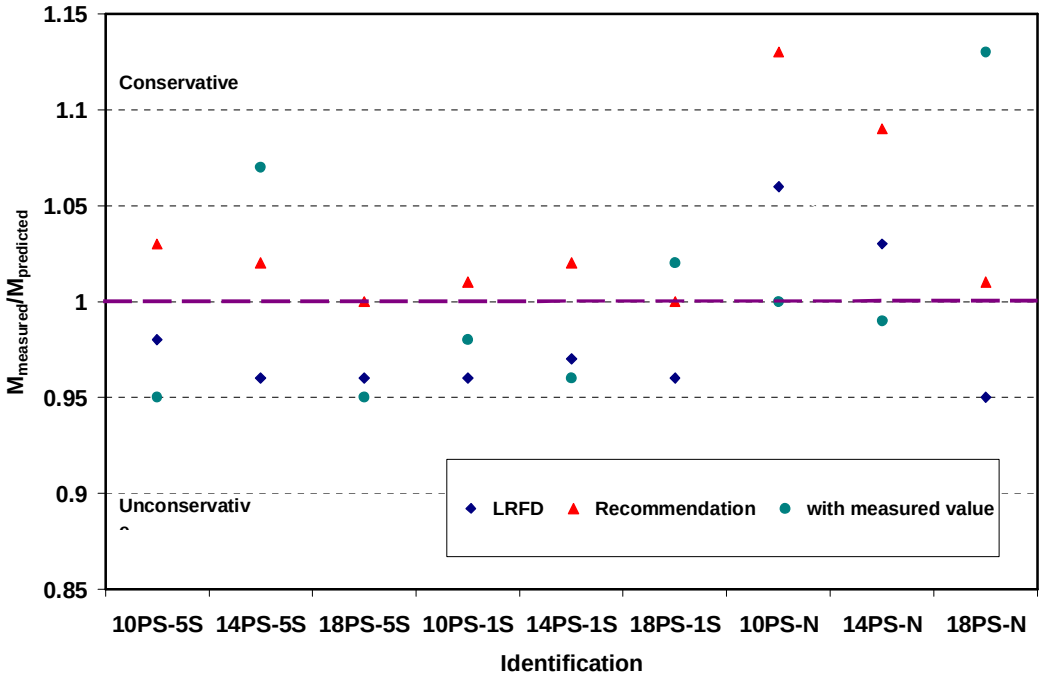

Figure 5-1 Cracking strength ratio for three different calculations

5.2.2 Analysis of Flexural Strength

Each girder is tested until failure under static loads to determine its nominal flexural strength. The observed flexural strength for each specimen can be determined using the following equation:

$$M_n = a \cdot (P/2) + M_D \,, \qquad \textbf{Equation 5-3}$$

where

M_n = observed flexural strength, ft.-kips;

a = length of shear span, ft.;

P = total applied load at ultimate load, kips; and

M_D = dead load moment.

According to Section 5.7.3 in the LRFD specifications (2004), a T-shape member subjected to flexure can be analyzed as a rectangular section if the distance $a = \beta_1 c$ from the extreme compression fiber is no less than the flange thickness, h_f, in which the distance c shall be measured perpendicular to the neutral axis, and the distance a can be determined by the force equilibrium condition using the approximate stress distribution. The flexural moment may be computed by using the following equations, described in Table 5.2.

Table 5.2 Calculation Method for the Flexural Strength

	AASHTO LRFD specifications (2004)	**NCHRP 12-64 (2006)**
The average stress in prestressing steel, f_{ps} f_{pe} is not less than 0.5 f_{pu}	$f_{ps} = f_{pu}\left(1-k\frac{c}{d_p}\right)$ in which : $k = 2\left(1.04 - \frac{f_{py}}{f_{pu}}\right)$	
For rectangular section behavior	$c = \frac{A_{ps}f_{pu} + A_s f_y - A_s' f_y'}{0.85 f_c' \beta_1 b + kA_{ps}\frac{f_{pu}}{d_p}}$	$c = \frac{A_{ps}f_{pu} + A_s f_y - A_s' f_y'}{a_1 f_c' b_1 b + kA_{ps}\frac{f_{pu}}{d_p}}$
For rectangular section, the nominal flexural resistance , in which case b_w shall be taken as b	$M_n = A_{ps}f_{ps}\left(d_p - \frac{a}{2}\right) + A_s f_y\left(d_s - \frac{a}{2}\right) - A_s' f_y'\left(d_s' - \frac{a}{2}\right) + 0.85 f_c'(b-b_w)h_f\left(\frac{a}{2} - \frac{h_f}{2}\right)$	$M_n = A_{ps}f_{ps}\left(d_p - \frac{a}{2}\right) + A_s f_y\left(d_s - \frac{a}{2}\right) - A_s' f_y'\left(d_s' - \frac{a}{2}\right) + a_1 f_c'(b-b_w)h_f\left(\frac{a}{2} - \frac{h_f}{2}\right)$

A_s = area of mild steel tension reinforcement (in.^{2});

A'_s = area of compression reinforcement (in.^{2});

A_{ps} = area of prestressing steel (in.^{2});

f_{pu} = specified tensile strength of prestressing steel (ksi);

f_{py} = yield strength of prestressing steel (ksi);

f_y = yield strength of tension reinforcement (ksi);

f'_y = yield strength of compression reinforcement (ksi);

b = width of the compression face of the member (in.);

b_w = width of web (in.);

c = distance between the neutral axis and the compressive face (in.);

d_p = distance from extreme compression fiber to the centroid of the prestressing tendons (in.);

d_s = distance from extreme compression fiber to the centroid of nonprestressed tensile reinforcement (in.);

d'_s = distance from extreme compression fiber to the centroid of compression reinforcement (in.);

f'_c = specified compressive strength of concrete at 28 days, unless another age is specified (ksi);

β_1 = stress block factor;

h_f = compression flange depth of an I or T member (in.);

a = $c\beta_1$; depth of the equivalent stress block (in.)

The parameters of the stress-strain distribution in the compressive zone of concrete – k_1, k_2, k_3, α_1 and β_1 – are used to determine the ultimate flexural resistance in both the ACI 318-05 and AASHTO-LRFD specifications (2004). k_1 is the ratio of average compressive stress to maximum compressive stress. k_2 is the ratio of the distance from the extreme fiber to the resultant of the compressive force to the neutral axis. k_3 is the ratio of the compressive strength of the flexural test to the compressive strength of the cylinder test. α_1 and β_1 can be obtained by using the relationships of k_1, k_2, and k_3 as follows:

$$a_1 = \frac{k_1 k_3}{2k_2} \quad \text{and} \qquad \textbf{Equation 5-4}$$

$$b_1 = 2k_2. \qquad \textbf{Equation 5-5}$$

Both the ACI and AASHTO specifications use these parameters to generalize the equivalent rectangular stress block for the compressive stress distribution in concrete. The current specification is defined such that the α_1 parameter has a constant value of 0.85, and states that "β_1 shall be taken as 0.85 for concrete strength, f'_c, up to and including 4,000 psi. For strengths above 4,000 psi, β_1 shall be reduced continuously at a rate of 0.05 for each 1,000 psi of strength in excess of 4,000 psi, but β_1 shall not be taken as less than 0.65." These parameters considered to be validated up to 10,000 psi concrete strength. As part of the NCHRP 12-64 research project, the experimental study for the equivalent rectangular stress block for HSC up to 18,000 psi concrete strength has been investigated by NCHRP12-64 (2006) at North Carolina State University. On the basis of the NCHRP 12-64 research findings, the research team proposes that the equivalent rectangular stress block parameters,

α_1, shall be taken as 0.85 for concrete strengths not exceeding 10,000 psi. For concrete strengths exceeding 10,000 psi, α_1 shall be reduced at a rate of 0.02 for each 1,000 psi of strength in excess of 10,000 psi, except that α_1 shall not be taken to be less than 0.75. The proposed equation for α_1 is as follows:

$$a_1 = \begin{Bmatrix} 0.85 & for & f_c' \le 10ksi \\ 0.85 - 0.02(f_c' - 10) \ge 0.75 & for & f_c' > 10ksi \end{Bmatrix}. \quad \textbf{Equation 5-6}$$

The data in the literature and the test results from this research indicate that the equation for β_1 specified by the ACI 318 and AASHTO LRFD Bridge Design Specifications is still valid for the compressive strength in concrete up to 18,000 psi (Mertol, 2006). Therefore, the equation for β_1 can be specified as follows:

$$b_1 = \begin{Bmatrix} 0.85 & for & f_c' \le 4ksi \\ 0.85 - 0.05(f_c' - 4) \ge 0.65 & for & f_c' > 4ksi \end{Bmatrix}. \quad \textbf{Equation 5-7}$$

In addition to these proposed equivalent rectangular stress block parameters investigated by NCHRP 12-64 (2006), the recommended equations for material properties and prestress losses for HSC to evaluate the flexural behavior in this study are shown in Table 5.3.

As described earlier in this chapter, Table 5.3 shows the final three design calculation methods, including the sectional analysis method discussed in the following section.

Table 5.3 Comparison of Design Calculation

		Design Calculation		
		AASHTO LRFD Specifications	**Recommended Method**	**Section Analysis**
Concrete	**f_c**	C.C.S at test day	C.C.S at test day	Measured Results
	E_c	$E_c = 33{,}000\, w_c^{1.5}\, \sqrt{f_c'}$	$E_c = w_c^{2.5} \cdot (f_c')^{0.33}$	
	f_r	$7.5\sqrt{f_c}$ psi	$6\sqrt{f_c}$ psi	
Prestressing Strands	**f_{ps}**	$f_{pu}\left(1-k\frac{c}{d_p}\right)$	$f_{pu}\left(1-k\frac{c}{d_p}\right)$	
Prestress Loss		Tadros Eq., (2003)	Tadros Eq., (2003)	
Stress Block	**HSC**	Not available but α_1: 0.85, β_1: 0.65 Used in this study	α_1: $0.75 \le 0.85-(f_c-10\text{ ksi})0.02 \le 0.85$ β_1: 0.65	Strain Compatibility
	HSC & NSC	Not available	Base on the deck concrete	
	NSC	α_1:0.85, β_1:$0.65 \le 0.85-(f_c-4\text{ ksi})0.05 \le 0.85$	α_1:0.85, β_1:$0.65 \le 0.85-(f_c-4\text{ ksi})0.05 \le 0.85$	

C.C.S. is the cylinder concrete strength

5.2.2.1 AASHTO Girders with a 5 ft. Wide Deck

For a composite girder section in which the neutral axis is located within the deck, the nominal flexural moment, M_n of such specimens can be determined using the AASHTO LRFD specifications. The design compressive strengths of concrete for the three girders are 10,000, 14,000 and 18,000 psi. The design strength of concrete for the deck slab is 4,000 psi. In these cases, the neutral axis is located at the deck, and the compression force is developed in the NSC. The nominal flexural resistance, M_n, is computed by using the concrete compressive strength of the deck, as shown in Figure 5-2.

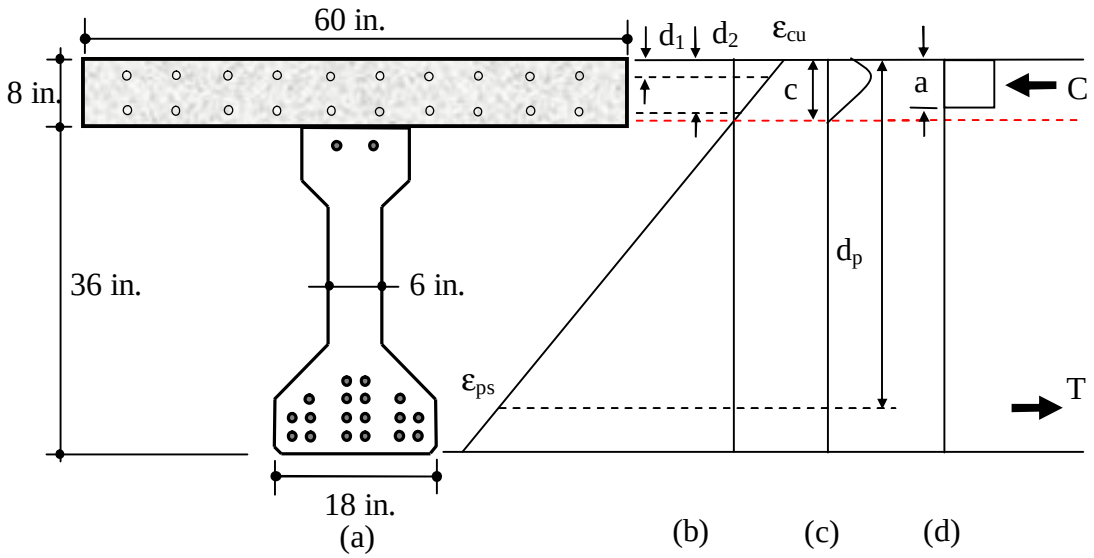

Figure 5-2 Compressive stress distribution (a) cross-section; (b) strain compatibility; (c) meausred strain-stress distribution in compression zone; (d) equivalent rectangular stress block in compression zone

The flexural resistance of the composite girder with flanged sections depends on whether the neutral axis is located within the flange or within the girder. If the neutral axis depth (c) is greater than the thickness of the deck, the composite girder displays a T-section behavior.

However, this configuration, seen in Figure 5-2 (b), shows that the neutral axis is located within the deck. Therefore, the composite girder is considered as a rectangular section. The stress block parameters for computing the flexural strength of the composite AASHTO girders can be determined by the AASHTO LRFD specifications (2004), as given in Table 5.2. Test results, as discussed in Section 4.5.1, confirm that the neutral axis is located within the deck at failure. Comparisons of the three analytical models – LRFD specifications, recommendations and section analyses – are given in Table 5.4.

Table 5.4 Design Calculations for Composite AASHTO Girders with a 5ft Wide Deck

I.D.	Experiment	Computed Flexural Strength					
		AASHTO LRFD		Recommendation		Section analysis	
	(kips-ft)	(kips-ft)	Exp. /Pre.	(kips-ft)	Exp. /Pre.	(kips-ft)	Exp. /Pre.
10PS-5S	2123	1904	1.12	1904	1.12	1977	1.07
14PS-5S	2349	2181	1.08	2181	1.08	2246	1.05
18PS-5S	2543	2344	1.08	2344	1.08	2445	1.04

The experimental results provide an 8 to 12% greater strength than the computed flexural strength in the AASHTO LRFD specifications and the recommended design calculations. On the other hand, the computed flexural strength in the section analysis provides the more accurate results in the range of 4 to 7 percent. It is generally accepted that the flexural behavior of concrete structures with NSC correlates well with the design calculations.

5.2.2.2 AASHTO Girders with a 1 ft. Wide Deck

For a composite girder section, in which the neutral axis is located below the deck, typically two types of concrete compressive strength in the compression zone must be considered. However, the current AASHTO specifications (2004) do not specify the design method to determine flexural strength with two types of concrete in the compression zone.

Figure 5-3 shows the stress distribution of the composite girder section in which the neutral axis is located below the deck. As shown in Figure 5-3 (b), because the neutral axis is located below the deck, the actual compressive stress, seen in Figure 5-3 (c), is distributed starting from the flange of the girder with HSC to the NSC deck. Once the simplified stress distribution is considered with only the stress distribution of the deck concrete, as shown in Figure 5-3 (d), the location of the compressive resultant force moves downward slightly due to an increase in the neutral axis depth. It may results in slight reduction of the lever arm of the flexural moment. Therefore, the resultant decrease in flexural moment provides conservative, yet quite accurate results. Finally, the equivalent rectangular stress block is created using the simplified compressive stress distribution, as given in Figure 5-3 (e).

For the composite girder section that has a relatively small deck flange, as well as two types of compressive strength subjected to the flexure, the nominal flexural resistance, M_n, may be determined by using the AASHTO LRFD specifications, as listed in Table 5.2, with an analysis based on the compressive strength of the deck concrete, which is usually lower than that of the girder concrete.

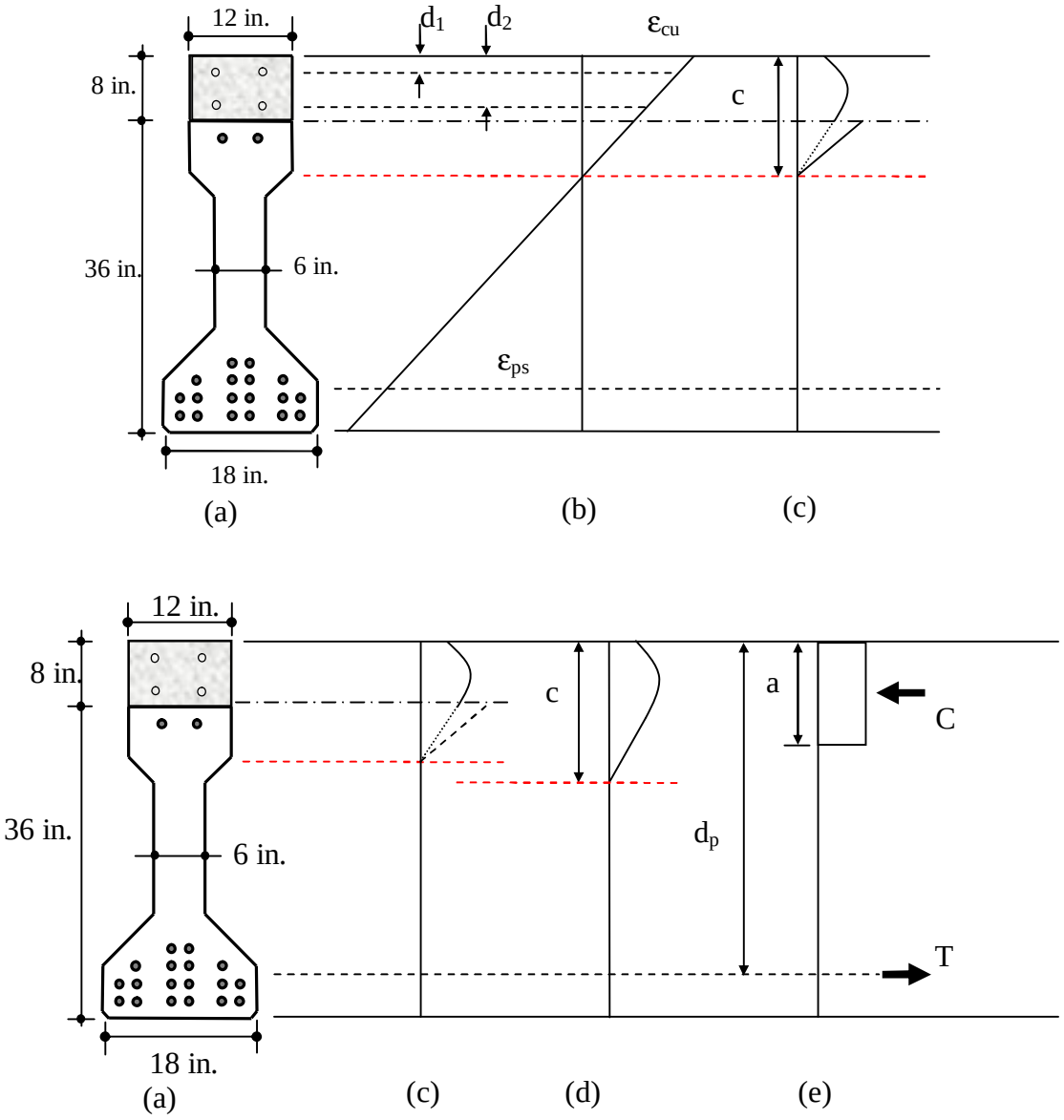

Figure 5-3 Compressive stress distribution (a) cross-section; (b) strain compatibility (c) measured strain-stress distrubution in compression zone, (d) simplified stress distribution (e) the equvalent rectagular stress block

A comparison between the measured flexural strength and the design calculation based on code provisions and recommendations is shown in Table 5.5. The computed flexural strength based on the section analysis is also given in the table.

Table 5.5 Design Calculation for Composite AASHTO Girders with a 1 ft. Wide Deck

I.D.	Experiment	Computed Flexural Strength					
		AASHTO LRFD		Recommendation		Section Analysis	
	(kips-ft)	(kips-ft)	Exp. /Pre.	(kips-ft)	Exp. /Pre.	(kips-ft)	Exp. /Pre.
10PS-1S	1752	N.A	-	1558	1.12	1735	1.01
14PS-1S	1941	N.A	-	1706	1.14	1928	1.01
18PS-1S	2083	N.A	-	1830	1.14	2107	0.99

These results confirm that the recommended method to determine the nominal flexural resistance, M_n, is reasonably conservative. However, the predicted nominal flexural resistance based on the section analysis method using the measured material properties and prestress losses shows more accurate results.

5.2.2.3 AASHTO Girders without a Deck

For a girder section in which the neutral axis is located within the flange, in the same manner as Section 5.2.2.1, the nominal flexural moment of such specimens can be determined using the AASHTO LRFD specifications. However, the current AASHTO LRFD specifications (2004) have limits that restrict the use of α_1 and β_1 over 10,000 psi compressive concrete strength. According to the part of NCHRP 12-64 (2006), the proposed equivalent rectangular stress block parameters for HSC up to 18,000 psi was conducted to determine the flexural strength for HSC girders. Figure 5-4 indicates the stress distribution of the girder section in

which the neutral axis is located within the flange of the girder and that can be computed as a rectangular section.

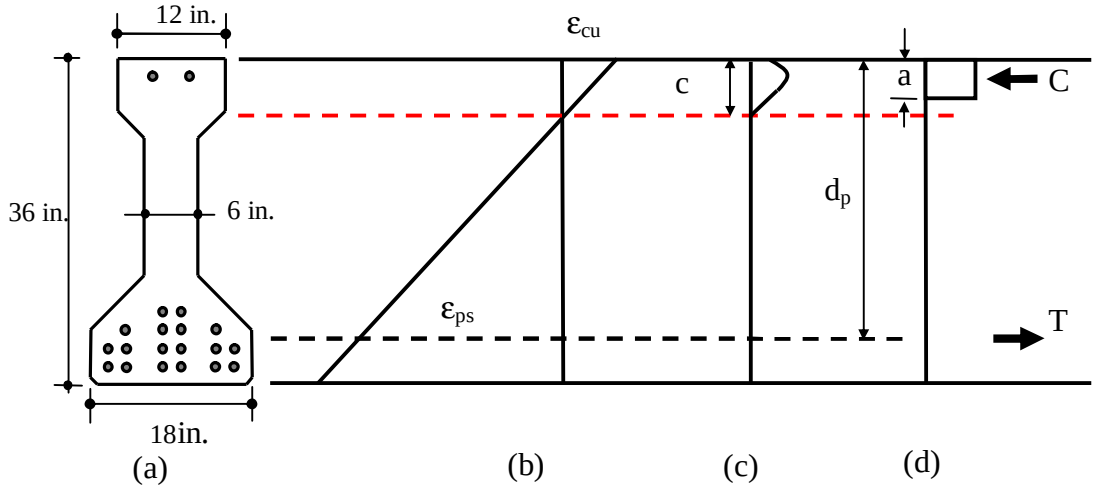

Figure 5-4 Compressive stress distribution (a) cross-section; (b) strain compatibility; (c) measured strain-stress distribution in compression zone; (d) equivalent rectangular stress block

The flexural resistance of the HSC girder can be calculated using the same equation addressed in Table 5-2, with the exception of the rectangular stress block parameters. As described previously in Section 5.2.2, the factor, a_1 , shall be taken as 0.85 for concrete strengths not exceeding 10,000 psi. For concrete strengths exceeding 10,000 psi, a_1 shall be reduced at a rate of 0.02 for each 1,000 psi of strength in excess of 10,000 psi, except that a_1 shall not be taken to be less than 0.75. The test results in this research and in the literature indicate that the equation for b_1, specified by ACI 318 and AASHTO LRFD Bridge Design Specifications, is still valid for HSC up to 18,000 psi (NCHRP 12-64, 2006).

A comparison between the measured flexural strength and the design calculation based on the code provisions and recommendations is shown in Table 5.6. The computed flexural strength based on the sectional analysis is also given in the same table.

Table 5.6 Design Calculation for AASHTO Girders without a Deck

I.D.	Experiment	Computed Flexural Strength					
		AASHTO LRFD		Recommendation		Section Analysis	
	(kips-ft)	(kips-ft)	Exp. /Pre.	(kips-ft)	Exp. /Pre.	(kips-ft)	Exp. /Pre.
10PS-N	1465	1334	1.10	1324	1.11	1433	1.02
14PS-N	1688	1548	1.09	1519	1.11	1623	1.04
18PS-N	1808	1723	1.05	1692	1.07	1813	1.00

As indicated in Table 5.6, the calculated flexural strength using the AASHTO LRFD specifications is slightly less conservative than that using the recommended conditions due to the reduced a_1 value. The calculated flexural strength shows that the reduced a_1 value assures the safety of the flexural strength of AASHTO girders with HSC. For the section analysis, the computed flexural strength using actual material properties and prestress losses provides the most accurate prediction.

5.2.3 Failure Evaluation

The failure evaluation provides a comprehensive behavior analysis of the prestress girder. This evaluation provides the potential to capture the flexural behavior of the tested girder

specimens. Figure 5-5 gives the failure evaluation, which is the moment ratio for the mid span applied moment at the continuous loading stage and the computed nominal flexural resistance using the current AASHTO LRFD specifications. The applied load does not include the dead load.

As described in the previous section, all of the specimens with three configurations of the neutral axis location can be determined using the current LRFD specifications (2004) except in the case of a composite girder section in which the neutral axis is located below the deck, as discussed previously. For this failure evaluation, the flexural strength is computed using the recommended method based on the LRFD design conditions set out in Table 5.3. Figure 5-5 includes a representation of each phase of the girders, 18PS-5S, 10PS-1N, and 18PS-N.

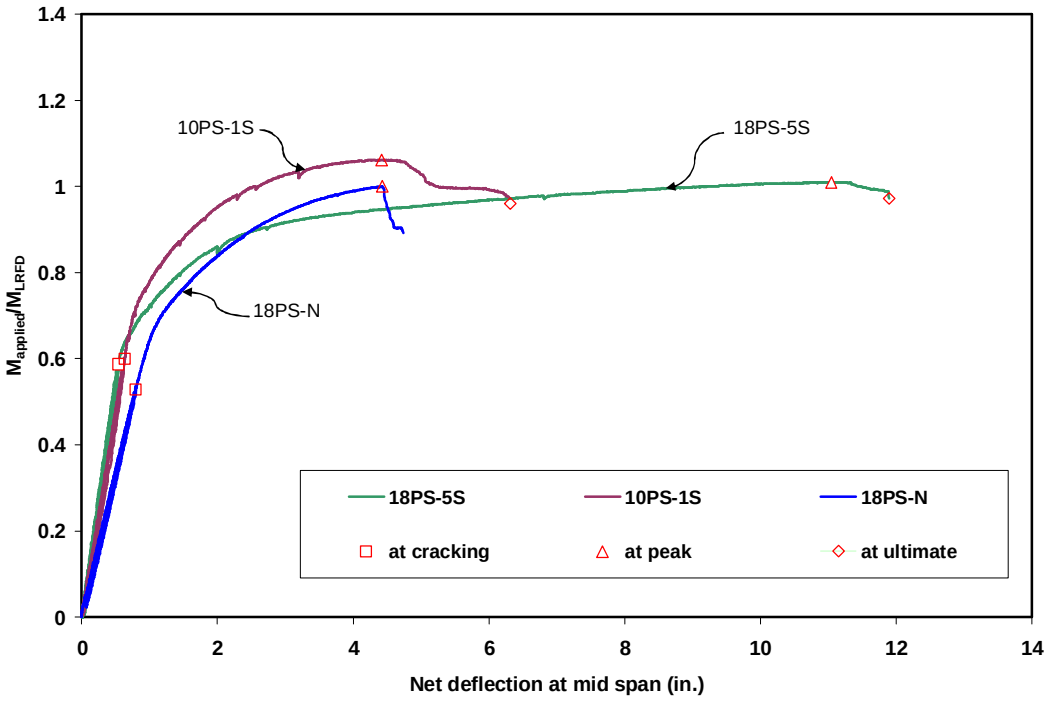

Figure 5-5 Failure evaluation for each configuration

It is difficult to draw general conclusions given the limited number of test results. As shown in Table 5.7, it can be concluded that the initial cracking of the tested specimens is approximately 60 percent of the flexural resistance using the current AASHTO LRFD specifications. This range of the load may be considered as the service loading condition. The calculated ultimate moment at the peak load is an average of 4 percent greater than the computed flexural resistance using the LRFD specifications.

Table 5.7 Failure Evaluation for All Specimens

I.D.	M_{LRFD}	M_{cr} (observed)	M_{cr}/M_{LRFD}	M_{peak} (at mid span)	M_{peak}/M_{LRFD}
10PS-5S	1904	1097	0.58	1947	1.02
14PS-5S	2181	1267	0.58	2172	1.00
18PS-5S	2344	1377	0.59	2366	1.01
10PS-1S	1558	935	0.60	1655	1.06
14PS-1S	1706	1054	0.62	1845	1.08
18PS-1S	1830	1131	0.62	1986	1.09
10PS-N	1334	799	0.60	1388	1.04
14PS-N	1548	867	0.56	1611	1.04
18PS-N	1723	918	0.53	1731	1.00
Average			0.59		1.04
St. Dev.			0.027		0.033

5.3 SECTIONAL ANALYSIS

The computed ultimate flexural strength based on the sectional analysis is presented in Section 5.2.2. This Section 5.3 presents a sectional analysis procedure to compute the moment-curvature and load-deflection behavior of prestressed girders subjected to flexure. Before conducting the sectional analysis, the material properties used in this experimental study need to be defined using the proper equations.

5.3.1 Flexural Model

For the sectional analysis, the material properties for the concrete and the prestressing strands used for the AASHTO girders tested under static loading conditions are determined by testing representative concrete cylinders and prestressing strands, as discussed in Chapter 3. The measured stress-strain curves for the concrete and the strands are used to gain accurate material properties to be input into the analytical model. The material models are used to generate a best fit to the experimentally determined stress-strain curves.

Based on the assumption that a plane remains in a plane after deformation, the strain profile at any depth through the section can be determined from two variables: the strain of the top surface of concrete (ε_c) and the depth of the neutral axis (c), as shown in Figure 5-6. The corresponding curvature is defined as:

$$f = \frac{e_c}{c}. \qquad \textbf{Equation 5-8}$$

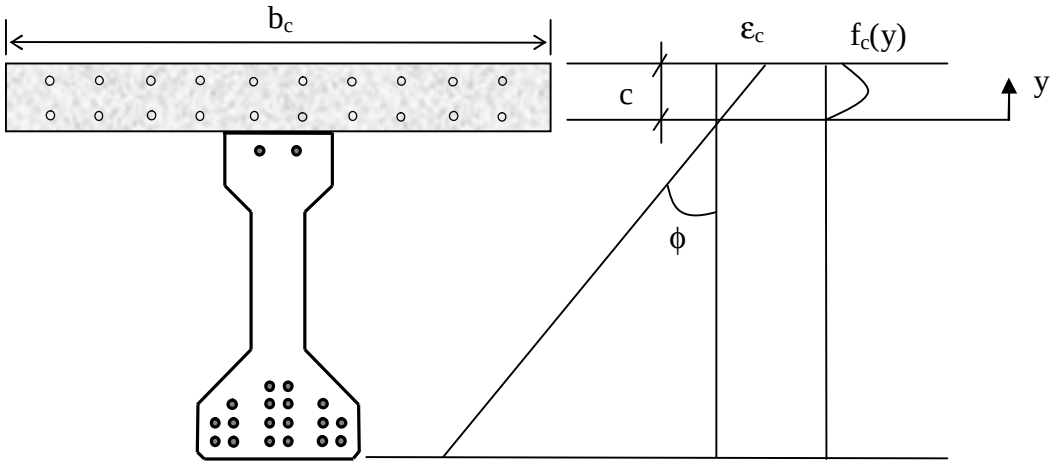

Figure 5-6 Cross-section and assumed strain profile for 18PS - 5S

Once the strain in the extreme compression fiber (ε_c) is fixed, the force distribution of concrete, F_c, can be determined by the force equilibrium conditions with the variable, c. The force contribution, F, of the different materials at a given section can be determined by the integrating the stress profile into the equation.

First of all, the force contribution of the deck concrete, F_c, can be determined by the following equation:

$$F_c = \int_0^c b_c(y) \cdot f_c(y) dy, \qquad \textbf{Equation 5-9}$$

where $b_c(y)$ is the width of the deck, which is generally constant; c is the assumed neutral axis depth; and $f_c(y)$ is the stress distribution of the deck concrete.

Popovic's equation, presented in Collins and Mitchell (1991) to model the stress-strain curve of concrete, is used for this research. The stress in the concrete can be calculated using the equation, as follows:

$$f_c(y) = \frac{f_c' \cdot n \cdot (e_c(y)/e_c')}{n - 1 + (e_c(y)/e_c')^{nk}}, \qquad \textbf{Equation 5-10}$$

f_c' = the maximum strength of the concrete;

ε_c' = the corresponding strain; and n is a curve fitting factor defined as $E_c/(E_c-E_c')$, where E_c is the initial tangent modulus of the concrete and $E_c' = f_c'/\varepsilon_c'$; and

k = The post-peak decay in the concrete stress is defined by the curve fitting factor.

If the strength of the concrete, f_c', is the only known parameter, the remaining factors can be calculated from the following relationships:

$$E_c = 40{,}000\sqrt{f_c'} + 1{,}000{,}000,$$
$$n = 0.8 + \frac{f_c'}{2{,}00},$$
$$e_c' = \frac{f_c'}{E}\frac{n}{n-1} \quad \textit{and}$$
$$k = 0.67 + \frac{f_c'}{9{,}000} \qquad \textbf{Equation 5-11}$$

with f_c' in units of psi.

Alternatively, the values of f_c', ε_c', E_c and E_c' can be determined directly if the full stress-strain curve of a characteristic concrete cylinder is obtained experimentally. The value of k can then be determined from the measured post-peak stress-strain data to provide a best fit.

Consequently, the force contribution of the concrete, F_c, can be expressed by substituting Equation 5-11 into Equation 5-9, as follows:

$$F_c = b_c \int_0^c \frac{f_c' \cdot n \cdot (e_c(y)/e_c')}{n-1+(e_c(y)/e_c')^{nk}} dy \,. \qquad \textbf{Equation 5-12}$$

The material properties for the concrete used for the nine specimens tested under static loading conditions are determined by testing representative concrete cylinders, as discussed in Chapter 3. The measured stress-strain curves for the concrete and the steel are used to obtain the material properties to be used in the analytical model. The material models for concrete are used to generate a best fit of the experimentally determined stress-strain curves. Two cylinders from each girder specimen were tested to determine the stress-strain relationship of the concrete and a best-fit curve until failure at the final loading stage. Figure 5-7 represents the measured stress-strain curve of the cylinders as well as the best fits of the measured data from 10PS-5S. The coefficients used for the concrete material model are presented in Table 5.8. The remaining best-fit curves for each specimen are given in Appendix I.

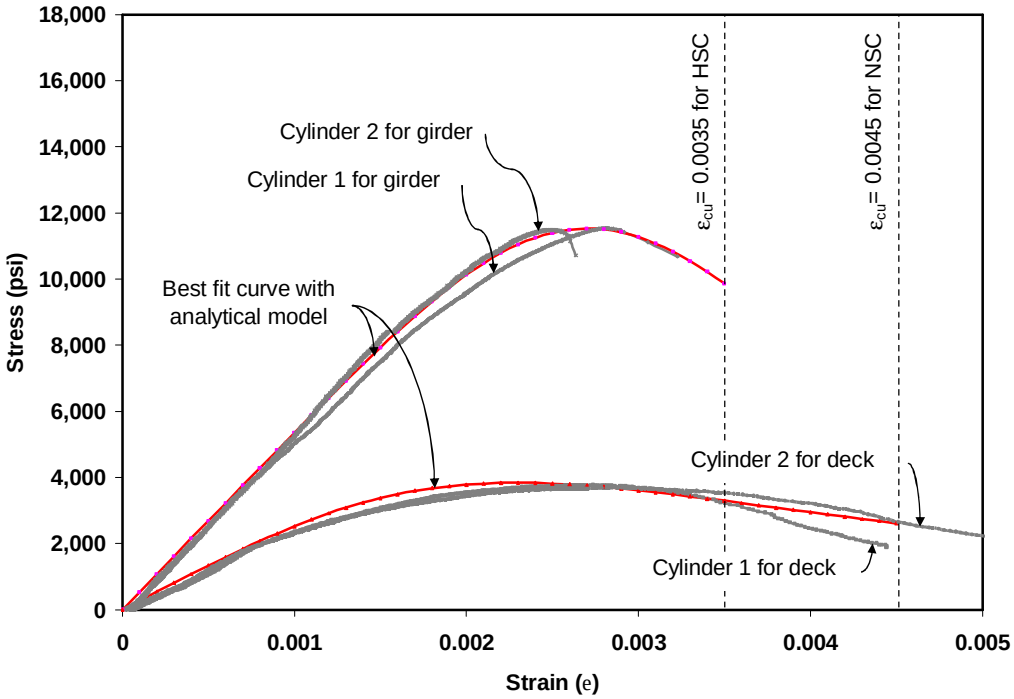

Figure 5-7 Measured stress-strain behavior of 10PS-5S and a best-fit curve with analytical model

Table 5.8 Concrete Material Model for the Specimens

	10PS-5S		14PS-5S		18PS-5S	
	Girder	**Deck**	**Girder**	**Deck**	**Girder**	**Deck**
Peak Strength, f'_c (psi)	11,520	3,730	15,900	5,340	17720	3,960
Strain at peak, e'_c	0.0026	0.0028	0.0033	0.0028	0.0032	0.0026
Elastic modulus, E_c (ksi)	5,364	2,692	5,557	3,301	5,969	2,656
Fitting Factor, n	5.28	2.01	7.79	2.43	13.13	2.34
Post peak, k	0.92	1.32	0.85	1.26	1.05	1.09
	10PS-1S		**14PS-1S**		**18PS-1S**	
	Girder	**Deck**	**Girder**	**Deck**	**Girder**	**Deck**
Peak Strength, f'_c (psi)	13,340	5,030	15,470	5030	14,430	5,030
Strain at peak, e'_c	0.0029	0.0031	0.0035	0.0031	0.0034	0.0031
Elastic modulus, E_c (ksi)	5,626	2,767	5,441	2,767	5,626	2,767
Fitting Factor, n	5.38	2.42	5.30	2.42	3.92	2.42
Post peak, k	0.38	1.06	1.02	1.06	0.66	1.06
	10PS-N		**14PS-N**		**18PS-N**	
	Girder		**Girder**		**Girder**	
Peak Strength, f'_c (psi)	11,930		15,610		18,270	
Strain at peak, e'_c	0.0027		0.0033		0.0035	
Elastic modulus, E_c (ksi)	5,534		5,325		6,019	
Fitting Factor, n	4.97		9.85		7.40	
Post peak, k	0.88		0.12		0.95	

Secondly, the force contribution of the prestressing strand, F_{pe}, can be determined by

$$F_{ps} = \sum A_{ps}(n) \cdot f_{ps}(y), \qquad \textbf{Equation 5-13}$$

where $A_{ps}(n)$ is the area of the prestressing strand at the nth layer, and $f_{ps}(y)$ is the stress distribution of a prestressing strand.

The actual material properties for the prestressing strands are provided by the supplier, as described in Chapter 3. For the purpose of the analytical modeling of the prestressing strands, the Ramberg-Osgood equation, given in Collins and Mitchell (1997), is used to model the tension behavior of the prestressing strand, as follows:

$$f_{ps} = E_{ps} e_{ps} \left\{ A + \frac{1 - A}{\left[1 + (Be_{ps})^{C}\right]^{1/C}} \right\} \leq f_u, \qquad \textbf{Equation 5-14}$$

where f_{ps} is the prestressing steel tensile stress; E_{ps} is the elastic modulus of the strand; and e_{ps} is the tensile strain of the strand. The four factors, A, B, C and E_{ps}, can be determined from the actual stress-strain curve.

Figure 5-8 shows the definition of each parameter in the stress-strain curve. Based on the defined parameters, the stress-strain curve of the prestressing strand used for the analytical model is generated in Figure 5-9. As given in Section 3.5.3, the ultimate elongation is 4.5%. The generated stress-strain curve shown in Figure 5-9 matches well with the measured stress-strain curve.

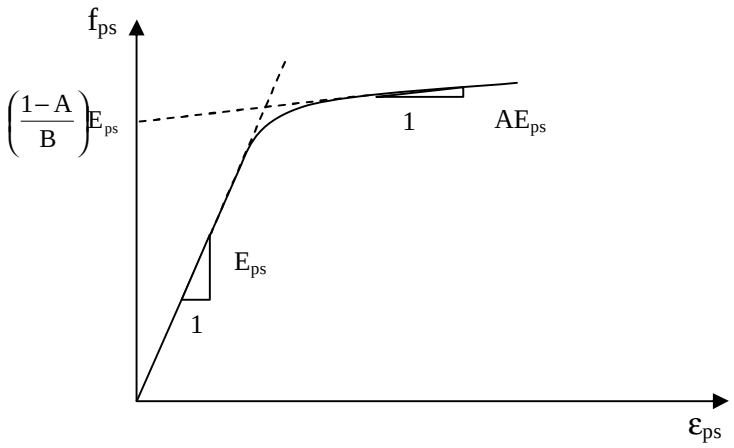

Figure 5-8 Definition of the four factors adopted from Collins (1997)

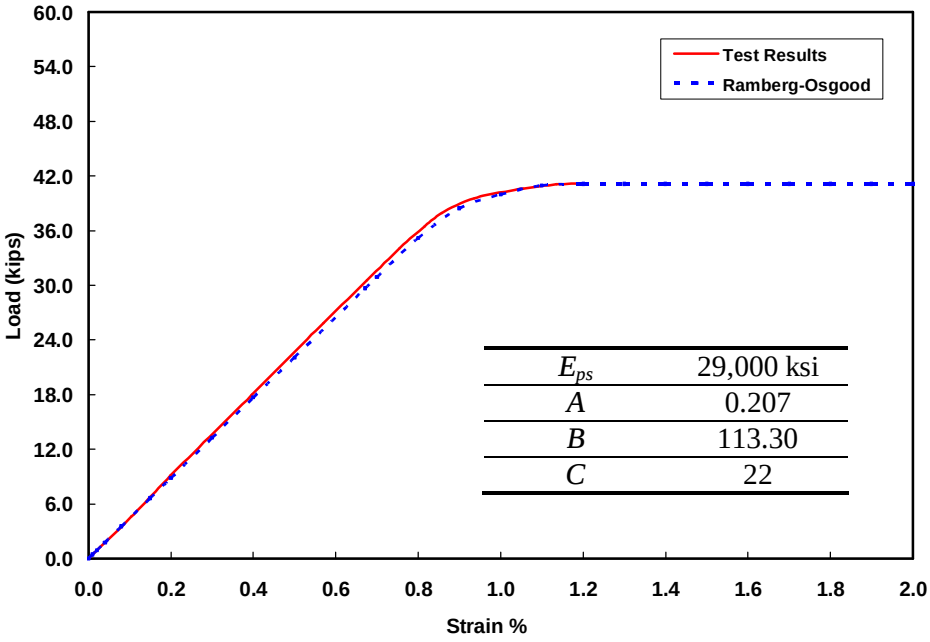

Figure 5-9 Analytical modeling of the prestressing strand

For simplification, due to the minor role of the force contribution, the longitudinal reinforcement in the deck can be calculated using a bilinear relationship, described as

$$F_s(y) = A_s \cdot f_s(y), \qquad \textbf{Equation 5-15}$$

where A_s is the area of the longitudinal reinforcement in the deck concrete and $f_s(y)$ is the stress of the steel. Typically, the elastic modulus of steel, E_s, is 29,000 ksi, and the yield stress, f_y, is 60 ksi.

5.3.2 Flexural Behavior

After the section properties have been defined, as described above, the moment-curvature and the load-deflection response are determined by using the layer-by-layer approach. Once the moment-curvature response of the section is calculated, the load-deflection response of a beam under known loading and support conditions can be determined by integrating the curvature into the given moment value.

Once the strain in the extreme compression fiber (ε_c) is fixed, the force distribution of each material in the section can be determined by the force equilibrium conditions with the variable, c. For the first equilibrium equation, the resultant force acting on the section should be equal to zero, if there is no axial load, *N*.

$$N = F_c + F_s + \sum F_{ps} \quad \text{.} \qquad \textbf{Equation 5-16}$$

Here, the neutral axis depth, c, can be determined using the first equilibrium equation. For the second equilibrium equation, the flexural moment can be taken at the location of the neutral axis depth from the top fiber.

$$M = F_c \cdot y_1 + F_s \cdot y_2 + \sum F_{ps} \cdot y_n \quad \text{,} \qquad \textbf{Equation 5-17}$$

where F_c = the force contribution of concrete; y_1 = the distance from the location of the neutral axis to the location of the resultant force of concrete; F_s = the force contribution of the reinforcement; y_2 = the distance from the location of the neutral axis to the location of the reinforcement; F_{ps} = the force contribution of the prestressing strands; and y_n = the distance from the location of the neutral axis to the location of each prestressing strand layer.

From the two equilibrium conditions, the moment corresponding to the curvature of the section can be obtained by the iteration method. The full moment-curvature relationship of the section is obtained using the various strain levels at the top surface fiber. Then, the load-deflection envelope of the member can be calculated using the moment-curvature relationship by using numerical integration.

Using the defined analytical model for each material used in the specimen, the load-deflection envelopes for the nine AASHTO girders are predicted. As described in Chapter 4, the measured material properties and prestress losses for each specimen are input for the design calculations. All of the girders are modeled to predict the behavior up to the ultimate strain of the top surface of the extreme fiber. The ultimate strain for each specimen is determined by the measured ultimate strain, discussed in Chapter 4. For a direct comparison of the predicted values using the experimental results, the predicted deflection at midspan in the analytical model offsets the camber of the prestressed girder. A comparison between the predicted load-deflection envelope and the measured load-deflection envelope under static loading conditions at the midspan is given in Figures 5-10 to 5-12, respectively.

As can be seen in the figures below, the predicted load-deflection relationship shows good agreement with the measured response for the specimens.

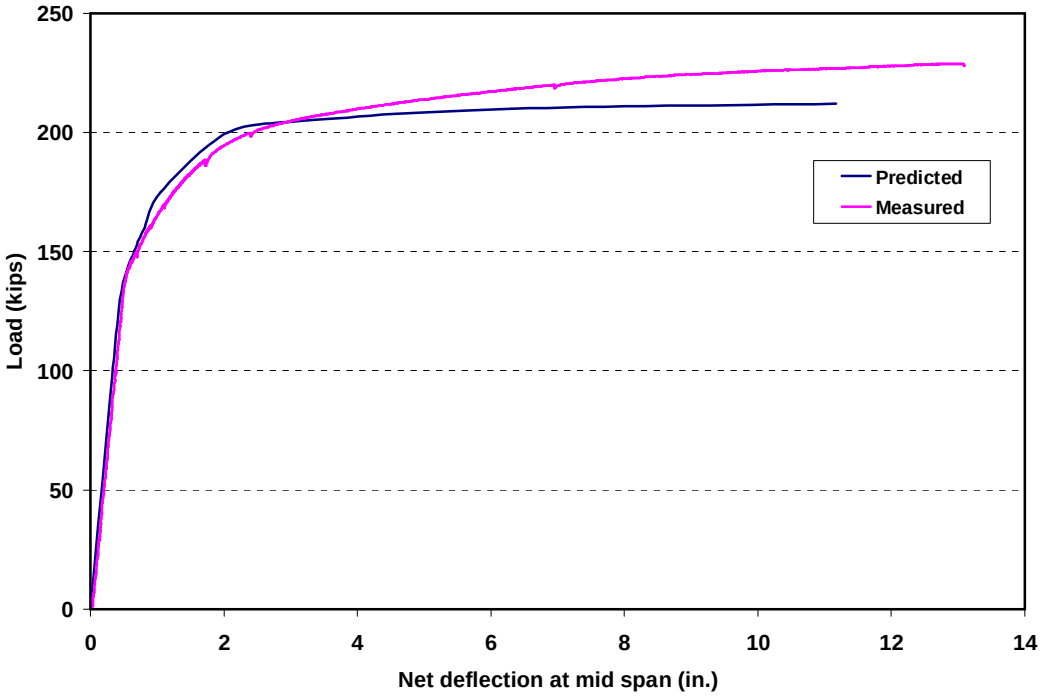

a) 10PS–5S

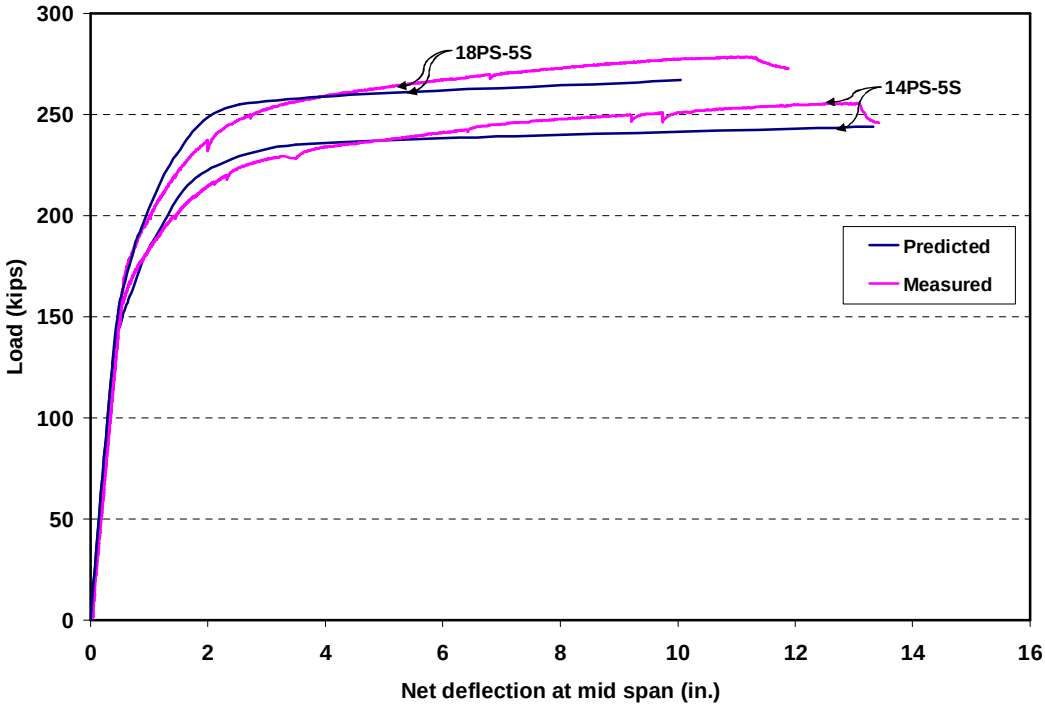

b) 14PS-5S and 18PS-5S

Figure 5-10 Measured and predicted load deflection responses

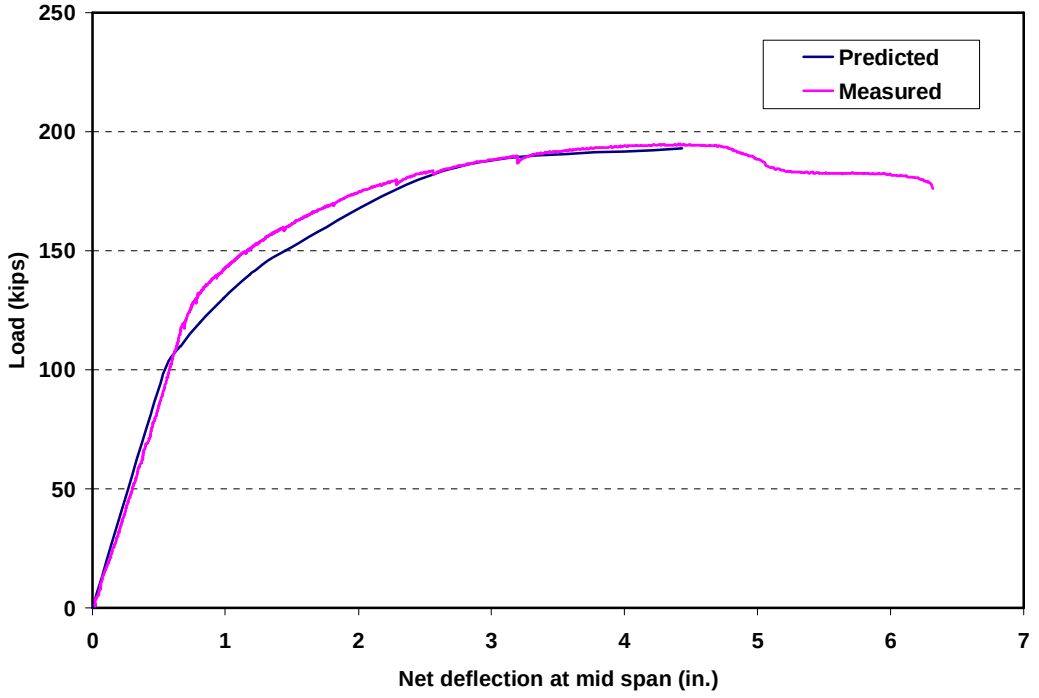

a) 10PS-1S

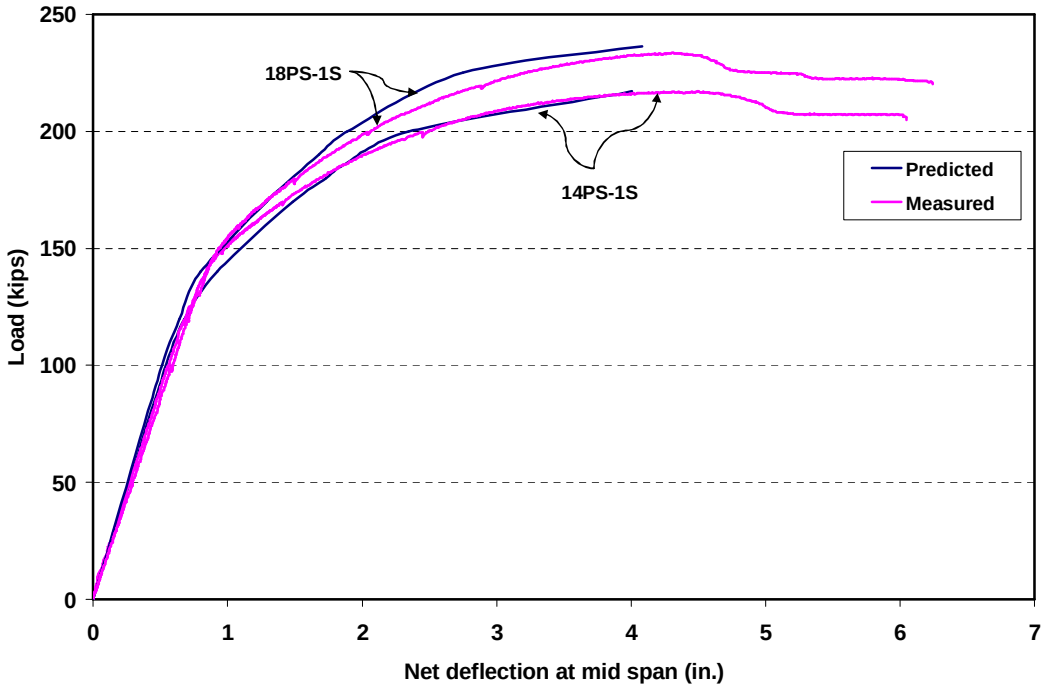

b) 14PS-1S and 18PS–1S

Figure 5-11 Measured and predicted load deflection responses

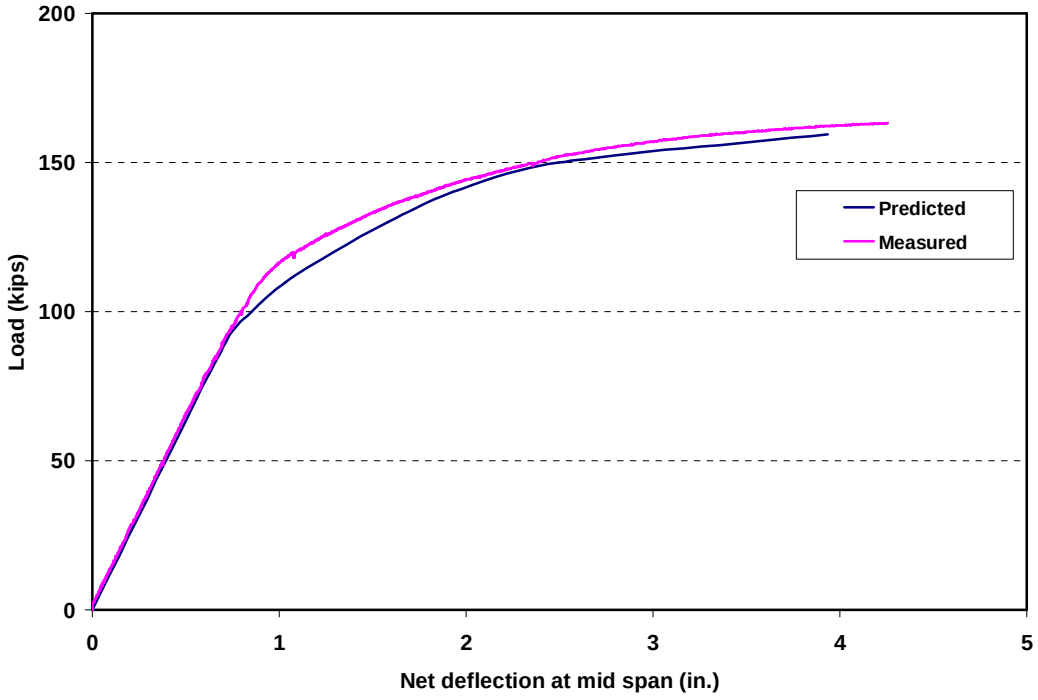

a) 10PS-N

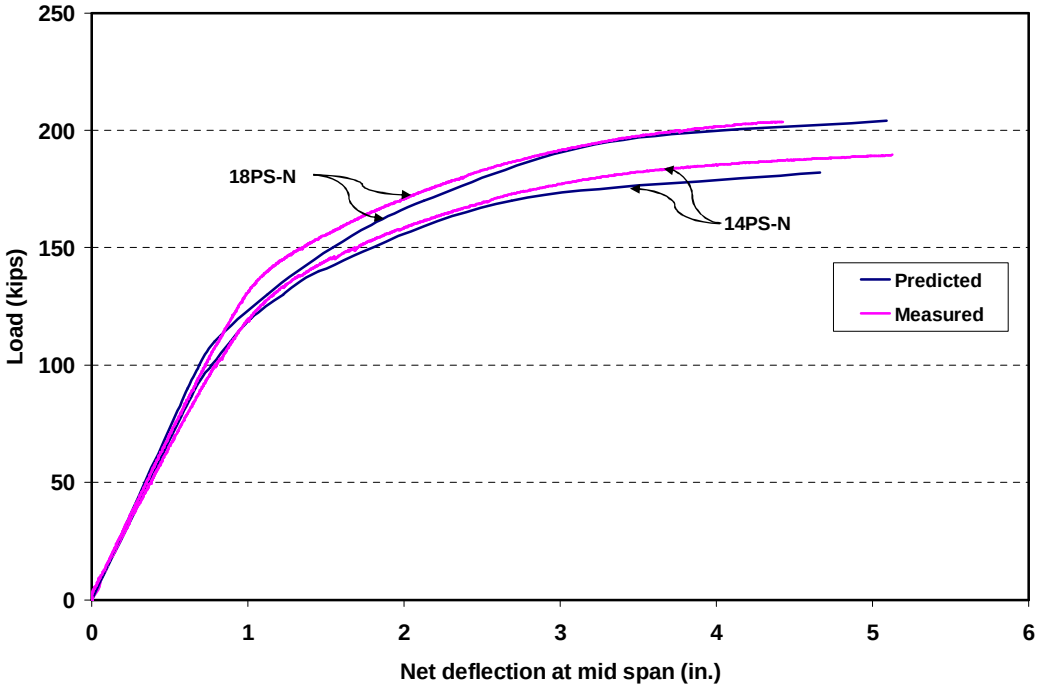

b) 14PS-N and 18PS–N

Figure 5-12 Measured and predicted load deflection responses

5.3.3 Summary of flexural strength behavior

The flexural strength determined in the second loading phase is used to evaluate the flexural strength ratio ($M_{measured}/M_{predicted}$) for the three design calculations.

The first three specimens;10PS, 14PS and 18PS-5S in Figure 5-13, which are prestressed girders with a 5 ft. wide deck, are investigated to evaluate the flexural response for NSC. The flexural strength ratio for these three specimens shows that the AASHTO LRFD specifications provide a generally conservative estimate for the flexural strength of NSC.

For the three specimens; 10PS, 14PS and 18PS-1S in Figure 5-13, which are the composite girders with a 1 ft. wide deck, the composite girder sections that have a relatively small deck flange and that have two types of compressive strength subjected to the flexure, the current AASHTO specifications (2004) do not specify the design method needed to determine the flexural strength of girders with two types of concrete in the compression zone. In this study, the nominal flexural resistance is recommended to be used to determine the flexural strength by using the AASHTO LRFD specifications using an analysis based on the compressive strength of deck concrete, which is usually lower than that of girder concrete. The flexural strength ratio for these three specimens confirms that the recommended method to determine the nominal flexural resistance, M_n, is reasonably conservative, yet still accurate.

Finally, the three specimens; 10PS, 14PS and 18PS-N in Figure 5-13, which are the girders without a deck, are designed to evaluate the flexural response for HSC. The rectangular stress block parameters in the current LRFD specifications are limited in their use to help determine the flexural strength of HSC girders up to 10, 000 psi. On the basis of the research findings

from the related research presented in Section 2.2.2, the recommended stress block parameters is applicable to determine the flexural strength for these three specimens.

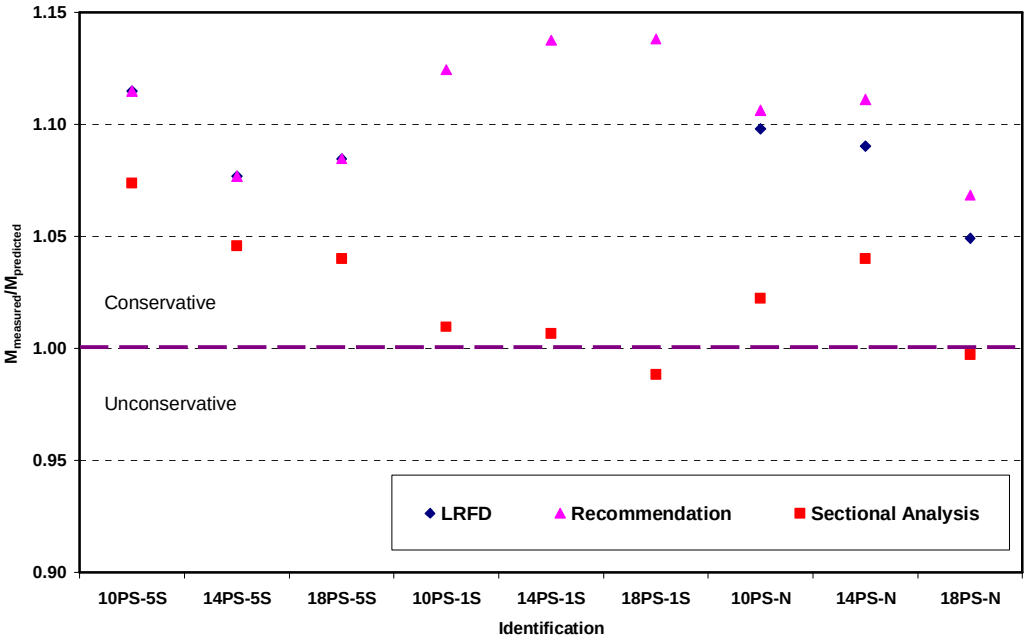

Figure 5-13 Flexural strength ratio of the measured versus predicted results

6 SUMMARY AND CONCLUSIONS

6.1 SUMMARY

The use of HSC has increased due to the advantages of its material characteristics that can reduce the section depth or extend the span length in bridge construction. However, the current code provisions cannot meet the demands of HSC design. The limits of the current code provisions, the AASHTO LRFD specifications, lead to uncertainty regarding its ability to predict the flexural response with reasonable accuracy. In order to validate the analytical models typically used to determine the flexural response of prestressed HSC girders with and without a cast-in-place deck, a total of nine girders were tested under static loading. In the experimental program, valuable test results, which include material properties, transfer length, prestress losses, cracking strength, and flexural strength, were obtained. In the analytical program, these test results were evaluated by the current AASHTO LRFD specifications (2004) or by using related equations from other research. On the basis of the research findings, the proposed equation for the elastic modulus is in good agreement with the measured test results. The modulus rupture, the transfer length and prestress losses equations in the current AASHTO LRFD specifications correlate well with the measured values. Additionally, the revised equivalent rectangular stress block parameters used to determine the flexural response were reassessed for prestressed girders with HSC.

6.2 CONCLUSIONS

The objective of this research is to reassess the current AASHTO LRFD specifications as they apply to prestress girders with HSC, especially in terms of flexural response. On the basis of the research findings along with the experimental and analytical programs, the material properties, transfer length, prestress losses and equivalent rectangular stress block parameters for the flexural response, several conclusions can be drawn. The following conclusion section is divided according to the flexural behavior of each prestress girder with HSC.

6.2.1 Material properties

In the experimental program, the equation addressed in ACI 363R-92 correlates well with the measured elastic modulus with regard to the HSC region, whereas the current equation in the AASHTO LRFD specifications overestimates the elastic modulus for all the tested specimens. According to the statistical method using the collected data that include the various compressive strength ranges and unit weights, the predicted value by ACI363R-92 is slightly conservative. On the other hand, the proposed equation in Equation 6-1 for the elastic modulus provides a more appropriate estimation, regardless of the compressive strength and a unit weight of concrete.

$$E_c = w_c^{2.5} \cdot \left(f_c'\right)^{0.33}, \text{ (pcf, psi)} \qquad \textbf{Equation 6-1}$$

Due to moisture conditions, the equation presented in ACI 363R-92 overestimates the measured modulus of rupture for the air-cured cylinder. However, the equation in AASHTO LRFD suggests an applicable prediction of the modulus of rupture regardless of the

compressive strength. The equation for the modulus of rupture in the current AASHTO LRFD specifications (2004) may be appropriate for HSC up to 18,000 psi. However, on the basis of research findings, the lower bound equation for modulus of rupture, $6\sqrt{f'_c}$ (psi) is recommended to determine the cracking moment in this study.

6.2.2 Prestress losses

The total prestress loss, including elastic shortening, creep, shrinkage and relaxation, is evaluated with the predicted results based on the recent AASHTO LRFD specifications (2004). On the basis of these research findings, the instantaneous losses at transfer due to elastic shortening and the prestress losses are approximately 7.6 percent and 15 percent of the initial prestressing stress, respectively. Based on the research findings, among the prestress losses, the elastic shortening results are slightly higher than found from the AASHTO LRFD equation. However, the calculated prestress losses by the measured cracking moment and modulus of rupture shows that the total prestress losses for each specimen at test day shows a good agreement with the prediction in the LRFD specification.

6.2.3 Flexural behavior

For composite girder sections in which the neutral axis is located in the deck, the nominal flexural resistance can be calculated using the current AASHTO LRFD specifications. The computed flexural resistance is approximately 8 to 12 percent less strength than the measured value. It is evident that the flexural behavior for NSC in the compression zone can be estimated using the equivalent rectangular stress block parameters currently found in the AASHO LRFD specifications for concrete strengths up to 10,000 psi. In addition to the code

equation, the sectional analysis using measured material properties and prestress losses provides more precise results with 4 to 7 percent less loss than the measured flexural resistance.

The current AASHTO LRFD specifications (2004) do not specify a design method to determine the flexural strength of two types of concrete in the compression zone. Typically, the compressive concrete strength of the deck is less than the girder concrete strength. For composite girder sections in which the neutral axis is located below the deck, two types of concrete compressive strength in the compression zone must be considered. The nominal flexural resistance can be determined by using AASHTO LRFD specifications based on the compressive strength of the deck concrete. The computed flexural strengths using the recommended method are approximately 12 to 14% less strength than the measured flexural strengths. These results confirm that the recommended method to determine the nominal flexural resistance, M_n, is reasonably conservative. Based on the same results, the predicted nominal flexural resistance based on the sectional analysis that uses the measured material properties and prestress losses shows more accurate results within a ±1% difference of the measured flexural resistance.

For prestressed girder sections in which the neutral axis is located in the flange of the girder subjected to flexure, the nominal flexural resistance computed by using the proposed equivalent rectangular stress block parameters with the AASHTO LRFD specifications

equation is approximately 5 to 10 percent less strength than the measured flexural strength. This finding seems reasonably conservative. Therefore, the revised equivalent rectangular stress block parameters listed below for the approximate stress in concrete may be applicable for prestressed girders with HSC up to 18,000 psi.

$$a_1 = \begin{Bmatrix} 0.85 & for & f_c' \le 10ksi \\ 0.85 - 0.02(f_c' - 10) \ge 0.75 & for & f_c' > 10ksi \end{Bmatrix}. \qquad \textbf{Equation 6-2}$$

$$b_1 = \begin{Bmatrix} 0.85 & for & f_c' \le 4ksi \\ 0.85 - 0.05(f_c' - 4) \ge 0.65 & for & f_c' > 4ksi \end{Bmatrix}. \qquad \textbf{Equation 6-3}$$

In addition to the computed flexural strength based on the LRFD equation, the predicted nominal flexural resistance based on the section analysis with the measured material properties and prestress losses is 0 to 4 percent less than the measured flexural resistance.

6.2.4 Transfer length and failure mode

An assessment of the transfer length presented in the current LRFD specifications has been conducted. The calculated transfer length computed by the average end slippage measurement of prestressing strands correlates well with the estimation obtained from the AASHTO LRFD specifications.

Failure evaluation of the prestressed girders with and without a deck has been conducted. Under a given applied load at the midsection, the failure procedure can be evaluated by comparing the applied moment at mid-span to the computed flexural moment at mid-span in

the current specifications. On the basis of this comparison, it is concluded that the initial cracking of the tested specimens is approximately 60 percent of the computed flexural resistance found in the current AASHTO LRFD specifications.

6.3 RECOMMENDATION AND FUTURE WORK

6.3.1 Recommendation

The following changes are recommended to the current LRFD specification.

5.4.2.4 Modulus of Elasticity

In the absence of measured data, the modulus of elasticity, E_c, for concretes with unit weights between 0.090 and 0.155 kcf and specified compressive strengths up to 18.0 ksi may be taken as:

$$E_c = 310{,}000 K_1 w_c^{2.5} (f_c')^{0.33} \qquad (5.4.2.4\text{-}1)$$

K_1 = correction factor for source of aggregate to be taken as 1.0 unless determined by physical test, and as approved by the authority of jurisdiction;

w_c = unit weight of concrete (kcf);

f'_c = specified compressive strength of concrete (ksi)

5.7.3.2.6 Composite Girder Section

For composite girder section in which the neutral axis is located below the deck, the nominal flexural resistance, M_n, may be determined by Eqs. 5.7.3.2.2-1, based on the lower compressive strength of the deck concrete.

6.3.2 Future work

The experimental and analytical program in this study is mainly focused on the girders subjected on the flexure under static loading. Therefore, further investigation for the fatigue and shear behavior of the prestressed girder with high strength concrete is necessary.

REFERENCES

AASHTO LRFD Bridge Design Specifications, Second Edition, American Association of State Highway and Transportation Officials, Washington DC, 2005.

ACI Committee 318, "Building Code Requirements for Structural Concrete (ACI 318-02) and Commentary (318R-02)", American Concrete Institute, Farmington Hills, MI, 2002, 443 pp.

ACI Committee 363, "State-of-the-Art Report on High-Strength Concrete (ACI 363R-92)", American Concrete Institute, Detroit, 1992 (Revised 1997), 55 pp.

ACI Committee 363, "Guide to Quality Control and Testing of High-Strength Concrete (ACI 363.2R-98)", American Concrete Institute, Detroit, 1998, 18 pp.

Ahlborn, T. M., French, C. E. and Shield, C. K., "High-Strength Concrete Prestressed Bridge Girders: Long Term and Flexural Behavior", *Final Report 2000-32*, Minnesota Department of Transportation, 2000, 390 pp.

Ahmad, S. H. and Lue, D. M., "Flexure-Shear Interaction of Reinforced High-Strength Concrete Beams", *ACI Structural Journal*, Vol. 84, No.4, 1987, pp. 330-341.

Bae, S. and Bayrak, O., "Stress Block Parameters for High-Strength Concrete Members", *ACI Structural Journal*, Vol. 100, No. 5, 2003, pp. 626-636.

Bayrak, O. and Sheikh, S. A., "Confinement Reinforcement Design Considerations for Ductile HSC Columns", *Journal of Structural Engineering*, Vol. 124, No. 9, 1998, pp. 999-1010.

Bernhardt, C. J. and Fynboe, C. C., "High Strength Concrete Beams", *Nordic Concrete Research*, No. 5, 1986, pp. 19-26.

Bhatia, S., "Continuous Prestressed Concrete Beams in the Inelastic Range", *M.Sc. Thesis*, Department of Queen's University, Kingston, Ontario, Canada, 1984.

Bing, L., Park, R. and Tanaka, H., "Stress Strain Behavior of High Strength Concrete Confined by Ultra-High- and Normal-Strength Transverse Reinforcement", *ACI Structural Journal*, Vol. 98, No. 3, 2001, pp. 395-406.

Burns N. H., Gross S. P. and Byle K.A., "Instrumentation and Measurements - Behavior of Long-Span Prestressed High Performance Concrete Bridges", *PCI/FHWA International Symposium on High Performance Concrete October 20-22*, New Orleans, Louisiana, 1997.

Canadian Standards Association, "Design of Concrete Structures, CSA A23.3 1994", Rexdale, Ontario, 1994, pp.199.

Carino, N. J., "Prediction of Potential Strength at Later Ages", *Concrete and Concrete-Making Materials*, 1994, pp. 140.

Carrasquillo, R. L., Nilson, A. H. and Slate, F., "Properties of High Strength Concrete Subject to Short- Term Loads", *ACI Structural Journal*, Vol. 78, No.3, 1981, pp. 171-178.

Carrasquillo, R. L., Slate, F. and Nilson, A. H., "Micro-Cracking and Behavior of High Strength Concrete Subject to Short- Term Loading", *ACI Structural Journal*, Vol. 78, No.3, 1981, pp. 179-186.

Chin, M. S., Mansur, M. A. and Wee, T. H., "Effect of Shape, Size and Casting Direction of Specimens on Stress-Strain Curves of High-Strength Concrete", *ACI Materials Journal*, Vol. 94, No. 3, 1997, pp. 209-219.

Cohn, M. Z. and Lounis, Z., "Moment Redistribution in Structural Concrete Codes", *Canadian Journal of Civil Engineering*, Vol.18, No. 1, 1991, pp. 97-108.

Collins, T. M., "Proportioning High-Strength Concrete to Control Creep and Shrinkage" *ACI Materials Journal*, Vol. 86, No. 6, 1989, pp. 576-580.

Collins, M. P., Mitchell, D. and MacGregor, J. G., "Structural Design Considerations for High-Strength Concrete", *Concrete International*, Vol. 15, No. 5, 1993, pp. 27-34.

Comite Europeen de Normalisation (CEN), "Eurocode 2 : Design of Concrete Structures, Part 1 – General Rules and Rules for Buildings", prEN 1992-1, 2002, pp. 211.

Criteria for Prestressed Concrete Bridges, 1954, citation details not available.

Cusson, D. and Paultre, P., "High-Strength Concrete Columns Confined by Rectangular Ties", *Journal of Structural Engineering*, Vol. 120, No. 3, 1994, pp. 783-804.

Hognestad, E., Hanson, N. W. and McHenry, D., "Concrete Stress Distribution in Ultimate Strength Design", ACI Journal, Vol. 52, No. 4, 1955, pp. 455-479.

Hueste, M. B. D. and Cuadros G. G., "Survey of Current Practice for Design of High Strength Concrete Prestressed Bridge Girders", *TRB Annual Meeting*, Transportation Research Board, Washington, D.C., January 2004.

Ibrahim, H. H. H. and MacGregor, G., "Tests of Eccentrically Loaded High-Strength Concrete Columns", *ACI Structural Journal*, Vol. 93, No. 5, 1996, pp. 585-594.

Ibrahim, H. H. H. and MacGregor, G., "Modification of the ACI Rectangular Stress Block for High-Strength Concrete", *ACI Structural Journal*, Vol. 94, No. 1, 1997, pp. 40-48.

Iravani, S., "Mechanical Properties of High-Performance Concrete", *ACI Materials Journal*, Vol. 93, No. 5, 1996, pp. 416-426.

Le Roy, R., "Instantaneous and Time Dependant Strains of High-Strength Concrete", Laboratoire Central des Ponts et Chaussees, Paris, France, 1996, pp. 376.

Legeron, F. and Paultre, P., "Prediction of Modulus of Rupture of Concrete", *ACI Materials Journal*, Vol. 97, No. 2, 2000, pp. 193-200.

Mansur, M. A., Chin, M. S. and Wee, T. H., "Flexural Behavior of High-Strength Concrete Beams", *ACI Structural Journal*, Vol. 94, No. 6, 1997, pp. 663-674.

Miller, R. A., Castrodale, R., Mirmiran, A., and Hastak, M., "Connection between Simple Span Precast Concrete Girders Made Continuous", *Draft Final Report*, NCHRP Project 12-53, University of Cincinnati, Cincinnati, OH, October 2003.

Mokhtarzadeh, A. and French, C. E., "Mechanical Properties of High-Strength Concrete", *Final Report No. 1998-11*, Minnesota Department of Transportation, 1988.

Naaman, A. E. "Rectangular Stress Block and T-Section Behavior", *PCI Journal*, Vol. 47, No.5, 2002, pp. 106-112.

Nagashima, T., Sugano, S., Kimura, H. and Ichikawa, A., "Monotonic Axial Compression Test on Ultra-High-Strength Concrete Tied Columns", *Earthquake Engineering Tenth World Conference*, Balkema, Rotterdam, the Netherlands, 1992, pp. 2983-2988.

Nedderman, H., "Flexural Stress Distribution in Very-High Strength concrete", *M.Sc. Thesis*, University of Texas at Arlington, 1973, 182 pp.

Neville, A. M., Properties of Concrete, Fourth and Final Edition, New York: J. Wiley, New York, 1996, pp. 884..

Noguchi Laboratory Data, Department of Architecture, University of Tokyo, Japan, (http://bme.t.u-tokyo.ac.jp/index_e.html).

Park, R. and Paulay, T., "Reinforced Concrete Structures", John Wiley and Sons, New York, N. Y., 1975.

Parrot, L. J., "The Properties of High-Strength Concrete", *Technical Report No. 42.417*, Cement and Concrete Association, Wexham Springs, 1969, 12 pp.

Paultre, P. and Mitchell, D., "Code Provisions for High-Strength Concrete - An International Perspective", *Concrete International*, 2003, pp. 76-90.

PCI Industry Handbook Committee, "PCI Design Handbook – Precast and Prestressed Concrete", Precast/Prestressed Concrete Institute, Chicago, Illinois, 1999.

Priestley, M. J. N. and Park, R., "Moment Redistribution in Continuous Prestressed Concrete Beams", Magazine of Concrete Research, Vol. 24, No. 80, 1972, pp. 157-166.

Razvi, S. R. and Saatcioglu, M., "Confinement Model for High Strength Concrete", *Journal of Structural Engineering*, Vol. 125, No. 3, 1999, pp. 281-289.

Russell B. W. and Pang J. P., "Investigation of Allowable Compressive Stresses for High Strength, Prestressed Concrete Bridges", *PCI/FHWA International Symposium on High Performance Concrete October 20-22*, New Orleans, Louisiana, 1997.

Russell, H. G., "ACI Defines High-Performance Concrete", Concrete International, February, 1999, pp. 56-57.

Russell, H. G., Miller, R. A., Ozyildirim, H. C. and Tadros, M. K., "Compilation and Evaluation of Results from High Performance Concrete Bridge Projects, Volume 1", *Federal Highway Administration*, 2003.

Russell, H. G., Miller, R. A., Ozyildirim, H. C. and Tadros, M. K., "Compilation and Evaluation of Results from High Performance Concrete Bridge Projects, Volume 2", *Federal Highway Administration*, 2003.

Russell, H. G., Miller, R. A., Ozyildirim, H. C. and Tadros, M. K., "High Performance Concrete", *Compact Disc*, Federal Highway Administration, Version 3.0, 2003.

Sarkar, S., Adwan, O. and Munday, J. G. L., "High Strength Concrete: An Investigation of the Flexural Behavior of High Strength RC Beams" *Structural Engineer*, Vol. 75, No. 7, 1997, pp. 115-121.

Schade, J. E., "Flexural Concrete Stress in High Strength Concrete Columns", *M. S. Thesis in Civil Engineering*, the University of Calgary, Calgary, Alberta, Canada, 1992.

Stallings, J. M., Barnes, R. W. and Eskildsen, S., "Camber and Prestress Losses in Alabama HPC Bridge Girders", *PCI Journal*, Vol. 48, No. 5, 2003, pp. 90-104.

Stanton, J. F., Barr, P. and Eberhard, M. O., "Behavior of High-Strength HPC Bridge Girders", *Research Report*, University of Washington, Seattle, WA, 2000.

Swartz, S. E., Nikaeen, A., Narayan Babu, H. D., Periyakaruppan, N. and Refai, T. M. E., "Structural Bending Properties of Higher Strength Concrete", *ACI Special Publication-87*, High-Strength Concrete, 1985, pp. 145-178.

Tadros, M., Al-Omaishi, N., Seguirant, J. S. and Galit, J. G., "Prestress Losses in Pretensioned High-Strength Concrete Bridge Girders", *NCHRP Report 496*, Transportation Research Board, 2003.

Zia, P., Leming, M. L., Ahmad, S., Schemmel, J. J., Elliot, R. P. and Naaman, A. E., "Mechanical Behavior of High Performance Concrete, Vol. 1 – Summary Report", *SHRP Report C- 361*, Strategic Highway Research Program, National Research Council, Washington, D. C., 1993.

Zia, P., Leming, M. L., Ahmad, S., Schemmel, J. J. and Elliot, R. P., "Mechanical Behavior of High Performance Concrete, Vol. 2, - Production of High Performance Concrete", *SHRP ReportC-362*, Strategic Highway Research Program, National Research Council, Washington, D. C., 1993.

Zia, P., Ahmad, S., Leming, M. L., Schemmel, J. J. and Elliot, R. P., "Mechanical Behavior of High Performance Concrete, Vol. 3 - Very Early Strength Concrete", *SHRP Report C-363*, Strategic Highway Research Program, National Research Council, Washington, D. C., 1993.

Zia, P., Ahmad, S., Leming, M. L., Schemmel, J. J. and Elliot, R. P., "Mechanical Behavior of High Performance Concrete, Vol. 4 - High Early Strength Concrete", *SHRP Report C-364*, Strategic Highway Research Program, National Research Council, Washington, D. C., 1993.

Zia, P., Ahmad, S., Leming, M. L., Schemmel, J. J. and Elliot, R. P., "Mechanical Behavior of High Performance Concrete, Vol. 5 - Very High Strength Concrete", *SHRP Report C-365*, Strategic Highway Research Program, National Research Council, Washington, D. C., 1993.

Zia, P., "State-of-the-Art of HPC: An International Perspective", *Proceedings of the PCI/FHWA International Symposium on High Strength Concrete*, New Orleans, Luisiana, 1997, pp. 49-59.

Zollman, C. C., "Prestressed Concrete Construction", *The Military Engineer*, No.291, 1951.

APPENDICES

Appendix A: Related Study for Stress Block Parameters (adopted from Mirmiran, 2003)

Reference[2]	α_1	β_1
LRFD and ACI 318-02 (2002)	0.85	$0.85 \quad for \quad f'_c \le 4KSI$ $0.85 - 0.05(f'_c - 4) \ge 0.65 \quad for \quad f'_c > 4KSI$
NZS 3101 (1995) (see Li, Park and Tanaka 1994)	$0.85 \quad for \quad f'_c \le 8KSI$ $0.85 - 0.02758(f'_c - 8) \ge 0.75 \quad for \quad f'_c > 8KSI$	$0.85 \quad for \quad f'_c \le 4.35KSI$ $0.85 - 0.05516(f'_c - 4.35) \ge 0.65 \quad for \quad f'_c > 4.35KSI$
CSA A23.3 (1994)	$0.85 - 0.01034 f'_c \ge 0.67$	$0.97 - 0.01724 f'_c \ge 0.67$
EC2-02 (2002)	$a_{cc} \quad for \quad f'_{ck} \le 7.25KSI$ $a_{cc}\left(1 - \frac{f'_{ck} - 7.25}{29}\right) \quad for \quad 7.25KSI \le f'_{ck} \le 13.05KSI$	$0.80 \quad for \quad f'_{ck} \le 7.25KSI$ $0.80 - \frac{f'_{ck} - 7.25}{68} \quad for \quad 7.25KSI \le f'_{ck} \le 13.05KSI$
CEB-FIB (1990)	$0.85\left(1 - \frac{f'_c}{36.3}\right)$	1
AFREM (1995)	0.85	$1.0 - \left(\frac{0.7}{4.5 - 0.1724 f'_c}\right)$
ACI 441-R96 (1996)	$0.85 - 0.05033(f'_c - 10) \ge 0.60 \quad for \quad f'_c > 10KSI$	$0.67 \quad for \quad f'_c \ge 10KSI$

[1] For consistency, the equations have been converted from SI units.

[2] ACI 441-R96 (1996) is not a design code, and is only shown for comparison. For other design codes, see Appendix A as well as Paultre and Mitchell (2003) and Zia (1997).

Appendix B : Shop Drawing for AASHTO Girder

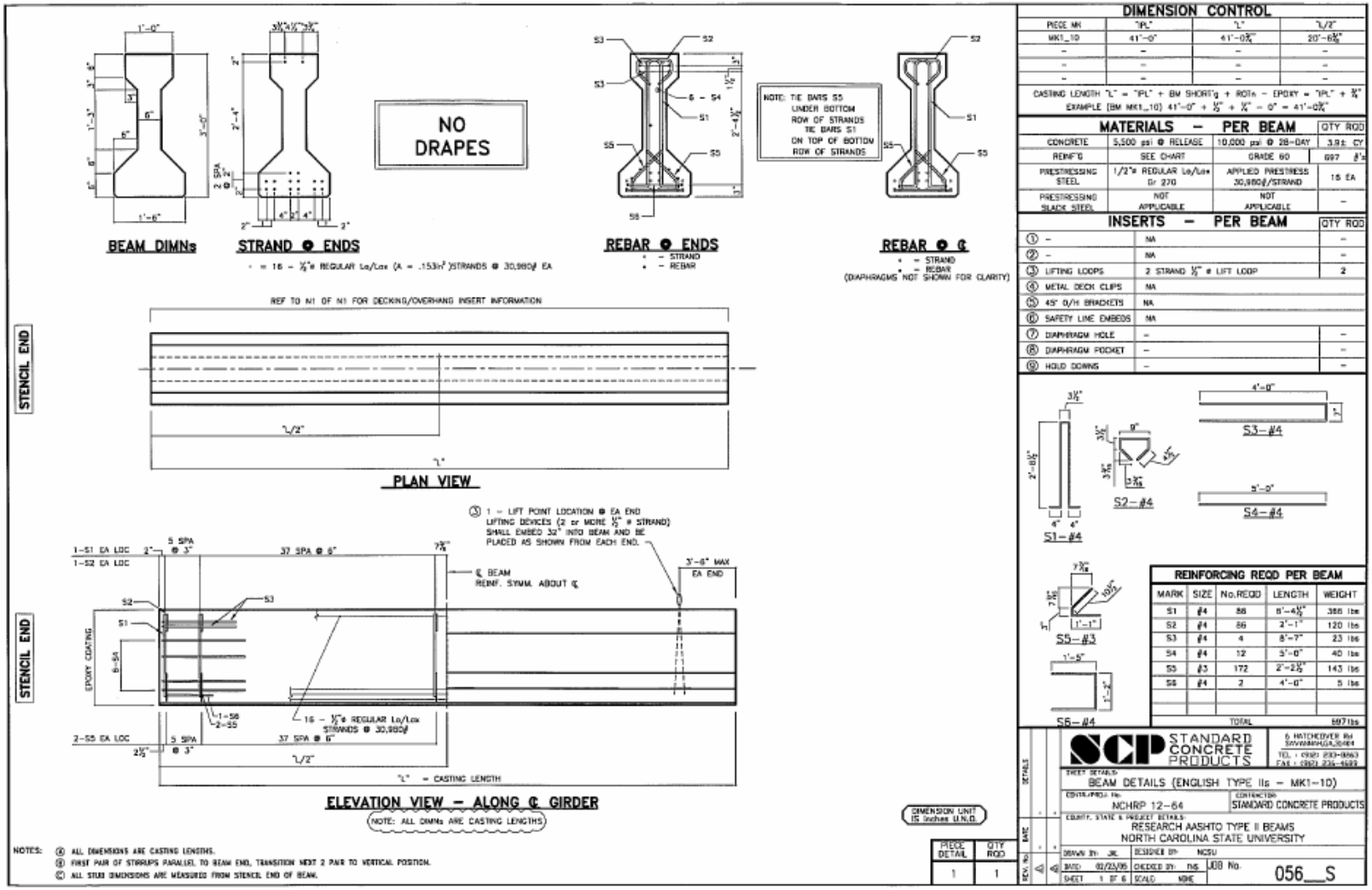

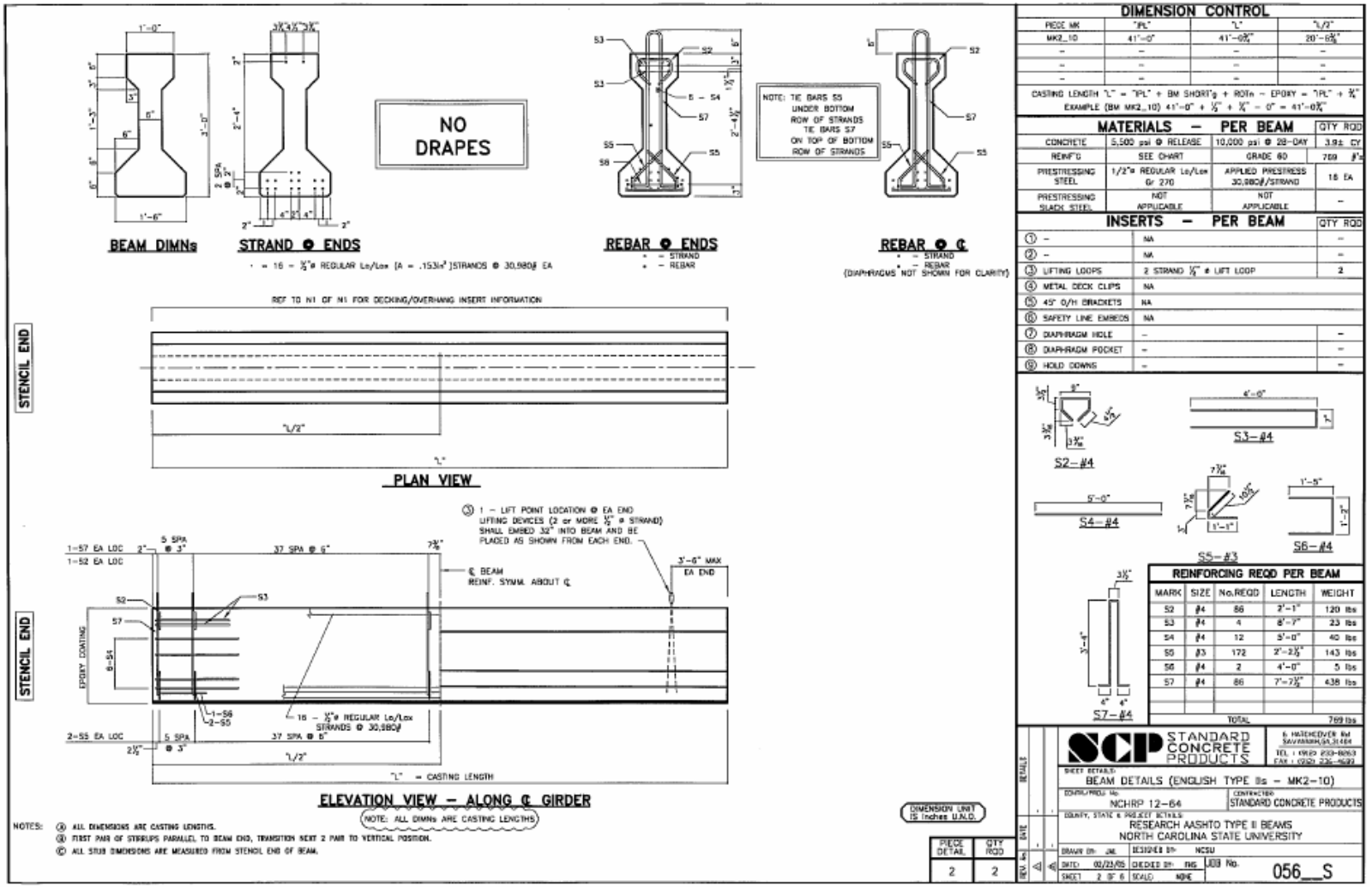

DIMENSION CONTROL

PIECE MK	"PL"	"L"	"L/2"
MK2_10	41'-0"	41'-0⅜"	20'-6⅜"
–	–	–	–
–	–	–	–
–	–	–	–
–	–	–	–

CASTING LENGTH "L" = "PL" + BM SHORT'g + ROTn – EPOXY = "PL" + ¾"
EXAMPLE (BM MK2_10) 41'-0" + ½" + ¾" – 0" = 41'-0⅜"

MATERIALS – PER BEAM

			QTY ROD
CONCRETE	5,500 psi @ RELEASE	10,000 psi @ 28-DAY	3.9± CY
REINF'G	SEE CHART	GRADE 60	769 #'s
PRESTRESSING STEEL	1/2"ø REGULAR Lo/Lox Gr 270	APPLIED PRESTRESS 30,980#/STRAND	18 EA
PRESTRESSING SLACK STEEL	NOT APPLICABLE	NOT APPLICABLE	–

INSERTS – PER BEAM

		QTY ROD
① –	NA	–
② –	NA	–
③ LIFTING LOOPS	2 STRAND ½" ø LIFT LOOP	2
④ METAL DECK CLIPS	NA	
⑤ 45° O/H BRACKETS	NA	
⑥ SAFETY LINE EMBEDS	NA	
⑦ DIAPHRAGM HOLE	–	–
⑧ DIAPHRAGM POCKET	–	–
⑨ HOLD DOWNS	–	–

REINFORCING REQD PER BEAM

MARK	SIZE	No.REQD	LENGTH	WEIGHT
S2	#4	86	2'-1"	120 lbs
S3	#4	4	8'-7"	23 lbs
S4	#4	12	5'-0"	40 lbs
S5	#3	172	2'-2½"	143 lbs
S6	#4	2	4'-0"	5 lbs
S7	#4	86	7'-7½"	438 lbs
			TOTAL	769 lbs

PIECE DETAIL	QTY ROD
2	2

STANDARD CONCRETE PRODUCTS
6 HATCHCOVER Rd SAVANNAH, GA 31404
TEL: (912) 233-8263 FAX: (912) 236-4689

SHEET DETAILS: BEAM DETAILS (ENGLISH TYPE IIs – MK2-10)
CONTROLLING No.: NCHRP 12-64
CONTRACTOR: STANDARD CONCRETE PRODUCTS
COUNTY, STATE & PROJECT DETAILS: RESEARCH AASHTO TYPE II BEAMS NORTH CAROLINA STATE UNIVERSITY
DRAWN BY: JAK DESIGNED BY: NCSU
DATE: 02/23/05 CHECKED BY: RHS JOB No. 056__S
SHEET 2 OF 6 SCALE: NONE

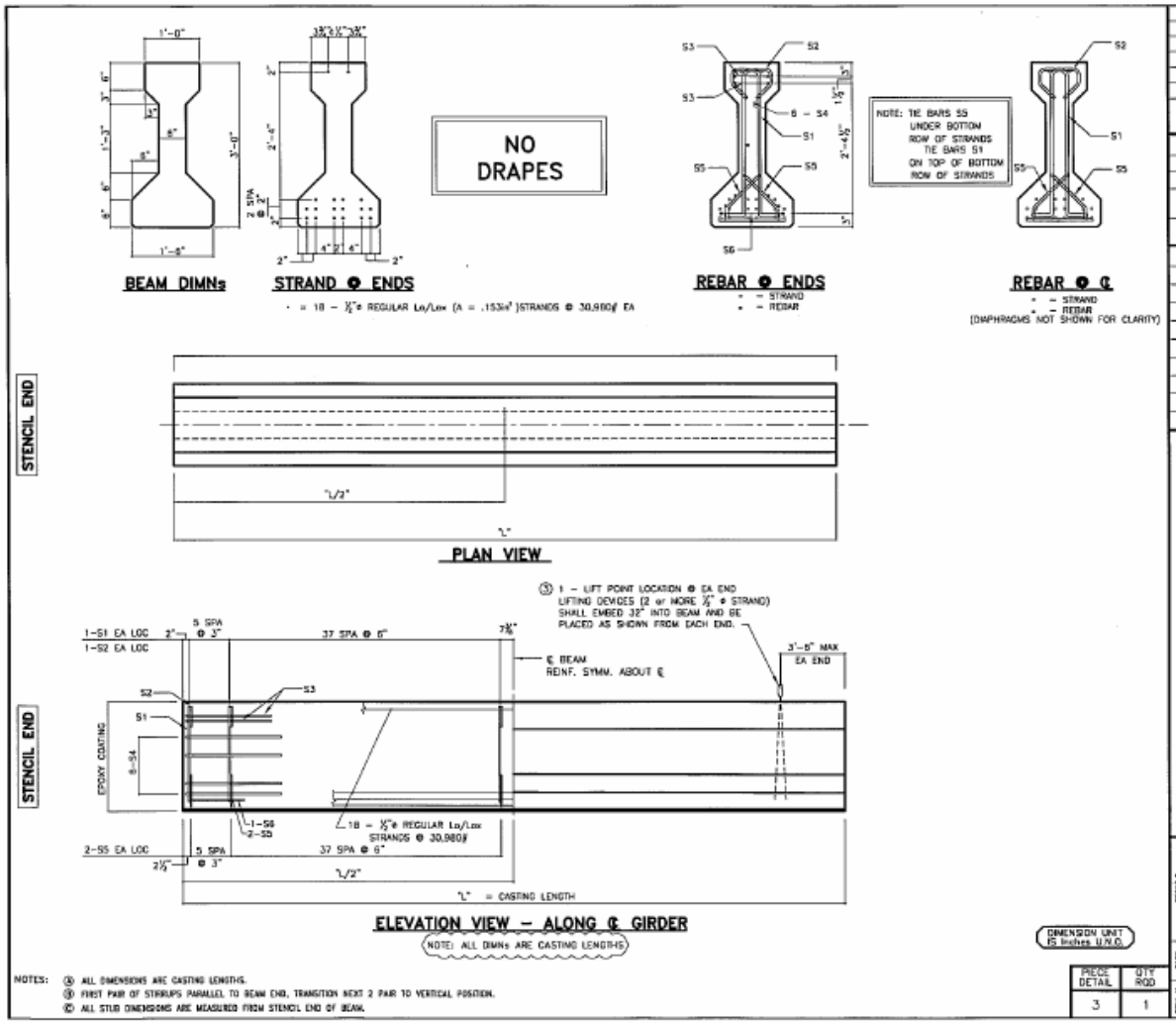

DIMENSION CONTROL			
PIECE MK	"IPL"	"L"	"L/2"
MK1_14	41'-0"	41'-0⅝"	20'-6⅝"
–	–	–	–
–	–	–	–
–	–	–	–

CASTING LENGTH "L" = "IPL" + BM SHORT'g + RDfn – EPOXY = "IPL" + ⅜"
EXAMPLE (BM MK1_14) 41'-0" + ½" + ½" – 0" = 41'-0⅝"

MATERIALS – PER BEAM			QTY RQD
CONCRETE	6,000 psi @ RELEASE	14,000 psi @ 28-DAY	3.9± CY
REINF'G	SEE CHART	GRADE 60	697 #'s
PRESTRESSING STEEL	1/2"ø REGULAR Lo/Lox Gr 270	APPLIED PRESTRESS 30,980#/STRAND	18 EA
PRESTRESSING SLACK STEEL	NOT APPLICABLE	NOT APPLICABLE	–

INSERTS – PER BEAM		QTY RQD
① –	NA	–
② –	NA	–
③ LIFTING LOOPS	2 STRAND ½" ø LIFT LOOP	2
④ METAL DECK CLIPS	NA	
⑤ 45° D/H BRACKETS	NA	
⑥ SAFETY LINE EMBEDS	NA	
⑦ DIAPHRAGM HOLE	–	–
⑧ DIAPHRAGM POCKET	–	–
⑨ HOLD DOWNS	–	–

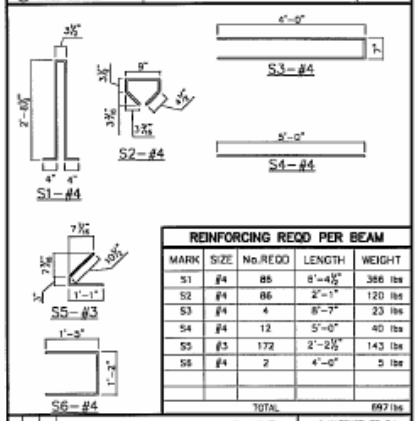

REINFORCING REQD PER BEAM				
MARK	SIZE	No.REQD	LENGTH	WEIGHT
S1	#4	85	8'-4½"	386 lbs
S2	#4	86	2'-1"	120 lbs
S3	#4	4	8'-7"	23 lbs
S4	#4	12	5'-0"	40 lbs
S5	#3	172	2'-2½"	143 lbs
S6	#4	2	4'-0"	5 lbs
			TOTAL	697 lbs

NOTES:
Ⓐ ALL DIMENSIONS ARE CASTING LENGTHS.
Ⓑ FIRST PAIR OF STIRRUPS PARALLEL TO BEAM END, TRANSITION NEXT 2 PAIR TO VERTICAL POSITION.
Ⓒ ALL STUB DIMENSIONS ARE MEASURED FROM STENCIL END OF BEAM.

PIECE DETAIL	QTY RQD
3	1

SCP STANDARD CONCRETE PRODUCTS
6 HATCHCOVER RD SAVANNAH, GA. 31404
TEL : (912) 233-9243
FAX : (912) 236-1687

SHEET DETAILS: BEAM DETAILS (ENGLISH TYPE IIs – MK1–14)
CONTR./PROJ. No.: NCHRP 12-64
CONTRACTOR: STANDARD CONCRETE PRODUCTS
COUNTY, STATE & PROJECT DETAILS: RESEARCH AASHTO TYPE II BEAMS NORTH CAROLINA STATE UNIVERSITY
DRAWN BY: JAL | DESIGNED BY: NCSU
DATE: 02/23/05 | CHECKED BY: TMS | JOB No. 056_S
SHEET 3 OF 8 | SEAL: NONE

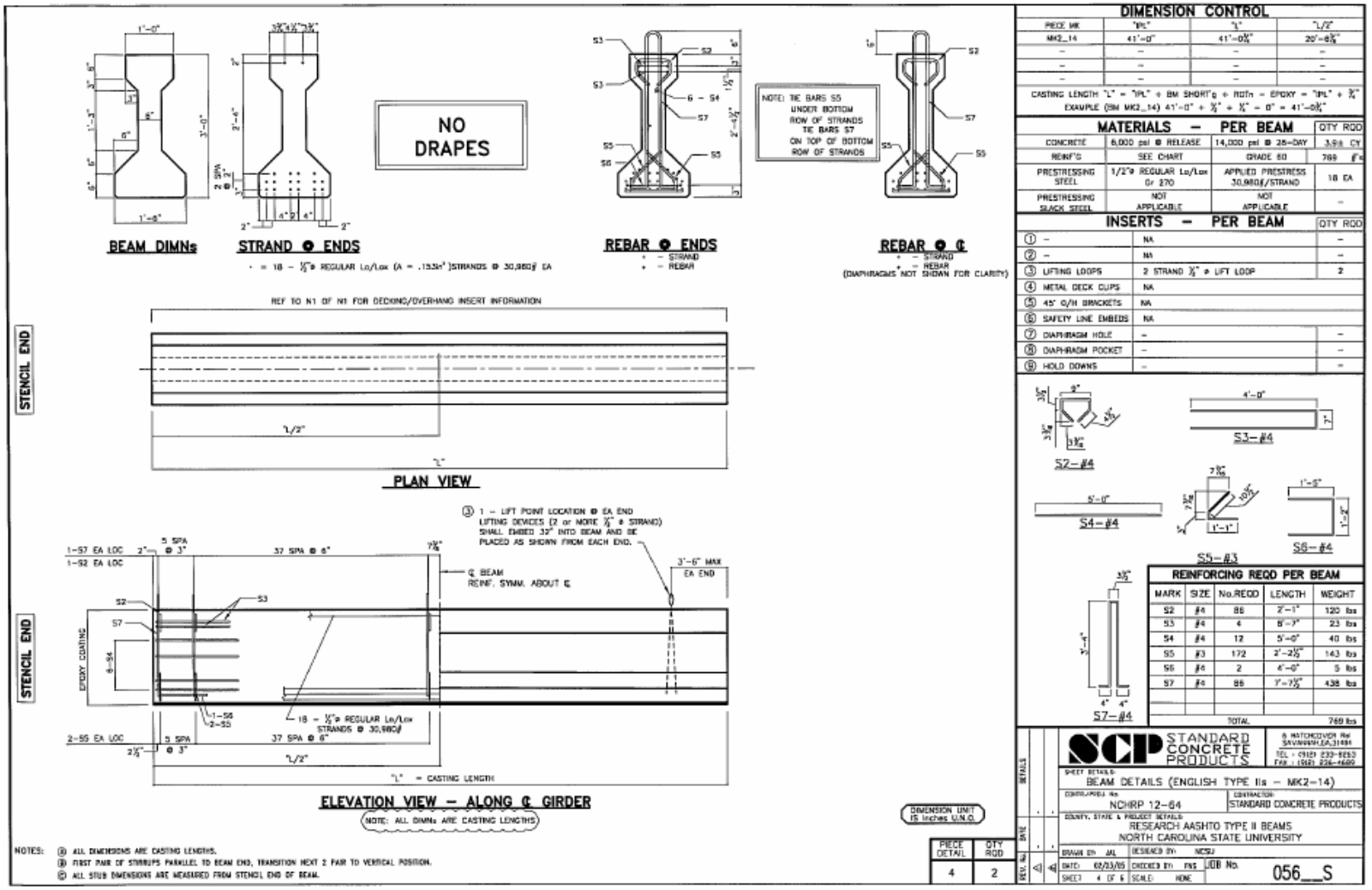

DIMENSION CONTROL

PIECE MK	"PL"	"L"	"L/2"
MK2_14	41'-0"	41'-0 1/16"	20'-8 1/16"
–	–	–	–
–	–	–	–
–	–	–	–

CASTING LENGTH "L" = "PL" + BM SHORT'g + RDTn – EPOXY = "PL" + 3/16"
EXAMPLE (BM MK2_14) 41'-0" + 3/16" + 3/16" – 0" = 41'-0 1/16"

MATERIALS – PER BEAM

			QTY RQD
CONCRETE	6,000 psi @ RELEASE	14,000 psi @ 28-DAY	3.96 CY
REINF'G	SEE CHART	GRADE 60	769 #'s
PRESTRESSING STEEL	1/2"ø REGULAR Lo/Lox Gr 270	APPLIED PRESTRESS 30,980#/STRAND	18 EA
PRESTRESSING SLACK STEEL	NOT APPLICABLE	NOT APPLICABLE	–

INSERTS – PER BEAM

		QTY RQD
① –	NA	–
② –	NA	–
③ LIFTING LOOPS	2 STRAND 3/8" ø LIFT LOOP	2
④ METAL DECK CLIPS	NA	
⑤ 45° O/H BRACKETS	NA	
⑥ SAFETY LINE EMBEDS	NA	
⑦ DIAPHRAGM HOLE	–	–
⑧ DIAPHRAGM POCKET	–	–
⑨ HOLD DOWNS	–	–

REINFORCING REQD PER BEAM

MARK	SIZE	No.REQD	LENGTH	WEIGHT
S2	#4	86	2'-1"	120 lbs
S3	#4	4	5'-7"	23 lbs
S4	#4	12	5'-0"	40 lbs
S5	#3	172	2'-2 1/2"	143 lbs
S6	#4	2	4'-0"	5 lbs
S7	#4	86	7'-7 1/2"	438 lbs
			TOTAL	769 lbs

NOTES:
(A) ALL DIMENSIONS ARE CASTING LENGTHS.
(B) FIRST PAIR OF STIRRUPS PARALLEL TO BEAM END, TRANSITION NEXT 2 PAIR TO VERTICAL POSITION.
(C) ALL STUB DIMENSIONS ARE MEASURED FROM STENCIL END OF BEAM.

PIECE DETAIL	QTY RQD
4	2

STANDARD CONCRETE PRODUCTS
6 HATCHCOVER Rd SAVANNAH, GA 31404
TEL : (912) 232-8253 FAX : (912) 236-4600

SHEET DETAILS: BEAM DETAILS (ENGLISH TYPE IIs – MK2–14)
CONTRACT No.: NCHRP 12-64
CONTRACTOR: STANDARD CONCRETE PRODUCTS
COUNTY, STATE & PROJECT DETAILS: RESEARCH AASHTO TYPE II BEAMS NORTH CAROLINA STATE UNIVERSITY
DRAWN BY: JAL | DESIGNED BY: NCSU
DATE: 02/23/05 | CHECKED BY: PNS | JOB No. 056__S
SHEET 4 OF 6 | SCALE: NONE

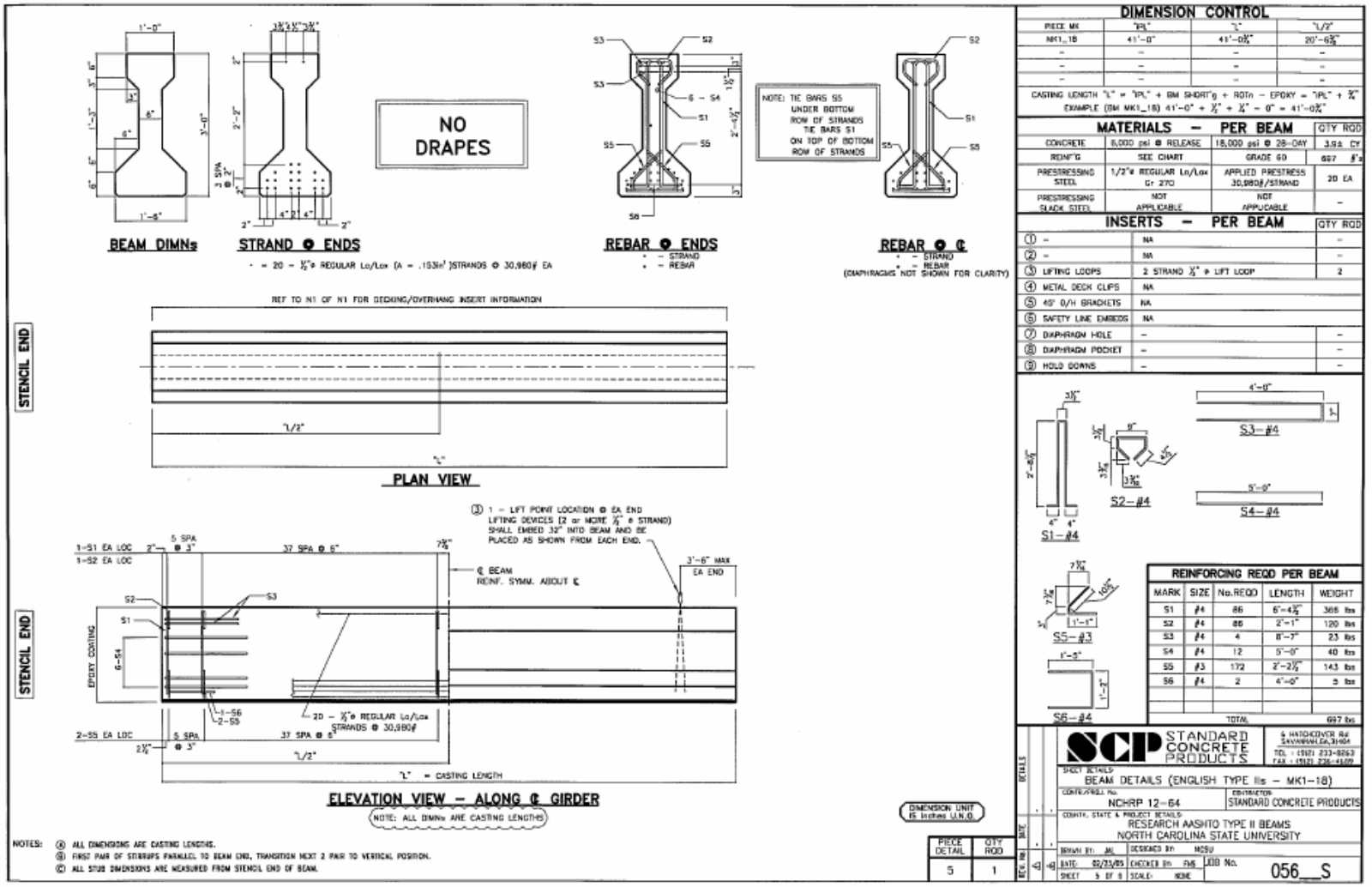

DIMENSION CONTROL

PIECE MK	"PL"	"L"	"L/2"
MK1_18	41'-0"	41'-0¾"	20'-6⅜"
–	–	–	–
–	–	–	–
–	–	–	–

CASTING LENGTH "L" = "PL" + BM SHORT'g + ROTn – EPOXY = "PL" + ¾"
EXAMPLE (BM MK1_18) 41'-0" + ½" + ¾" – 0" = 41'-0¾"

MATERIALS – PER BEAM

			QTY REQD
CONCRETE	8,000 psi @ RELEASE	10,000 psi @ 28-DAY	3.94 CY
REINF'G	SEE CHART	GRADE 60	697 lbs
PRESTRESSING STEEL	1/2"ø REGULAR Lo/Lox Gr 270	APPLIED PRESTRESS 30,980#/STRAND	20 EA
PRESTRESSING SLACK STEEL	NOT APPLICABLE	NOT APPLICABLE	–

INSERTS – PER BEAM

			QTY REQD
①	–	NA	–
②	–	NA	–
③	LIFTING LOOPS	2 STRAND ½" ø LIFT LOOP	2
④	METAL DECK CLIPS	NA	
⑤	45° D/H BRACKETS	NA	
⑥	SAFETY LINE EMBEDS	NA	
⑦	DIAPHRAGM HOLE	–	–
⑧	DIAPHRAGM POCKET	–	–
⑨	HOLD DOWNS	–	–

REINFORCING REQD PER BEAM

MARK	SIZE	No. REQD	LENGTH	WEIGHT
S1	#4	86	6'-4½"	365 lbs
S2	#4	86	2'-1"	120 lbs
S3	#4	4	8'-7"	23 lbs
S4	#4	12	5'-0"	40 lbs
S5	#3	172	2'-2½"	143 lbs
S6	#4	2	4'-0"	5 lbs
			TOTAL	697 lbs

NOTES:
Ⓐ ALL DIMENSIONS ARE CASTING LENGTHS.
Ⓑ FIRST PAIR OF STIRRUPS PARALLEL TO BEAM END, TRANSITION NEXT 2 PAIR TO VERTICAL POSITION.
Ⓒ ALL STUB DIMENSIONS ARE MEASURED FROM STENCIL END OF BEAM.

PIECE DETAIL	QTY REQD
5	1

SCP STANDARD CONCRETE PRODUCTS
4 HATCHCOVER Rd
SAVANNAH, GA, 31404
TEL: (912) 233-8263
FAX: (912) 236-4509

SHEET DETAILS: BEAM DETAILS (ENGLISH TYPE IIs – MK1–18)
CONTR/PROJ. No.: NCHRP 12-64
CONTRACTOR: STANDARD CONCRETE PRODUCTS
COUNTY, STATE & PROJECT DETAILS: RESEARCH AASHTO TYPE II BEAMS NORTH CAROLINA STATE UNIVERSITY
DRAWN BY: JML | DESIGNED BY: NCSU
DATE: 02/23/05 | CHECKED BY: FMS | JOB No. 056_S
SHEET 5 OF 5 | SCALE: NONE

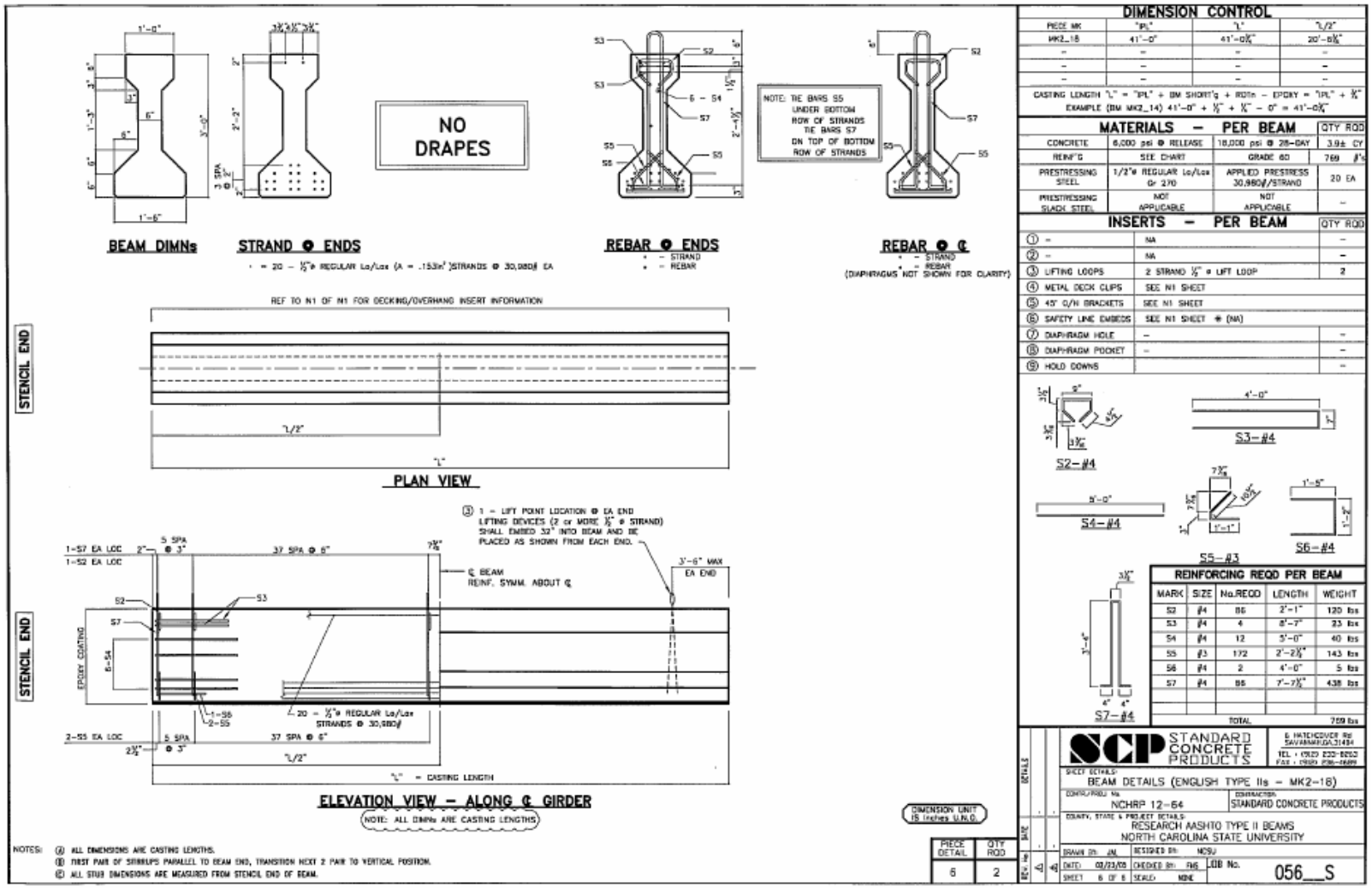

DIMENSION CONTROL

PIECE MK	"PL"	"L"	"L/2"
MK2_18	41'-0"	41'-0⅛"	20'-0⅛"
"	"	"	"
"	"	"	"
"	"	"	"
"	"	"	"

CASTING LENGTH "L" = "PL" + BM SHORT'g + RDTn – EPOXY = "PL" + ⅛"
EXAMPLE (BM MK2_14) 41'-0" + ½" + ⅛" – 0" = 41'-0⅛"

MATERIALS – PER BEAM

			QTY RQD
CONCRETE	6,000 psi @ RELEASE	10,000 psi @ 28-DAY	3.9± CY
REINF'G	SEE CHART	GRADE 60	769 #'s
PRESTRESSING STEEL	1/2"ø REGULAR Lo/Lox Gr 270	APPLIED PRESTRESS 30,980#/STRAND	20 EA
PRESTRESSING SLACK STEEL	NOT APPLICABLE	NOT APPLICABLE	–

INSERTS – PER BEAM

			QTY RQD
①	–	NA	–
②	–	NA	–
③	LIFTING LOOPS	2 STRAND ½" ø LIFT LOOP	2
④	METAL DECK CLIPS	SEE N1 SHEET	
⑤	45° C/N BRACKETS	SEE N1 SHEET	
⑥	SAFETY LINE EMBEDS	SEE N1 SHEET ⊕ (NA)	
⑦	DIAPHRAGM HOLE	–	–
⑧	DIAPHRAGM POCKET	–	–
⑨	HOLD DOWNS		–

REINFORCING REQD PER BEAM

MARK	SIZE	No.REQD	LENGTH	WEIGHT
S2	#4	86	2'-1"	120 lbs
S3	#4	4	8'-7"	23 lbs
S4	#4	12	5'-0"	40 lbs
S5	#3	172	2'-2½"	143 lbs
S6	#4	2	4'-0"	5 lbs
S7	#4	86	7'-7⅛"	438 lbs
			TOTAL	769 lbs

PIECE DETAIL	QTY REQD
6	2

SCP STANDARD CONCRETE PRODUCTS
6 WATERCOVER RD SAVANNAH,GA.31419
TEL : (912) 232-8262 FAX : (912) 236-6699

SHEET DETAILS: BEAM DETAILS (ENGLISH TYPE IIs – MK2-18)
CONTRACT No. NCHRP 12-64
CONTRACTOR: STANDARD CONCRETE PRODUCTS
COUNTY, STATE & PROJECT DETAILS: RESEARCH AASHTO TYPE II BEAMS NORTH CAROLINA STATE UNIVERSITY
DRAWN BY: JN DESIGNED BY: NCSU
DATE: 02/23/05 CHECKED BY: FHS JOB No. 056__S
SHEET 6 OF 6 SEALED: NONE

Appendix C : Shop Drawing for Cast-in place Deck

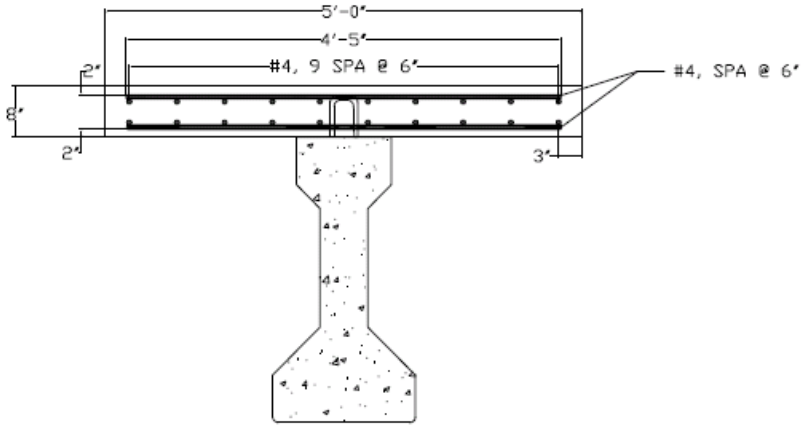

SECTION A

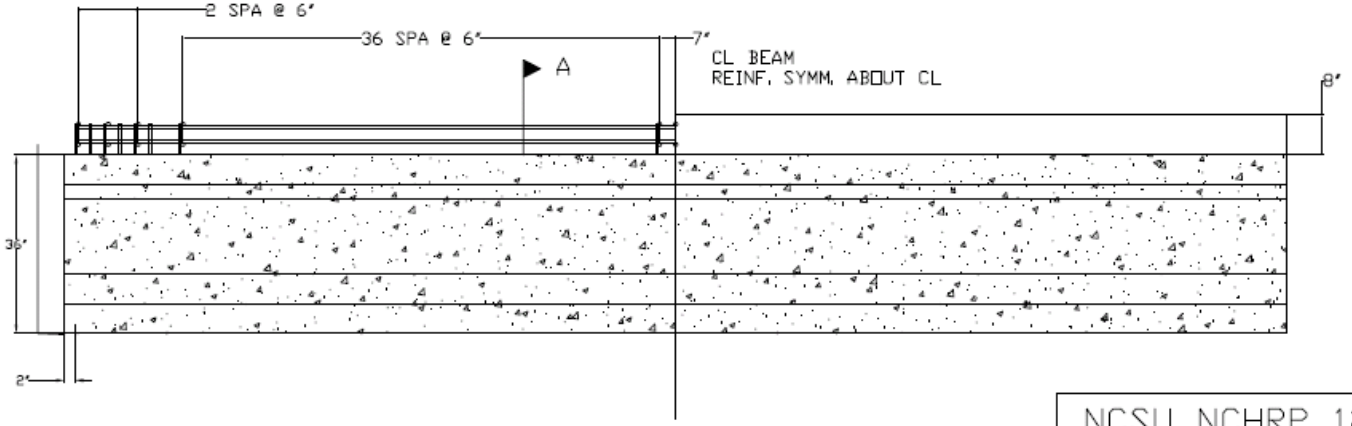

ELEVATION VIEW - ALONG GIRDER

NOTE: For one AASHTO Girder per Concrete Strength

QTY RQD	3	MK2_10, MK2_14, MK2_18

f'c for the deck slab = 4000psi

NCSU NCHRP 12-64

DECK CASTING SLAB WIDTH 5FT

Date : 08 / 05 2005

TEL : 919-513-1734
FAX : 919-513-1765

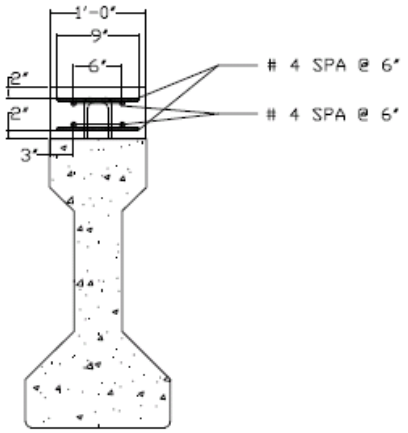

SECTION A

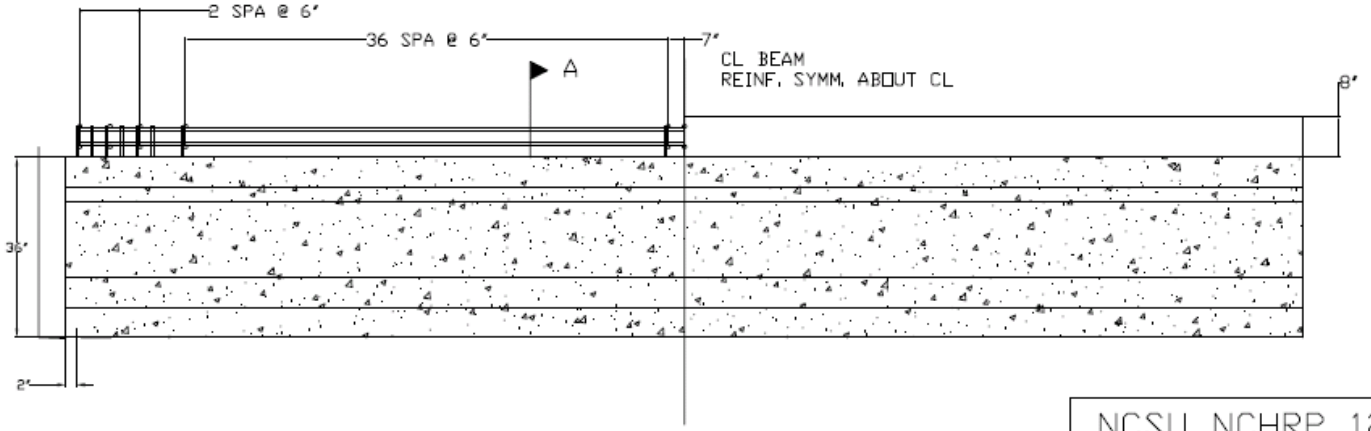

ELEVATION VIEW - ALONG GIRDER

NOTE: For one AASHTO Girder per Concrete Strength

QTY RQD	3	MK2_10, MK2_14, MK2_18

f'c for the deck slab = 4000psi

NCSU NCHRP 12-64

DECK CASTING SLAB WIDTH 1FT

Date : 08 / 05 2005

TEL : 919-513-1734
FAX : 919-513-1765

Appendix D : Concrete Batch Mixes

10 ksi Production (Mix 1P)			
	Batch 1	Batch 2	Batch 3
Cement	675	661	663
Flyash	166	156	150
Microsilica	47	48	51
#67 Granite	1697	1647	1719
Concrete Sand (River)	1084	1058	1087
Water	33	36	35
Recover	26	25	29
ADVA 170	97	94	98

14 ksi Production (Mix 2P)			
	Batch 1	Batch 2	Batch 3
Cement	692	699	698
Flyash	196	205	197
Microsilica	76	72	75
#67 Granite	1684	1674	1681
Concrete Sand (River)	1073	1079	1092
Water	29	30	30
Recover	37	50	50
ADVA 170	123	124	125

18 ksi Production (Mix 3P)			
	Batch 1	Batch 2	Batch 3
Cement	946	896	873
Flyash	196	191	189
Microsilica	86	79	79
#67 Granite	1784	1759	1667
Concrete Sand (River)	854	931	914
Water	25	29	32
Recover	38	37	36
ADVA 170	142	137	145

- Water gallon/cubic yard
- Recover oz/cubic yard
- ADVA oz/cubic yard

Appendix E : Compressive Concrete Strength from Girder Producer

Average Compressive Strength from 2, 4″x8″ Cylinders

Mix Design	Batch	1days (psi)	7days (psi)	14days (psi)	28days (psi)	56days (psi)
Mix 1P	1	6180	9750	10610	13090	14100
	3	6320	8310	10080	11640	10890
Mix 2P	1	6360	12750	13200	14170	14150
	2	5560	13890	14170	14330	15880
	3	5560	12920	13550	14660	17540
Mix 3P	1	7480	11120	14030	14430	15650
	2	7700	-	17230	16580	18710
	3	8100	13730	15320	16090	17880

Appendix F : Distribution of the collected data

Compressive Strength of Concrete (psi)

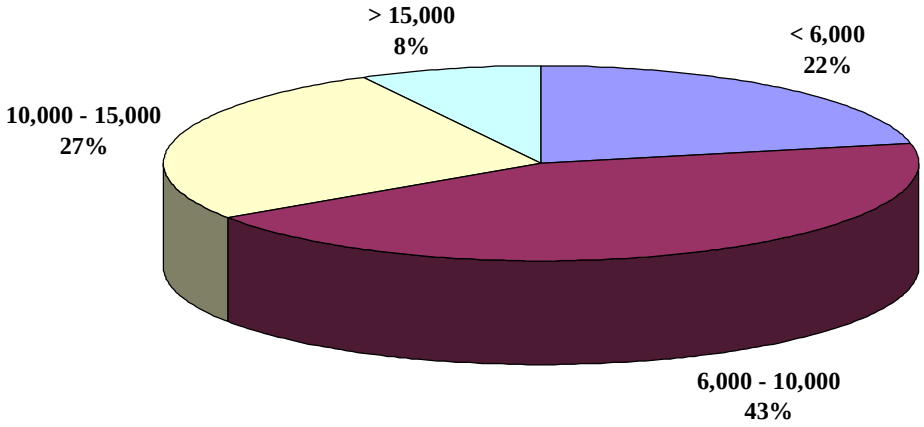

Unit Weight (pcf)

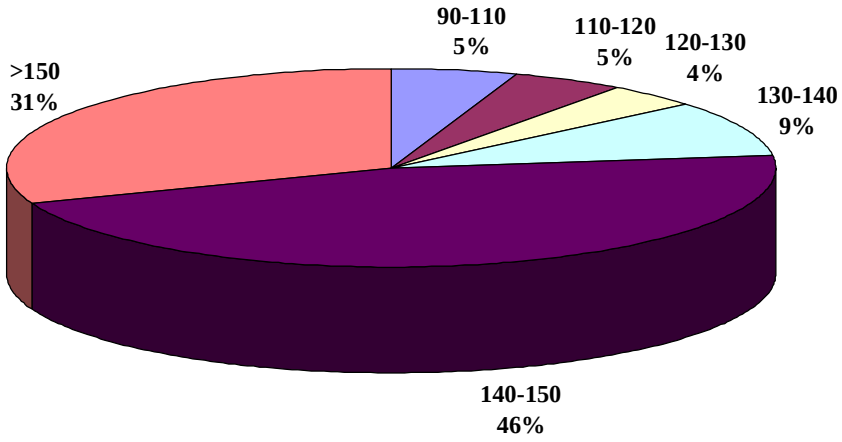

Appendix G : Stain envelopes for each specimens

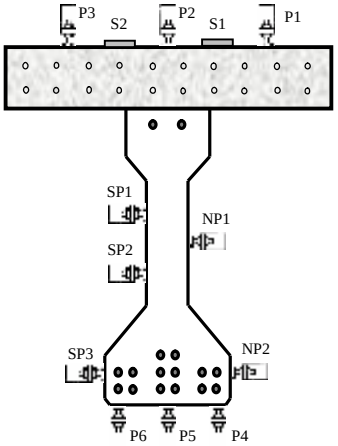

a) Strain gauge location

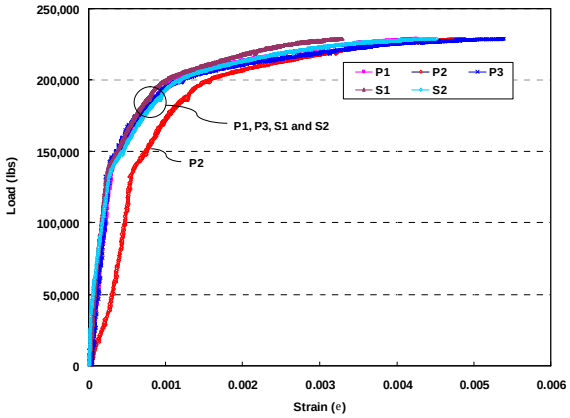

b) Strain at the top surface

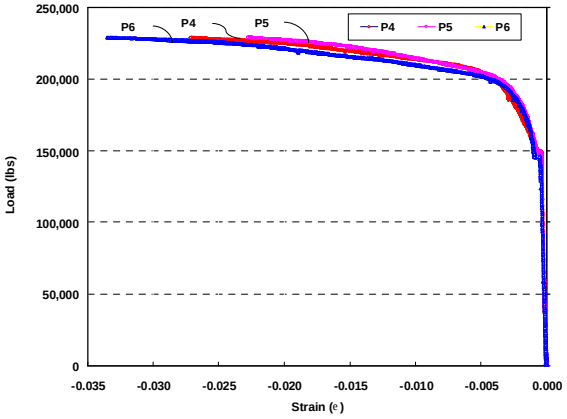

c) Strain at the bottom surface

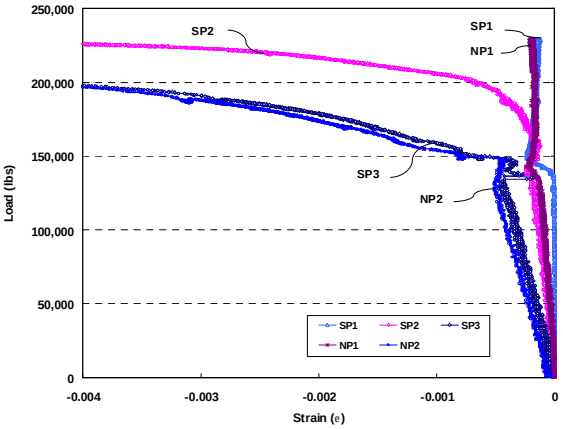

d) Strain at the side surface

Figure G-1 Strain envelopes for10PS-5S

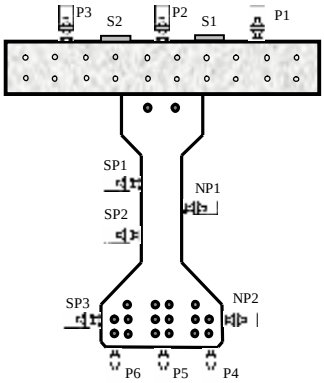

a) Strain gauge location

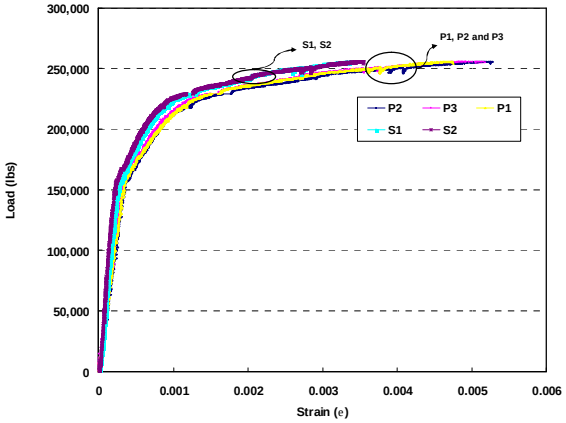

b) Strain at the top surface

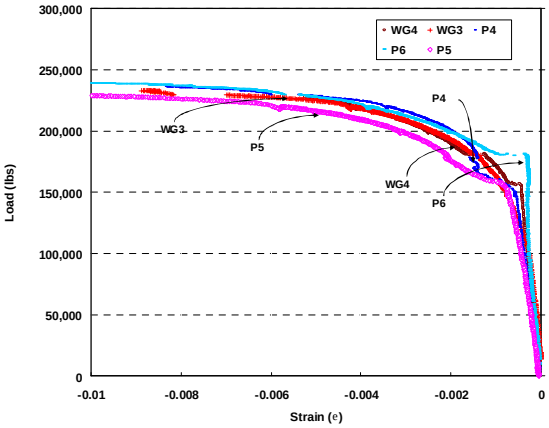

c) Strain at the bottom surface

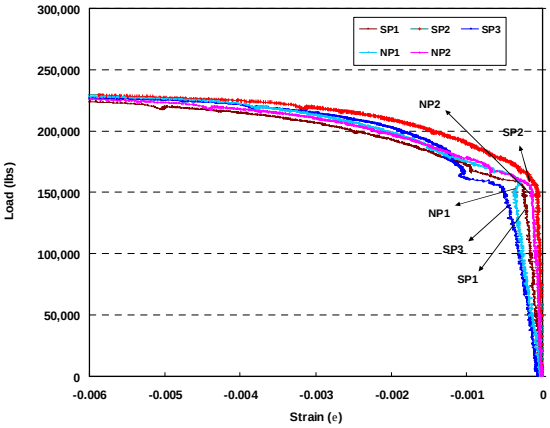

d) Strain at the side surface

Figure G-2 Strain envelopes for14PS-5S

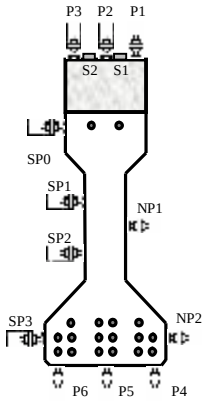

a) Strain gauge location

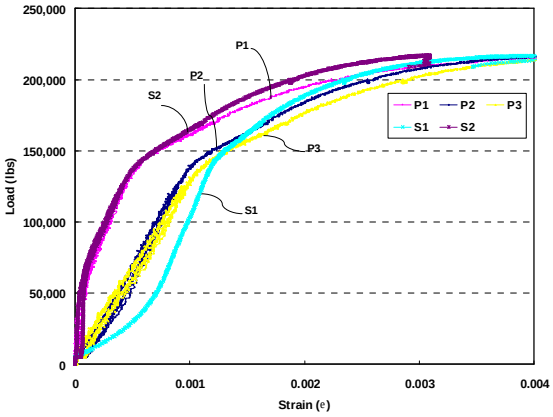

b) Strain at the top surface

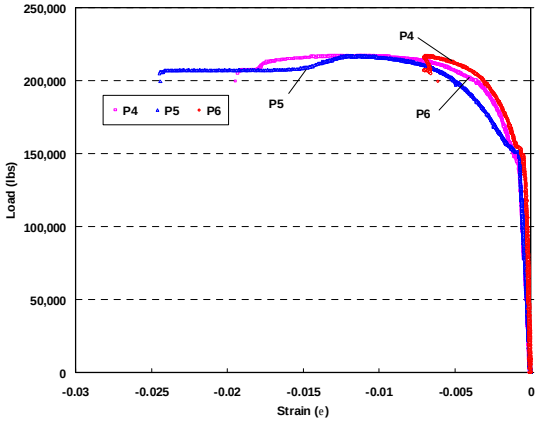

c) Strain at the bottom surface

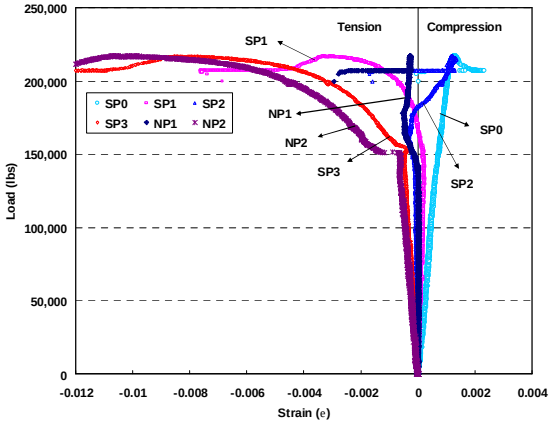

d) Strain at the side surface

Figure G-3 Strain envelopes for 14PS-1S

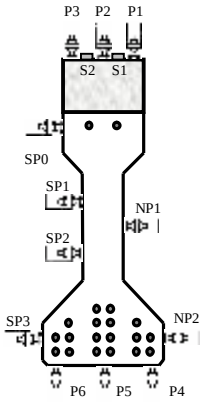

a) Strain gauge location

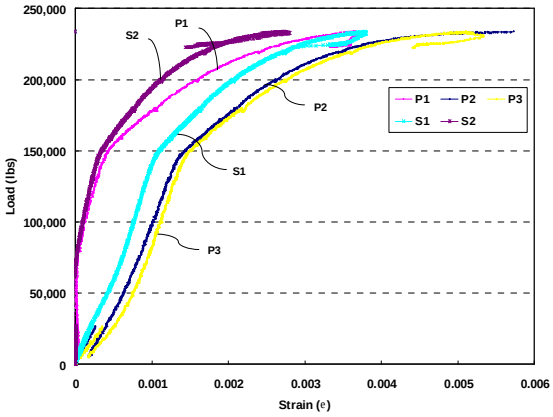

b) Strain at the top surface

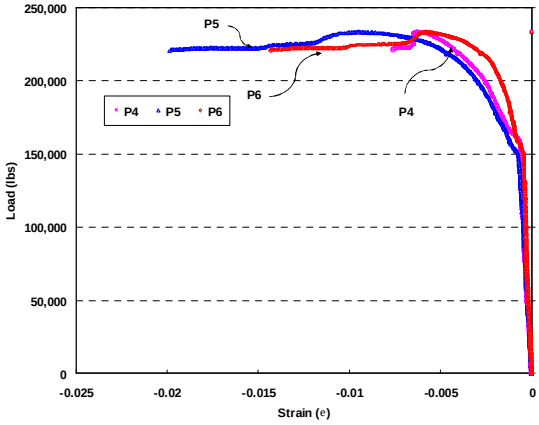

c) Strain at the bottom surface

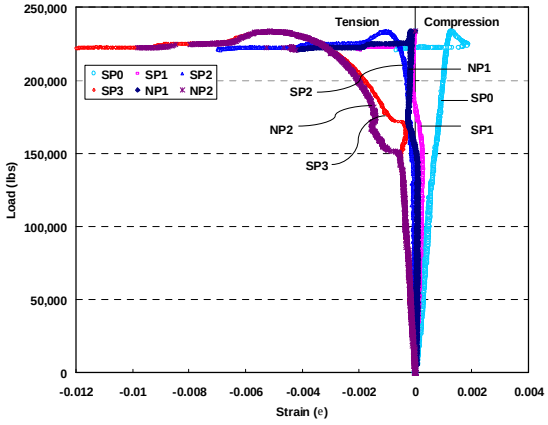

d) Strain at the side surface

Figure G-4 Strain envelopes for 18PS-1S

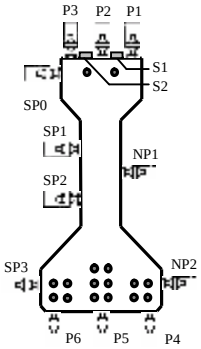

a) Strain gauge location

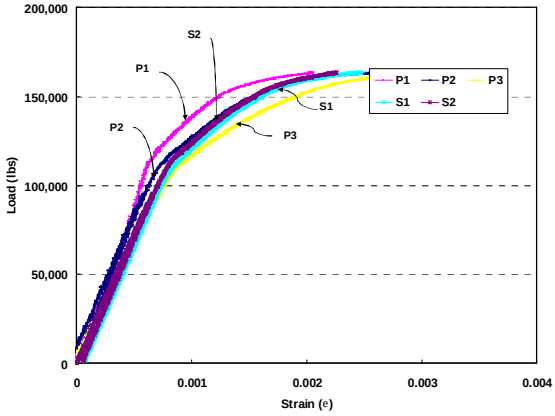

b) Strain at the top surface

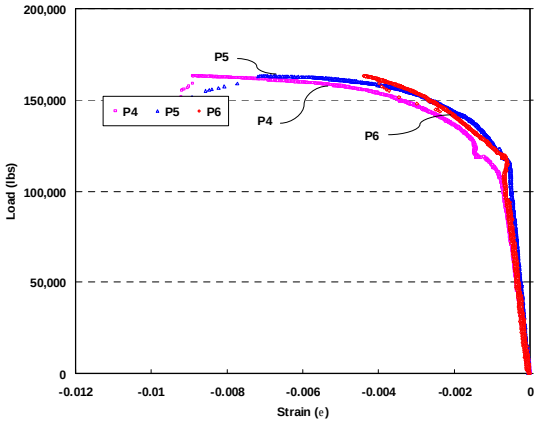

c) Strain at the bottom surface

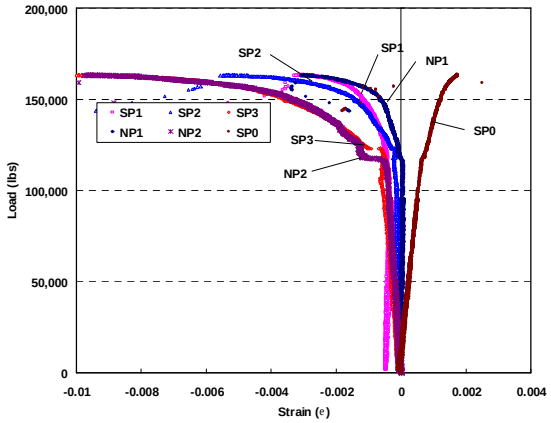

d) Strain at the side surface

Figure G-5 Strain envelopes for 10PS-N

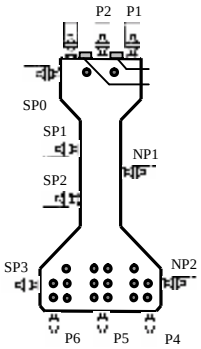

a) Strain gauge location

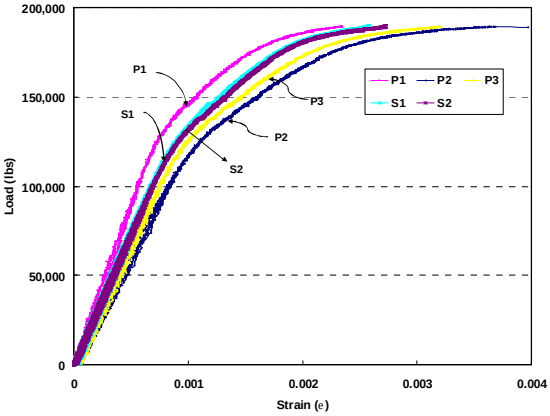

b) Strain at the top surface

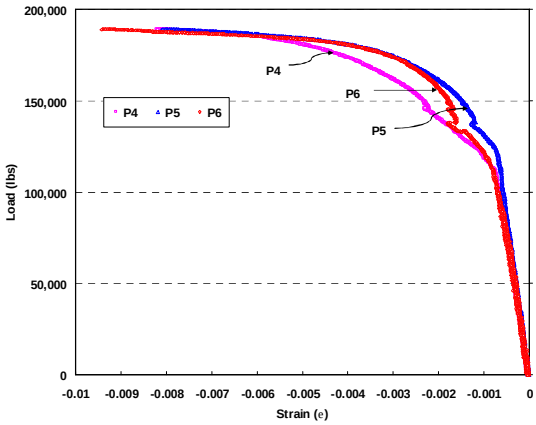

c) Strain at the bottom surface

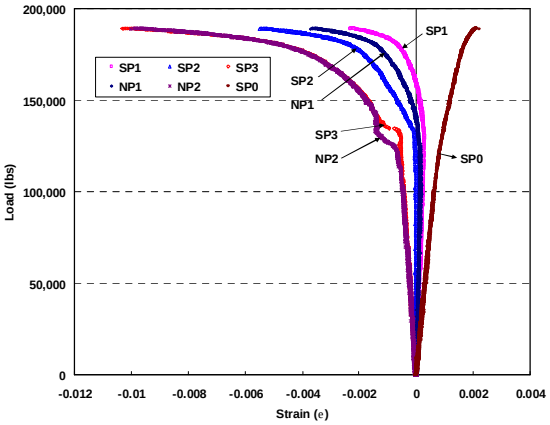

d) Strain at the side surface

Figure G-6 Strain envelopes for 14PS-N

Appendix H : Prestress losses Calculation (adopted from Tadros, 2003)

NCHRP 12-64 AAHSTO girder
Proposed Detailed Method Using Estimated Material Properties
Precast 10PS-5S

Span	40 ft		H	70 %	
A	369.00 in^2		f_{ci}	6.200 ksi	
I	50980 in^4		f'_c	11.490 ksi	
y_b	15.83 in				
h	36 in				
V/S	3.37 in				
Deck					
Width	60 in		f'_{cd}	3.78 ksi	
Thickness	8 in				
Area	480 in^2				
Steel			Age at release t_i	2 days	
A_{ps}	2.448 in^2		Age at deck placement	91 days	
f_{pi}	202.5 ksi		Age at Final	120 days	
E_s	29000 ksi				
y_{pb}	7.25 in				
Loads			**Midspan Moments**		
Girder self wt	0.3840 kip/ft		Girder self wt		922 kip-in
Deck wt	0.500 kip/ft		Deck wt	1200 kip-in	
Haunch wt	0.000 kip/ft		Haunch wt	0 kip-in	
Diaph. wt	0.000 kip/ft		Diaph. Wt	0.0 kip-in	1200 kip-in
SI dead ld.	0.000 kip/ft		SI dead ld.		0 kip-in
			Live load plus impact		0 kip-in

Solution

Modulus of Elasticity	$33000*w^{1.5}*(f'_c)^{0.5}$			Beam	E_{ci}	4726
	w=0.15	(kcf)			E_c	6434
				Deck	E_{cd}	3690
Shrinkage	$0.00043(5/(1+f_{ci}))k_s k_h k_{td}$			Beam	ε_{bif}	0.000259
	k_h	2.0-0.0143H			ε_{bid}	0.000241
	k_{td}	$t/(61-4f_{ci}+t)$	Precast		ε_{bdf}	0.000018
				Deck	ε_{ddf}	0.000182
Creep	$1.80*k_s*k_h*(5/(1+f_{ci}))*k_{la}*k_{td}$			Beam	ψ_{bif}	0.965
	k_h	(1.58-0.008*H)			ψ_{bid}	0.896
	k_{la}	t_i^-0.118	Formula for girder only		ψ_{bdf}	0.357
	k_{td}	$t/(61-4f_{ci}+t)$		Deck	ψ_{ddf}	1.294

Section Properties				**Precast Gross Section**	**Transf. Rel**	**Tr. Final**	**Deck**	**Composite Gross**	**Composite Tr.**
Steel modular ratio,n_i	E_s/E_{ci}	6.1363	A	369.00	381.57	377.59	275.31	644.31	652.90
Steel modular ratio,n	E_s/E_c	4.5076	y_b (to bottom fiber of beam)	15.83	15.55	15.63	40	26.16	25.91
Deck modular ratio	E_d/E_c	0.5736	I	50980	51875	51598	1468	144559	147588.3
			e_p	8.58	8.30	8.38		18.91	18.66
			e_d					-13.84	
			α=1+A*e2/I	1.5328				2.593	

Transfromed section factors, K	K_r Elastic (at release)	0.94126	K_{dc} Elastic(at SIDL)	0.95747
$K=1/(1+n*\alpha*A_s/A_c*(1+0.7*C))$	K_d Elastic(at deck pl.)	0.95617		
	K_{rd} Long-term	0.90535	K_{df} Long-term	0.90802

Stress Calculation		**Steel Stress Change**	**Steel Stress Net**	**Gross Section Concrete Stress Change**	**Gross Section Concrete Stress Net**	**Transf. Section Concrete Stress Change**	**Transf. Section Concrete Stress Net**
			202.500				
(1) Elastic due to P_i	$P_i*\alpha*K_r*n_i/A$	11.894	190.606	1.938	1.938	1.957	1.957
(2) Elastic due to self weight	$M*e/I*K_r*n_i$	-0.896	191.502	-0.146	1.792	-0.147	1.810
(3) Shrinkage between release and deck place	$\varepsilon_{bid}*E_p*K_{rd}$	6.318	185.183				
(4) Creep between release and deck place	$n_i*f_{cir}*K_r*\psi_{bid}*K_{rd}$	8.924	176.260				
(5) Relaxation between release and deck place		1.200	175.060	-0.167	1.625	-0.159	1.651
(6) Elastic due to deck weight	$n*\delta f_{cdp}*K_d$	-0.870	175.930	-0.193	1.432	-0.195	1.456
(7) Elastic due to superimposed DL (on composite section)	$n*\delta f_{csp}*K_{dc}$	0.000	175.930	0.000	1.432	0.000	1.456
(8) Shrinkage of beam bet.deck place and final	$\varepsilon_{bdf}*E_p*K_{df}$	0.485	175.445				
(9) Creep of beam bet.deck place and final, due to initial loads	$n_i*f_{pc}*(\psi_{bif}-\psi_{bid})*K_{df}$	0.685	174.761				
(10) Creep of beam due to deck and SIDL	$n*df_{pc}*\psi_{bdf}*K_{df}$	-0.527	175.288				
(11) Relaxation between deck place and final	$\phi_d*L_d*K_{df}$	1.200	174.088				
(12) Shrinkage of deck	$\varepsilon_{bdf}*E_{cd}/(1+0.7*\psi_{ddf})*A_d*\alpha/A*K_{df}*n*(1+0.7*\psi_{bdf})$	-0.223	174.311	-0.016	1.416	-0.015	1.440
Total Prestress Loss prior to Live Load Application		**28.189**					

Appendix I : Concrete material model

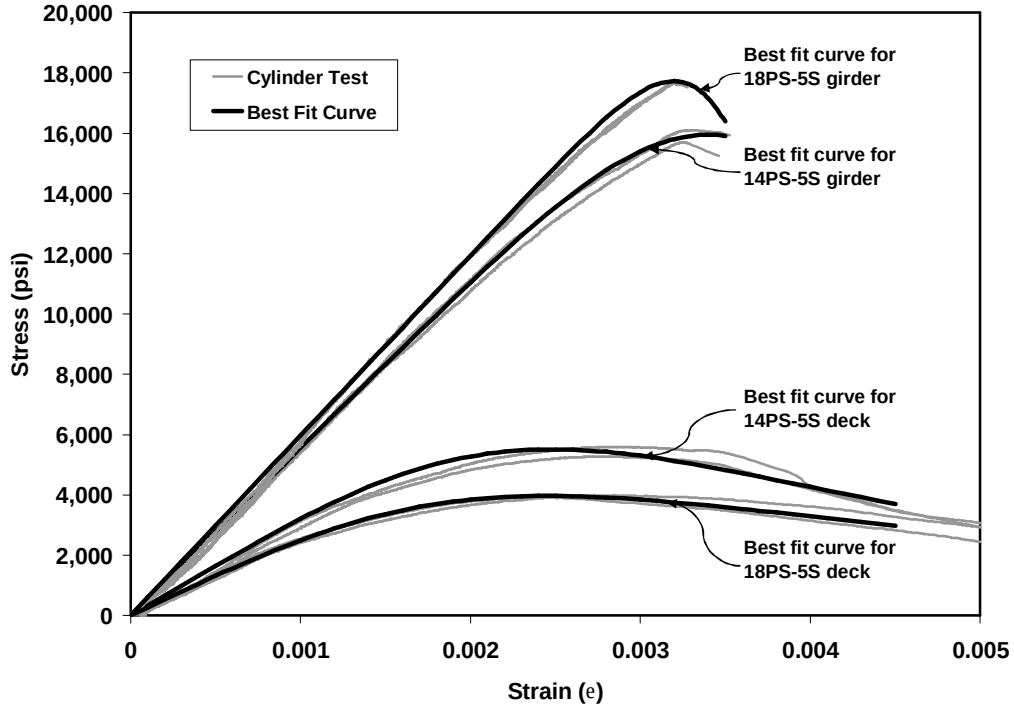

Figure I-1 Best fit curve for 14PS-5S and18PS-5S

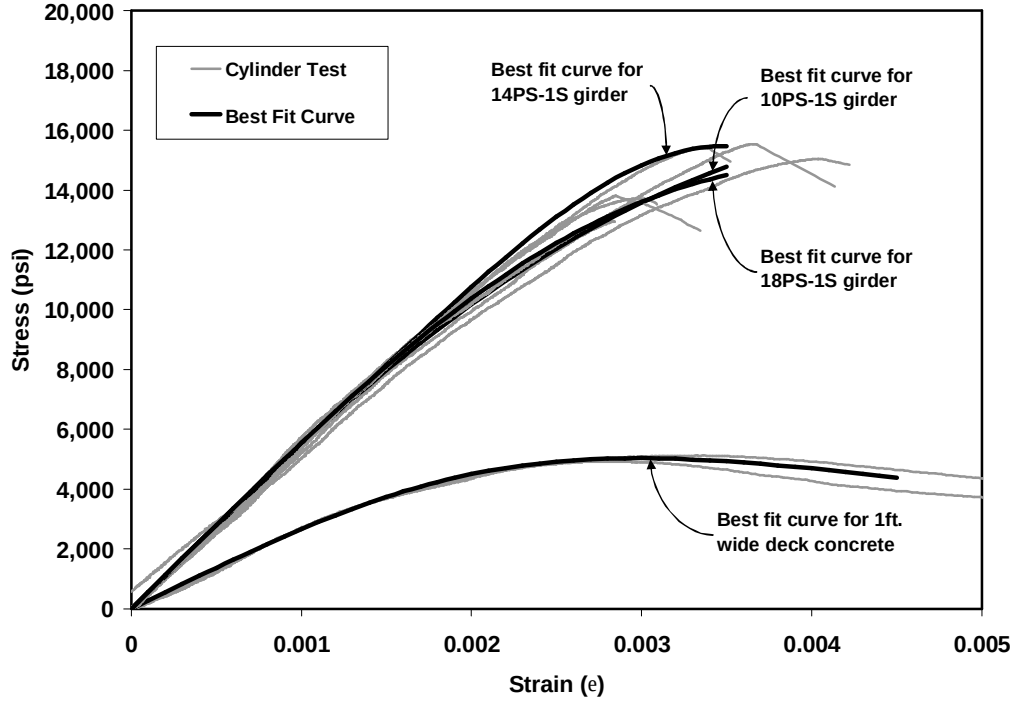

Figure I-2 Best fit curve for 10PS-1S, 14PS-1S and 18PS-1S

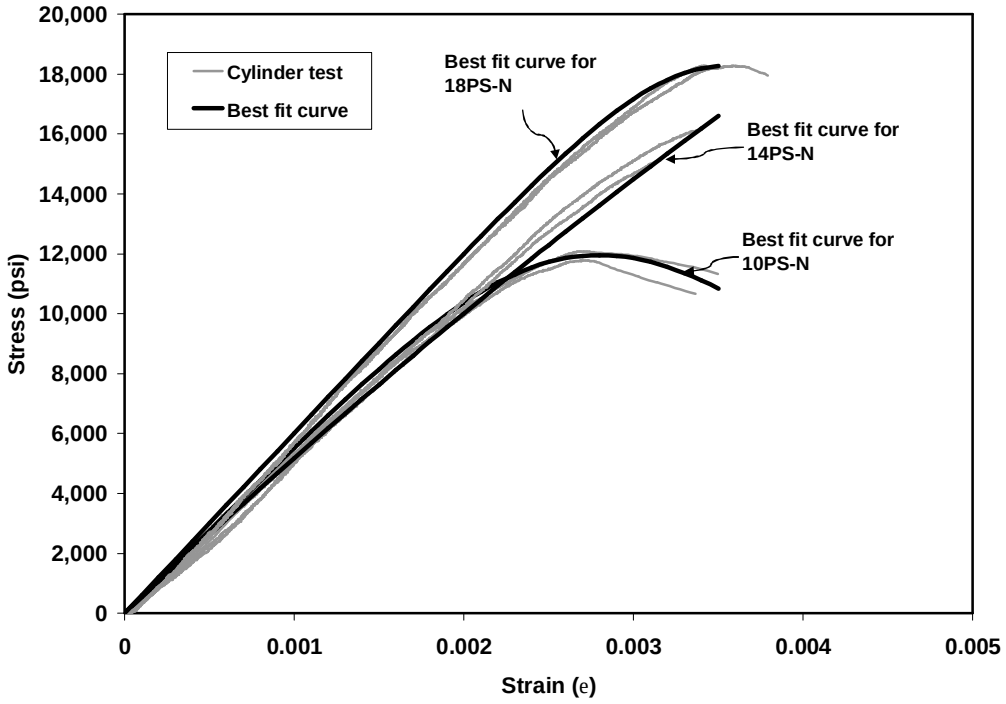

Figure I-3 Best fit curve for 10PS-N, 14PS-N and 18PS-N